ADVANCED, SMALL HIGH-TEMPERATURE-RISE COMBUSTOR PROGRAM. VOLUME II. DESIGN AND TEST OF FULL-SCALE COMBUSTION SYSTEM

Michael P. Wood, et al

AiResearch Manufacturing Company of Arizona

Prepared for:

Army Air Mobility Research and Development Laboratory

February 1974

DISCLAIMER NOTICE

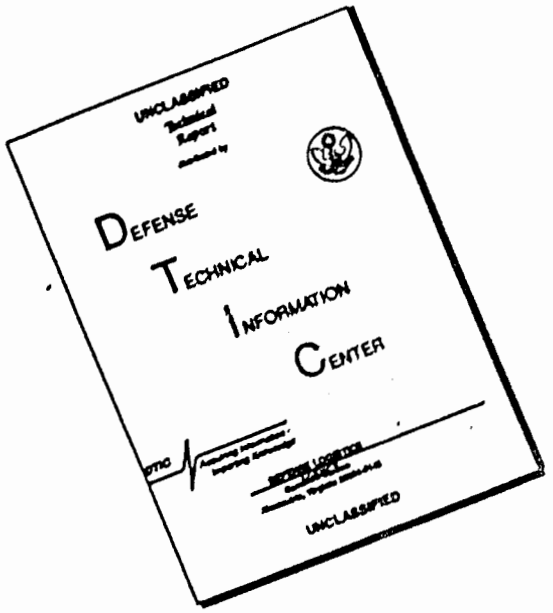

THIS DOCUMENT IS BEST QUALITY AVAILABLE. THE COPY FURNISHED TO DTIC CONTAINED A SIGNIFICANT NUMBER OF PAGES WHICH DO NOT REPRODUCE LEGIBLY.

Unclassified
Security Classification

AD776978

DOCUMENT CONTROL DATA - R & D

(Security classification of title, body of abstract and indexing annotation must be entered when the overall report is classified)

1. ORIGINATING ACTIVITY *(Corporate author)*
AiResearch Manufacturing Company of Arizona
A Division of The Garrett C rporation
Phoenix, Arizona

2a. REPORT SECURITY CLASSIFICATION
Unclassified

2b. GROUP

3. REPORT TITLE
ADVANCED, SMALL, HIGH-TEMPERATURE-RISE COMBUSTOR PROGRAM
VOLUME II - DESIGN AND TEST OF FULL-SCALE COMBUSTION SYSTEM

4. DESCRIPTIVE NOTES *(Type of report and inclusive dates)*
Final Report

5. AUTHOR(S) *(First name, middle initial, last name)*
M. P. Wood
K. M. Johansen

6. REPORT DATE	7a. TOTAL NO. OF PAGES	7b. NO. OF REFS
February 1974	116	8

8a. CONTRACT OR GRANT NO.	9a. ORIGINATOR'S REPORT NUMBER(S)
DAAJ02-70-C-0060	
b. PROJECT NO.	USAAMRDL Technical Report 74-3B
c. Task 1G162203D14413	9b. OTHER REPORT NO(S) *(Any other numbers that may be assigned this report)*
d.	

10. DISTRIBUTION STATEMENT
Approved for public release; distribution unlimited.

11. SUPPLEMENTARY NOTES	12. SPONSORING MILITARY ACTIVITY
Volume II of a 2-volume report.	Eustis Directorate, U.S. Army Air Mobility Research and Development Laboratory Fort Eustis, Virginia

13. ABSTRACT

This report describes an analytical and experimental study of advanced, small, high-temperature combustors. This volume describes the third and final phase of this program which included the design and performance verification tests of a full-scale combustion system. The objectives of the 32-month program were (a) to develop and validate an analytical design technique for small, high-temperature-rise, low-airflow combustors and related components, and (b) to define the limitations associated with these small combustors and related components and the effects of these limitations on the cycle and the configuration of advanced-technology engines.

Analytical models were developed to predict the characteristics and performance of the basic combustor elements including fuel injection, primary zone, dilution zone, and liner cooling. Nine combustor element rig test programs were conducted to provide data to update and validate the analytical models. Based on the analysis and rig test results, a full-scale combustor was designed, fabricated, and tested. Additionally, a material screening program was conducted to select the most suitable existing material for combustor application. A relatively new material (IN-586) was selected. Material-property tests were conducted to supplement published data for this material.

The analytical models were used to assess combustor design and performance limitations and the applicability of the design techniques over an airflow range of 2 to 5 pounds per second, cycle pressure ratio range of 10 to 16 (including recuperation), and a turbine inlet temperature range of 2300°F to 2700°F.

119

DD FORM 1 NOV 68 1473 REPLACES DD FORM 1473, 1 JAN 64, WHICH IS OBSOLETE FOR ARMY USE.

Unclassified
Security Classification

14 KEY WORDS	LINK A		LINK B		LINK C	
	ROLE	WT	ROLE	WT	ROLE	WT
Gas turbine engine Annular combustor Analytical combustor design Fuel injection						

DEPARTMENT OF THE ARMY
U. S ARMY AIR MOBILITY RESEARCH & DEVELOPMENT LABORATORY
EUSTIS DIRECTORATE
FORT EUSTIS, VIRGINIA 23604

The research described herein was conducted by AiResearch Manufacturing Company of Arizona, a Division of the Garrett Corporation, under Contract DAAJ02-70-C-0060. The work was performed under the technical management of Captain Frederick S. Sherwin (deceased), Mr. L. E. Bell, SP4 C. R. Roehrig, and Mr. R. G. Dodd, Technology Applications Division, Eustis Directorate, U.S. Army Air Mobility Research and Development Laboratory.

The objective of this contractual effort was to develop and validate analytical design techniques for small, high-temperature-rise, low-airflow gas turbine combustors and related components and to define the design limitations associated with these small advanced combustors. The analytical design models developed under this program were used to design a straight-through annular combustor with a W_a = 3 lb/sec, P_3 = 16 atm, and TIT = 2500°F. Combustor rig tests of this combustor indicate that the design models have the potential for reducing combustor development time and cost significantly.

Appropriate technical personnel of this Directorate have reviewed this report and concur with the conclusions contained herein.

The findings and recommendations outlined herein will be considered in planning future small gas turbine engine and combustor component development programs.

Task 1G162203D14413
Contract DAAJ02-70-C-0060
USAAMRDL Technical Report 74-3B
February 1974

ADVANCED, SMALL, HIGH-TEMPERATURE-RISE COMBUSTOR PROGRAM

Final Report

VOLUME II
DESIGN AND TEST OF FULL-SCALE COMBUSTION SYSTEM

By

M. P. Wood
K. M. Johansen

Prepared
By

AiResearch Manufacturing Company of Arizona
A Division of The Garrett Corporation
Phoenix, Arizona

for

EUSTIS DIRECTORATE
U.S. ARMY AIR MOBILITY RESEARCH AND DEVELOPMENT LABORATORY
Fort Eustis, Virginia

FOREWORD

The Advanced, Small, High-Temperature-Rise Combustor Program was conducted by the AiResearch Manufacturing Company of Arizona under Contract DAAJ02-70-C-0060, Task 1G162203D14413, with the Eustis Directorate U.S. Army Air Mobility Research and Development Laboratory. The primary objective of the three-phase, 32-month program was to develop and validate design techniques for advanced, small, high-temperature combustors for gas turbine engines in the 2- to 5-pound-per-second class.

This report is presented in two volumes. Volume I describes the derivation of the analytical models (Phase I) and combustor element rig tests (Phase II) that were conducted to provide data to validate the models. Volume II describes the design and test (Phase III) of a full-scale combustor that was derived from the results of Phases I and II.

The Program Manager was Mr. K. M. Johansen. Principal contributing engineers to Phase III were Dr. M. P. Wood (Principal Investigator), Dr. H. C. Mongia, and Ms. S. L. Trexler (Documentation Engineer). Other contributors to the program were Messrs. C. G MacKay, S. C. Hunter, E. L. Kumm, and J. A. Pyne, and Dr. D. E. Metzger of Arizona State University who was the major consultant on liner film cooling studies. The program was monitored by Messrs. L. Bell, Jr., R. Dodd and C. Roehrig from the Eustis Directorate, U.S. Army Air Mobility Research and Development Laboratory.

TABLE OF CONTENTS

	Page
ABSTRACT	iii
FOREWORD	v
LIST OF ILLUSTRATIONS	ix
LIST OF TABLES	xiii
LIST OF SYMBOLS	xiv
1.0 INTRODUCTION	1
1.1 General Information	1
1.2 Objectives	1
1.3 Summary	3
2.0 COMBUSTOR DESIGN	5
2.1 Combustor Element Selection	6
2.1.1 Fuel-Injection Element	6
2.1.2 Dilution-Zone Element	8
2.1.3 Liner Cooling Element	8
2.1.4 Material Selection	10
2.2 Combustor Design Considerations	10
2.2.1 Liner Cooling	11
2.2.2 Combustor Chamber Envelope	14
2.2.3 Combustor Liner Geometrical Relationships	14
2.2.4 Combustor Volume	14
2.3 Combustor Preliminary Design	17
2.3.1 Film Cooling Design	19
2.3.2 Fuel Injector Design	24
2.3.3 Primary-Zone Design	34
2.3.4 Dilution-Zone Design	34
2.4 Engine Conceptual Layout	35

Page

3.0 RIG TEST PROGRAM 37

3.1 Fuel Nozzle/Swirler Spray Testing . . . 37
3.2 Discharge Coefficient Testing 42
3.3 Atmospheric Rig Tests 45

3.3.1 Pressure Drop Measurement 45
3.3.2 Cold-Flow Mapping 45
3.3.3 Combustion Tests 56
3.3.4 Rich Limit Blowout Tests 57

3.4 Pressure Rig Tests 57

3.4.1 Performance Survey 65
3.4.2 Wall Temperature Measurement . . . 71
3.4.3 Performance Mapping Tests 71
3.4.4 Emission Tests 86
3.4.5 Structural Durability Test . . . 94

4.0 CONCLUSIONS AND RECOMMENDATIONS 97

4.1 Conclusions 97
4.2 Recommendations 98

LITERATURE CITED 99

APPENDIX. COMBUSTOR DESIGN AND PERFORMANCE DATA SUMMARY. 100

DISTRIBUTION 102

LIST OF ILLUSTRATIONS

		Page
1	Fuel Injector Element	9
2	Experience Curve for AiResearch Reverse-Flow Combustors, Comparing Average Coolant Flow Rates for Various Combustor Inlet Pressure Levels	12
3	Comparison of Total Airflow Required for Cooling Area at Design Point . . .	13
4	Combustor Liner Inner and Outer Radii vs Combustor Surface Area for Combustor Height of 1.25 Inches	15
5	Combustor Volume vs Liner Surface Area for Different Combustor Heights	16
6	Aerodynamic Loading Number vs Gas Generator Speed (45,000 Feet and Mach 0.85).	18
7	Combustor Schematic.	20
8	Combustor (AiResearch Part Number PAP211408-2). .	21
9	Calculated Liner Temperature as a Function of Panel Length for Two Assumed Mainstream Gas Velocities	23
10	Influence of Mainstream Turbulence Level on Film Effectiveness	25
11	Schematic of the Air-Shear Injector	27
12	SMD Correlation, Experimental Data From Fraser, et al[4] (1963)	29
13	Dependence of Liquid Film Thickness in Two-Phase Annular Flow on Function F' [Figure 9 from Levy[5]]	31
14	Predicted SMD From Air-Shear Atomizer	33
15	Conceptual Turboshaft Engine Layout	36

		Page
16	Combustor Fuel-Air Ratio as a Function of Maximum Rated Power	38
17	Pneumatic Impact/Swirler Test Rig	39
18	Modified Nozzle Designs for Fuel Nozzle/Swirler Assembly	40
19	Fuel Injection System	41
20	Fuel Manifold Pressure vs Fuel Flow Characteristics	43
21	Combustor Rig Instrumentation Schematic	46
22	Combustor Isothermal Pressure Drop	47
23	Combustor Cold-Flow Mapping Ports (After Weld Repair)	49
24	Axial Velocity Profile in Line With Swirler	50
25	Tangential Velocity Profiles in Line With Swirler	51
26	Combustor Velocity Profiles Comparing Experimental Data and Predictions From Gosman-Spalding Program	52
27	Combustor Axial Velocity Profiles Comparing Experimental Data and Predictions From Gosman-Spalding Program	53
28	Combustor Axial Velocity Profiles Comparing Experimental Data and Predictions From Gosman-Spalding Program	54
29	Comparison of Experimental and Analytical Models	55
30	Combustor Rig Schematic	59
31	Test Rig Instrumentation Layout	61
32	Combustor Exit Plane Instrumentation (Front Three-Quarter View)	62

		Page
33	Exhaust Gas Analyzer Flow System	63
34	Combustor Pressure Drop vs Corrected Inlet Airflow in Pressure Rig	66
35	Combustor Wall Thermocouples	67
36	Combustor Exit Circumferential Temperature Distribution (P_3 = 16.0 ATM) . . .	69
37	Radial Temperature Profile for Test 5(5) . . .	70
38	Temperature Traverse of USSAAMRDL Combustor (P_3 = 14.7 psi, W_{a3} = 0.239 lb/sec, T_3 = 717°R, f/a = 0.0287)	74
39	Temperature Traverse of USAAMRDL Combustor (P_3 = 235.5 psi, W_{a3} = 2.733 lb, sec, T_3 = 1205°R, f/a = 0.0095)	75
40	Correlation of Combustor Efficiency With Aerodynamic Loading for a Limited Range . . .	77
41	Combustor Efficiency of Designed Combustor	79
42	Combustor Efficiency Correlation With Lefebvre's Parameter	81
43	Effect of Combustor Inlet Temperature on Pattern Factor	82
44	Light-Off Fuel-Air Ratio of Combustor With Different Fuels	84
45	Light-Off Fuel-Air Ratio vs Altitude (Based on Data Correlation From Figure 44)	85
46	Lean Blowout Fuel-Air Ratio of Combustor With Different Fuels	87
47	Effect of T_3 on Carbon Monoxide and Hydrocarbon Emissions of Combustor With P_3, W_{a3}, and f/a as Parameters	89

48 Variation of Nitrogen Oxide Emissions of Combustor With P_3, W_{a3}, and f/a as Parameters 90

49 Exhaust Emissions of Combustor at Different Sea-Level Power Settings 91

50 Comparison of Combustor NO_x Emissions With State of the Art 93

51 Combustor Dome Buckling and Crack Failure 96

LIST OF TABLES

		Page
I	Fuel-Injector Comparison	7
II	Combustor Liner Effective Open Area (Swirler and Nozzle Not Included)	44
III	Pressure Rig Performance Data	68
IV	Inlet Conditions for Performance Mapping Test	72
V	Testing Results Summary	73
VI	Exhaust Emissions of USAAMRDL Combustor	88

LIST OF SYMBOLS

C_D	Discharge coefficient
C_m	Turbulence intensity
D	Cylinder diameter
F_1	Function of $\frac{(2\delta)}{D}$
K_1, K_2	Constants
LBO	Lean blowout
LO	Light off
M	Mach number
MRP	Maximum rated power
N_{GG}	Gas generator speed, pct
$N/\sqrt{\theta}_2$	Corrected engine speed, pct
PF	Pattern factor
P_T	Total pressure
P/P	Cycle pressure ratio
P_s	Static pressure
Q	Combustor loading parameter
Rn_A	Superficial air Reynolds number
Rn	Reynolds number
$R(AF/P_A)$	$(Pg/P_A)^{1/3}$
S.L.	Sea level
SMD	Sauter mean diameter, μ
T	Temperature, °F, °R

T_3	Combustor inlet temperature, °F, °R
T_4	Turbine inlet temperature, °F, °R
UHC	Unburned hydrocarbons
V_M	Mainstream gas velocity, ft/sec
V_{REF}	Mass mean velocity at combustor inlet conditions
V	Combustor volume, ft^3, or velocity, ft/sec
Ve^2	Mean square of relative fuel-air velocities on both sides of the fuel sheet, ft^2/sec^2
W_a	Airflow
W_f	Fuel flow, lb/hr
$\bar{W}$	Ratio of coolant mass velocity to the mainstream mass velocity
$\left(\frac{W_a\sqrt{\theta}}{\delta}\right)_3$	Corrected gas generator airflow, lb/sec
s	Slot height or fuel sheet thickness
β	Efflux angle
$\Delta P/P_3$	Combustor total pressure drop
δ	Thickness of film, cm
P_3	Combustor inlet pressure, atm
ε	Recuperative efficiency, pct
η_B	Combustor efficiency, pct
η_{film}	Film effectiveness
θ_3	$T_3/520$

ρ	Axial length of downstream cooling flux
ν	Fuel viscosity, centistokes
ρ_f	Density of fuel, gm/cm^3
ρ_g	Air density, lb_m/ft^3
σ	Surface tension of fuel, dynes/cm

1.0 INTRODUCTION

1.1 GENERAL INFORMATION

Small high-pressure-ratio high-turbine-inlet-temperature turboshaft engines impose conflicting requirements on the various elements of the combustor.

A large number of insertion points are desirable in order to provide a uniform temperature pattern over a large range of fuel flows. However, nozzle fuel passages should be large in order to tolerate contaminated fuels.

Small engine configurations dictate combustors with relatively high liner surface-to-airflow ratios requiring higher airflow percentages for cooling. Conversely, the liner cooling-air temperature increases with higher pressure ratio and less is available at higher turbine inlet temperatures, due to increased airflow required for combustion and turbine cooling.

AiResearch design procedures for small combustion systems are based largely on empirical correlations and experience derived from numerous APU and propulsion engine combustor development programs. One-dimensional simplified analytical models are included in the current design procedures but are of limited use. Two-dimensional and three-dimensional models are desirable; but due to computer time limitations and limited knowledge of the transport phenomenon in typical combustor flow fields, they have been extremely difficult to apply. The work in this program represents a concerted effort to advance the analytical capabilities available to the combustor designer to deal with these complex problems.

1.2 OBJECTIVES

This report describes the design and performance testing of a full-scale combustion system. The design of this system was based on data obtained during an analytical and experimental study of advanced, small, high-temperature-rise combustors.

The objectives of the three-phase, 32-month program were:

(a) To develop and validate an analytical design technique for small, high-temperature-rise, low-airflow combustors and related components

(b) To define the limitations associated with these small combustors and related components and the effect of these limitations on the cycle and configuration of advanced-technology engines

The approach that was employed included analysis and test of combustor elements, followed by the design and test of a complete combustor system. Volume I of this report describes the development of the analytical models and the combustor element rig tests that were conducted to obtain data for updating and validating the design technique. This volume describes the design and test of the full-scale combustion system.

The analysis was addressed to combustors and engines having the following characteristics:

(a) Airflow (W_a) = 2 to 5 pounds per second

(b) Cycle pressure ratio (P/P) = 10.0 to 16.0

(c) Turbine inlet temperature (T_4) = 2300°F to 2700°F

(d) Centrifugal last-stage compressor

(e) Axial or radial turbine

(f) Reverse-flow annular, straight-through annular, and single- or multiple-can combustors

(g) Simple or recuperative cycles (recuperative effectiveness $\varepsilon \approx 65$ percent)

Performance goals of combustors derived by the design techniques established by this study include:

(a) Combustor efficiency (η_B) = 99 percent

(b) Maximum total pressure loss ($\Delta P/P_3$) = 3 percent (excluding recuperator)

(c) Maximum combustor exit pattern factor, PF = 0.20

$$PF = \frac{T_{4\ max} - T_{4\ avg}}{T_{4\ avg} - T_3}$$

where T_3 and T_4 are the combustor inlet and discharge temperature respectively

(d) Stability over a wide range of fuel-air ratios, f/a

(e) Light-off/relight capability up to 25,000 feet altitude, M = 0 (the requirement for relight at an altitude of 45,000 feet, M = 0.85, was also examined)

(f) Multifuel capability including MIL-T-5424, Grades JP-4 and JP-5, MIL-T-83133, Grade JP-8, and Aviation Turbine Fuel, Type A-1

(g) Contamination tolerance in accordance with MIL-E-5007C

(h) Minimal formation of nitric oxide, carbon monoxide, and unburned hydrocarbons consistent with the system performance goals delineated above

(i) Smoke level below the visible limit

The performance goals are applicable to the air path between the compressor discharge and turbine stator inlet.

1.3 SUMMARY

Engine cycle studies (design and off-design) and preliminary combustor sizing (based on current techniques) were conducted to determine the approximate envelope, inlet-air conditions, and implications of the prescribed cycle and combustor performance goals. Computer programs were prepared for design assessment of the major combustor elements. Elements that were analyzed include:

- Fuel distribution and insertion devices, including L-pipe vaporizers, pneumatic-impact atomizers, and air-assist atomizers
- Primary combustion zone
- Mixing (or dilution) zone
- Liner structural design, including stresses, cooling, and radiant heat transfer

A series of combustor element tests was conducted to provide the data to update and verify the analytical models. Results of this contracted program provide for improved capability, with the following having been accomplished:

- Fuel atomization, evaporation, and distribution within the primary zone have been analyzed and refined.

- Primary zone recirculating flow analysis, heretofore totally intractable, has been demonstrated to be feasible within the limitations of other types of complex turbulent flows.

- Procedures for sizing and location of dilution holes and resultant mixing have been refined.

- Information on cooling performance of devices particularly applicable to small combustors has been considerably expanded.

- A new material, IN-586, has been evaluated and found to offer significant advantages as a combustor material.

The first volume describes the analytical model development and the combustor element rig tests. A full-scale combustion system was designed with the aid of the updated models. The design and rig tests of this system are presented in this volume. A tabular summary of the combustor design and performance characteristics is provided in the Appendix.

It should be noted that the objectives of the program were not to develop a combustor but to develop analytical design techniques and to demonstrate that combustion systems development can be significantly reduced by the use of these procedures. Therefore, the resulting Phase III combustor is not suitable for an engine application at this time. Since the data gathered and presented here is from initial design configuration, the relatively high level of performance obtained clearly demonstrates that the analytical modeling, though not fully developed, is a valid method of reducing combustor development time and cost.

2.0 COMBUSTOR DESIGN

This section presents the rationale that lead to the selection and design of the Phase III combustor elements. The information gathered during Phases I and II design, test and evaluation (Volume I of this report) was scrutinized to determine those elements best suited for the Phase III full-scale combustor. The following paragraphs discuss the selection of combustor elements and the combustion system preliminary design results.

The sea level, static design conditions for the combustor are summarized below:

Airflow, W_a	= 2.733 lb/sec
Corrected airflow, $\frac{W\sqrt{\theta}}{\delta}$	= 0.268 lb/sec
Combustor inlet total pressure, P_3	= 235.7 psi
Combustor total pressure drop, $\Delta P/P_3$	= 0.03
Combustor inlet temperature, T_3	= 1280°R
Combustor discharge temperature, T_4	= 2980°R
Fuel flow, W_f	= 280.9 lb/hr
Fuel-air ratio, f/a	= 0.0285

The objectives of the design effort were to provide a combustion system that would be suitable for an engine installation and to achieve the following performance goals:

Combustor efficiency, η_B	= 99 pct
Combustor total pressure loss, $\Delta P/P_3$	= $\leq$ 3.0 pct
Combustor exit pattern factor, PF	= 0.20
Combustor life	= 5000 hr

Altitude relight	= to 25,000 ft at M = 0
Multifuel capability	= including MIL-T-564, Grades JP-4 and JP-5, and MIL-T-83133, Grade JP-8
Fuel system contamination tolerance:	= in accordance with MIL-E-5007C
Minimal exhaust emissions formation UHC, CO, NO_x and smoke,	= Consistent with other performance goals

2.1 COMBUSTOR ELEMENT SELECTION

The elements selected for the Phase III combustor were:

- Straight-through annular configuration
- Fuel injection element - Pneumatic impact atomizer with radial swirler (air-shear system)
- Dilution zone element - opposed plunged or thick-wall opposed orifices
- Liner cooling element - impingement film with wiggle strips
- Material - IN-586

2.1.1 Fuel-Injection Element

Major considerations in the choice of the fuel injector are listed in Table I. This table shows some of the advantages and disadvantages of the three fuel systems considered.

Phase II experimental data demonstrated the necessity for matching the fuel-injection system with the primary air delivery, and resulted in the consideration of the following configurations:

- L-pipe injector with axial swirler
- Air-assist atomizer with radial swirler
- Pneumatic impact atomizer with radial swirler

The performance of each of these configurations has been discussed in Volume I, Section 4.0 and will not be repeated here. However, a brief summary of the logic used in final selection is presented.

The L-pipe configuration was eliminated from further consideration primarily due to fuel-distribution and potential durability problems. Fuel-backup problems were shown to exist at low differential air pressures (approximately 1 percent $\Delta P/P$) across the combustor and resulted in fuel puddling in the plenum (outer annulus) and attendant poor ignition and combustion characteristics.

TABLE I. FUEL-INJECTOR COMPARISON

	L-Pipe	Pneumatic Air Assist	Impact
Advantages	o Low cost o Low lean flammability limits o Low fuel pressure required	o Good atomization and distribution o Good ignition	o Moderate cost o Low fuel pressure required
Potential Problem Areas	o Possible fuel "backup" with low-pressure-drop combustors o L-pipe life o High ignition limits	o High-pressure air supply required o Small flow passages subject to contamination o Potential wall impingement (high metal temperatures) o High cost	o Moderate spray characteristics o Potential wall impingement (high metal temperatures)

The desired combustor life of 5000 hours also poses a possible durability problem to this injection configuration, where the sheet-metal L-pipe is suspended in the primary-zone reaction region and therefore is subjected to extremely severe temperatures and thermal stresses over the operating range.

The air-assist atomizer configuration was also eliminated because of the potential problems of contamination blockage due to small flow passages, high initial cost, and the requirement of an external air source during the engine start-cycle. It appeared that the fuel impingement on the wall experienced during Phase II tests and the resulting high metal temperatures could be prevented by reducing the core angle to almost axial injection, but at a cost that would partially compromise the advantages of the air-assist system.

The pneumatic-impact injector was chosen for the Phase III design. It appeared that the addition of the appropriate radial swirl configuration as shown in Figure 1 would sufficiently improve the degree of atomization and significantly reduce the fuel impingement on the liner walls. In the selected configuration, the pneumatic-impact atomizer discharges fuel onto the surface of a cylinder, where a film is formed. This film leaves the cylinder lip in the form of a fuel sheet with an axial component to keep it from the liner walls. Atomization takes place immediately following discharge from the lip due to the shearing action of the airflows on each side of the sheet. In this respect the pneumatic-impact atomizer-swirler combination performs in the same manner as an air-shear atomizer.

2.1.2 Dilution-Zone Element

The dilution-zone air is injected by means of opposed plunged or thick-wall opposed orifices located at the downstream limit of the primary zone. The opposing jets impinge at the combustor center and reinforce the primary zone recirculation. Thick-wall orifices were used to obtain an efflux angle approaching 90° and to ensure that this angle does not change significantly with varying annulus flow rates.

2.1.3 Liner Cooling Element

Cooling slots are the impingement-film type based on the results obtained in Phase II liner cooling tests (refer to Volume I, Section 7.0). Wiggle strips were incorporated to minimize the possibility of cooling-slot-gap closure from thermal distortion under operating conditions.

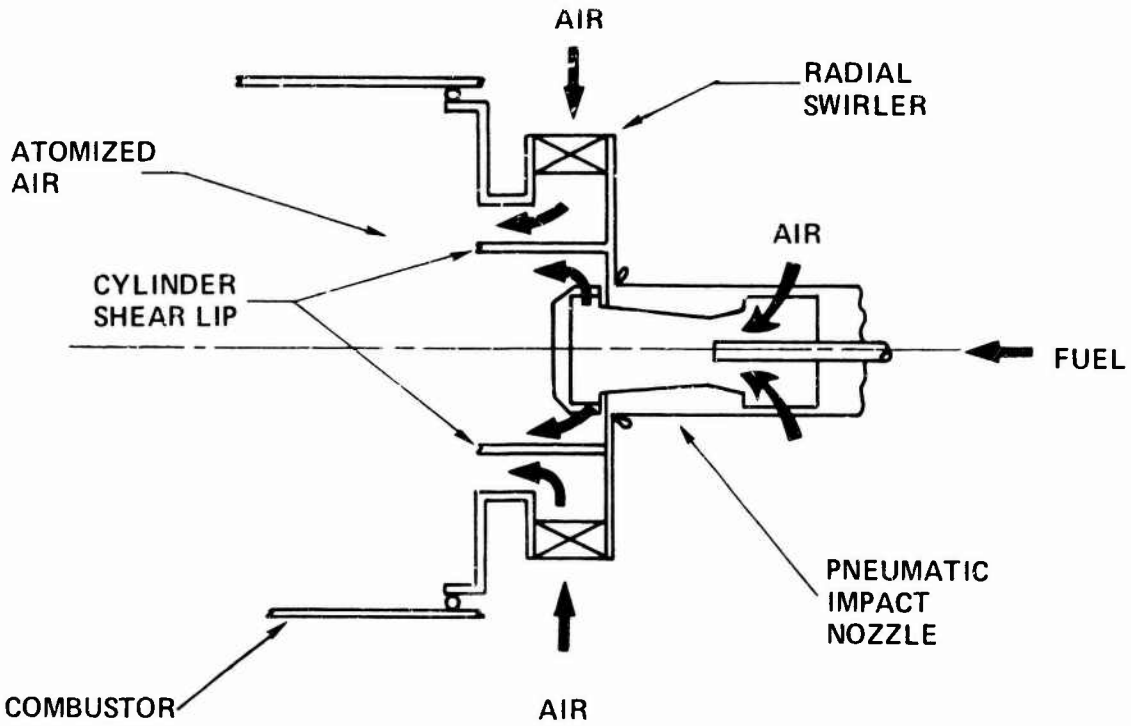

Figure 1. Fuel Injector Element.

2.1.4 Material Selection

The combustor material selection was based on material screening tests conducted during Phase I (refer to Volume I, Section 3.0). The results of these tests indicated that IN-586 is superior to the other materials considered with respect to the requirements desired for combustor application. To date, no known data is available on the use of this material in actual combustor operation; but from the Phase I material screening tests and the Phase II material property evaluation the material appeared to be well suited for this application.

2.2 COMBUSTOR DESIGN CONSIDERATIONS

Reverse-flow annular film-cooled combustion systems configured for a radial turbine were initially considered for the Phase III basic design (since that configuration was shown to provide the most compact engine), but they were subsequently eliminated because of wall cooling limitations. The relatively large pitch diameter and resultant large surface areas were determined to require film cooling airflows that greatly exceeded the total airflow available for the specified cycle. The axial through-flow annular combustor configurations afford smaller surface areas, and the required attendant film cooling flows were considerably reduced. This basic configuration was subsequently selected for detailed evaluation in Phase III.

To achieve the optimum combustion system configuration, a preliminary design effort was conducted. The design approach was semiempirical, supported by analytical models developed during Phase I and based upon AiResearch's overall development experience in the field of small combustors. The initial combustor design was fabricated and tested in the atmospheric rig. The intent was to use this initial test data along with the analytical models to confirm and/or refine the combustion system selected to achieve the performance goals. The initial task in the combustor preliminary design was to determine the airflow that is required by, and can be delivered to, each of the elements. A number of conflicting requirements were considered when determining the air distribution and size of the elements, including:

- Liner surface area and required cooling flow to achieve durability
- Combustor envelope limitations as influenced by adjacent engine components

- Combustor geometry (minimum length, length-to-height ratio, etc.) to provide adequate recirculation patterns and mixing lengths

- Combustor volume as related to efficiency and altitude ignition requirements

- Fuel nozzle spacing and size versus contamination tolerance and discharge gas temperature spread characteristics

- Annular flow split and velocities as related to required combustor pressure losses and overall performance characteristics

2.2.1 Liner Cooling

Wall cooling is generally recognized as a paramount design constraint that is experienced with small, high-pressure, high-temperature-rise combustors. The basic problem is illustrated by the following experimental correlations.

Figure 2 presents average coolant flow rates per surface area used for several current AiResearch combustion systems operating at various inlet pressure levels. From this correlation, a plot (Figure 3) of the percentage of total airflow required (for film cooling) against liner surface area was made for the sea-level static design-point conditions. Included in this figure is a similar curve based on information from Anderson[1]. The difference between the two curves is attributed to the fact that the latter curve is based on data for vaporizing combustors with premixed fuel-air, whereas the AiResearch curve is based on data from atomizing combustors with typically higher luminosity and radiant heat flux levels. The pneumatic-impact fuel injection system produces some premixing and requires a cooling flow rate between the two experience curves. A conservative approach was taken, and the upper curve was used initially for the combustor sizing presented below.

Initially, a range of allowable cooling flows was established for preliminary consideration. Sixty percent of the total combustor airflow was considered to be the feasible upper limit for cooling due to primary zone and dilution zone flow requirements, while minimum rates were limited to 40 percent based upon previous small combustor design experience. This range, in conjunction with the given airflow and Figure 3, provided a preliminary indication of liner surface area that could be film cooled. For example, for 50 percent cooling

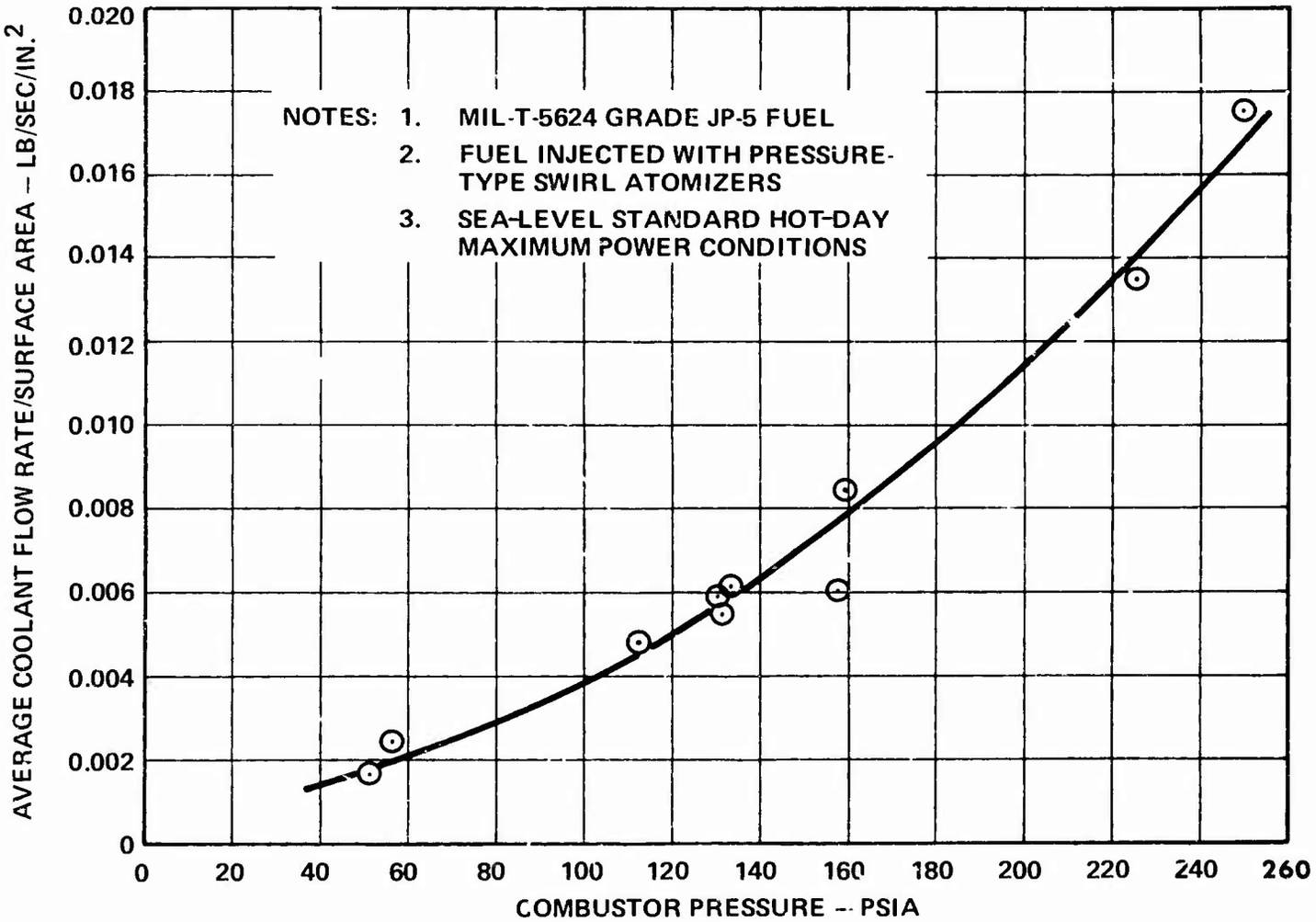

Figure 2. Experience Curve for AiResearch Reverse-Flow Combustors, Comparing Average Coolant Flow Rates for Various Combustor Inlet Pressure Levels.

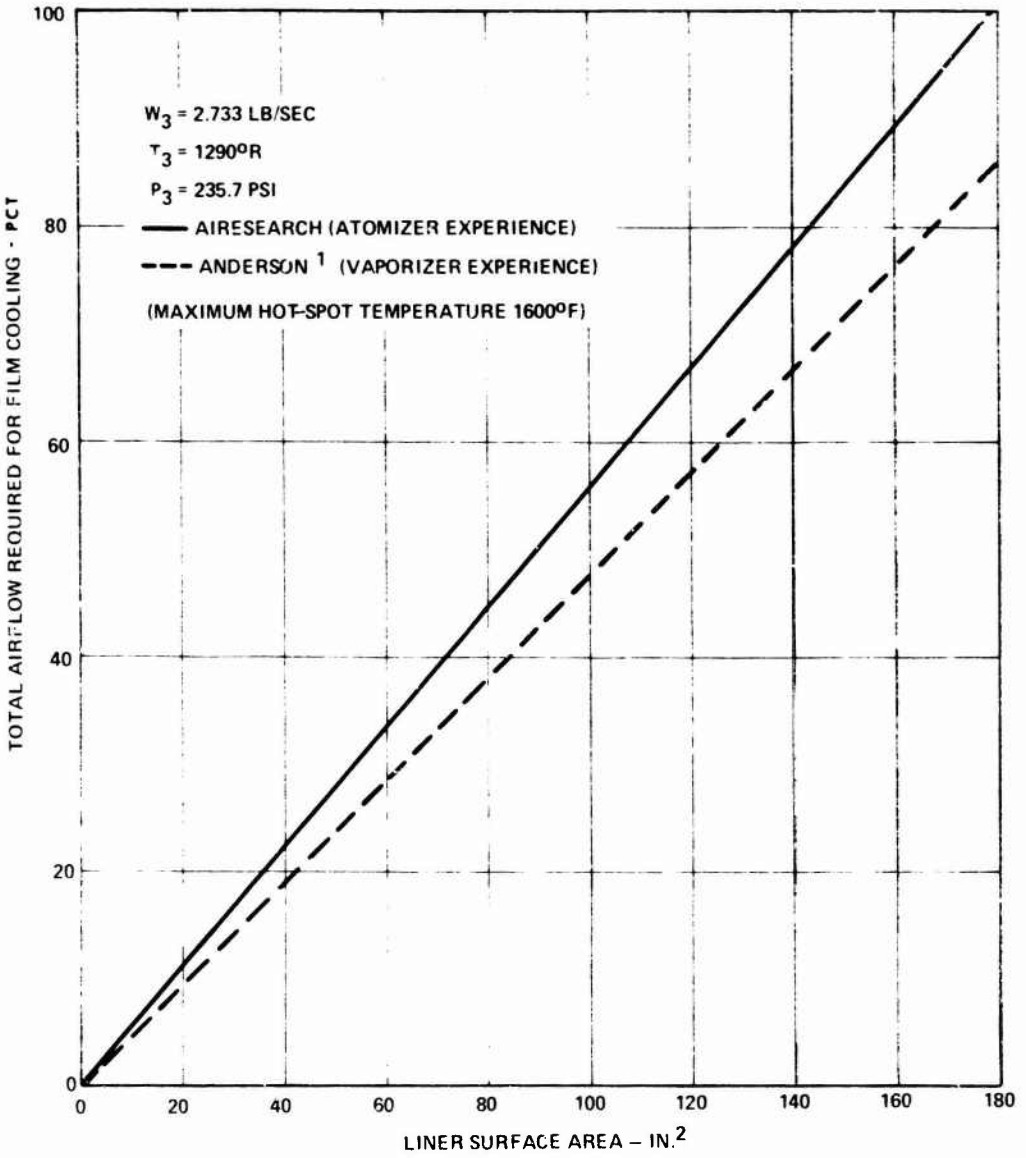

Figure 3. Comparison of Total Airflow Required for Cooling Area at Design Point.

maximum liner surface area would be approximately 90 square inches.

A series of curves was then generated for different combustor heights and lengths (h and L), relating inner and outer liner radii with combustor cylindrical wall surface areas. Typical results are shown in Figure 4 for h = 1.25 inches and L = 2.0h, 2.5h, and 3.0h. Similar curves were also prepared for combustor volume as a function of surface area (Figure 5).

2.2.2 Combustion Chamber Envelope

For a straight-through-flow annular combustor with an axial turbine, the minimum allowable inner wall radius is constrained by the gas generator shafting design. A conceptual engine layout (a turboshaft engine configuration with a front-drive power turbine shaft) was prepared and will be discussed later. A shaft dynamics analysis indicated that a minimum gas generator shaft radius of 0.80 inch would be required. Assuming a minimum clearance for a radiation shield above this shaft of 0.10 inch, material thickness of 0.025 inch, and a flow passage (inner annulus) height of 0.20 inch, the minimum inner liner radius was established to be 1.125 inches.

Since the engine configuration was constrained (by contract) to have a centrifugal compressor, the combustor outer diameter was not limited within the combustor height and height-to-length configurations being considered, except that a compatible transition section from the combustor exit to the turbine was to be maintained.

2.2.3 Combustor Liner Geometrical Relationships

Overall length of a straight-through annular configuration can significantly affect the engine shaft dynamic characteristics and directly influence combustor performance with regard to dilution mixing and pattern factor. Experience, as well as analysis, indicates (refer to Volume 1, Section 6.0) that a combustor length-to-height ratio of less than 2.0 is generally not sufficient and that typical values should be between 2.5 and 3.0 for satisfactory performance within the specified $\Delta P/P$ constraint of 3.0 percent.

2.2.4 Combustor Volume

Semiempirical correlations for combustor volume requirements were discussed in Volume I, Section 2.0. For ignition at 25,000 feet, M = 0, the minimum volume requirement was

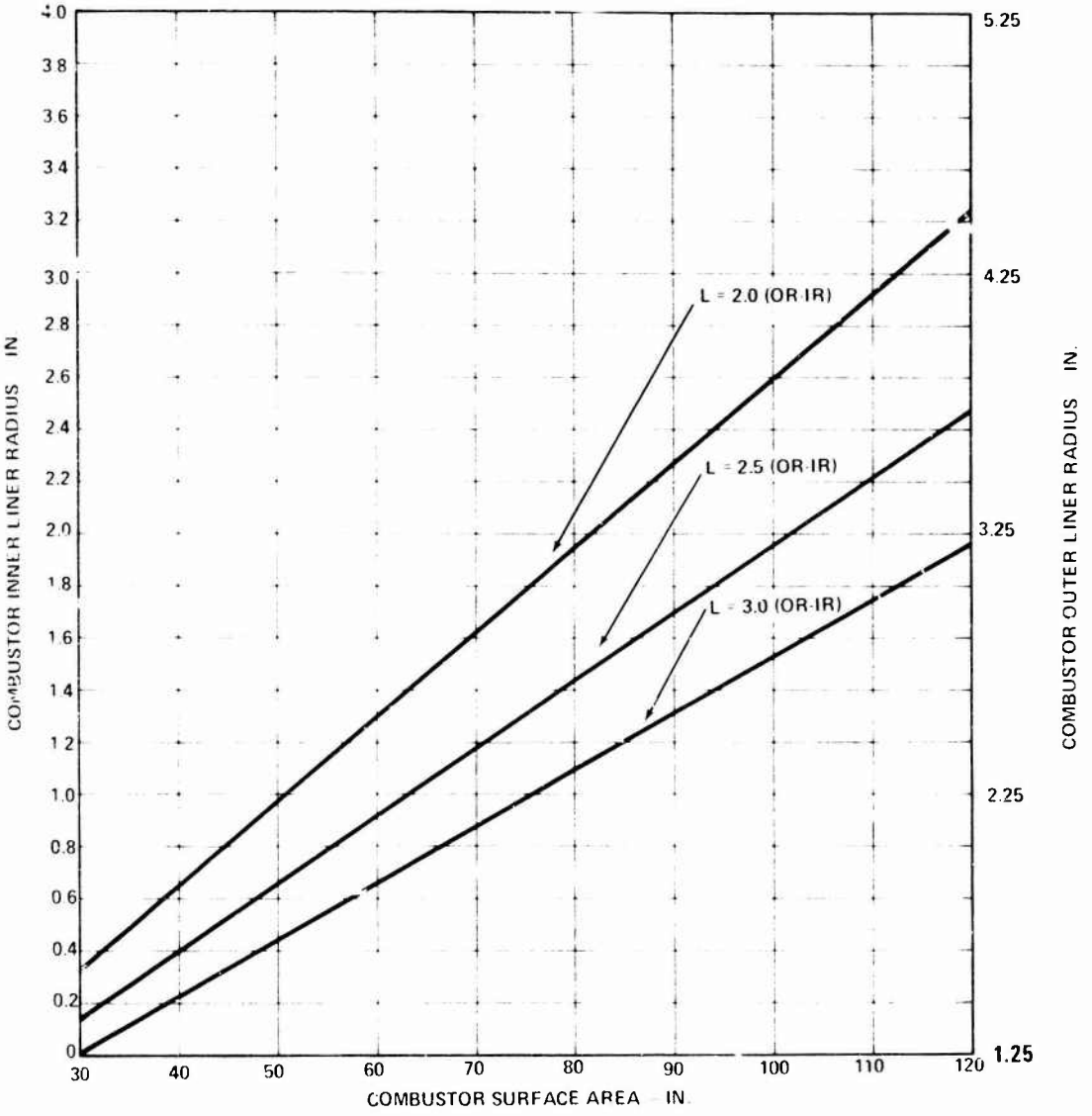

Figure 4. Combustor Liner Inner and Outer Radii vs Combustor Surface Area for Combustor Height of 1.25 Inches.

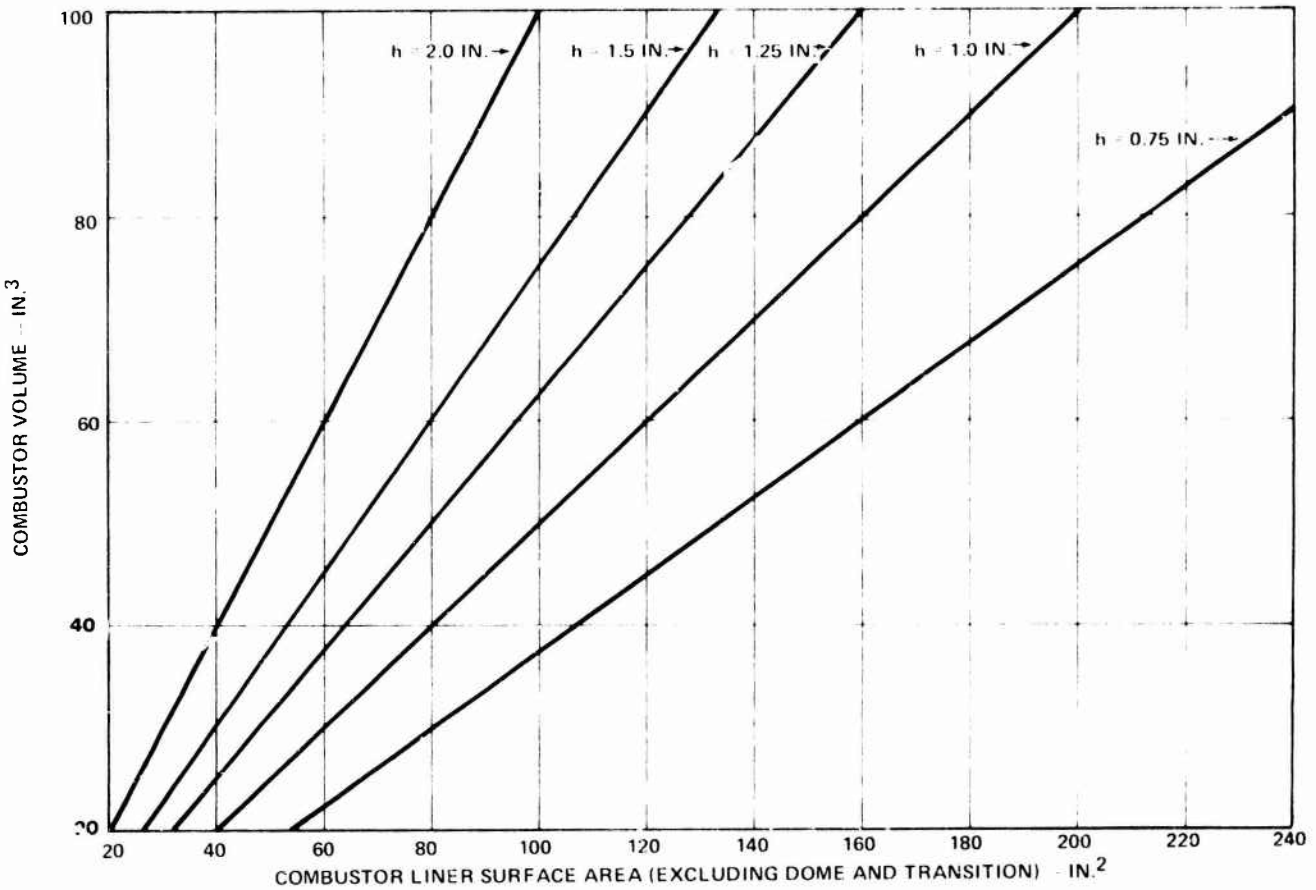

Figure 5. Combustor Volume vs Liner Surface Area for Different Combustor Heights.

determined to be 42 cubic inches at the peak loading conditions; at 45,000 feet, M = 0.85, the minimum volume requirement was 94 cubic inches. These volume requirements were based on a minimum combustion efficiency of 80 percent during acceleration as governed by the combustor loading parameter. Only the 60 percent cooling flow provision could provide the required volume for the latter condition, and even then, the inner liner radii which could be considered were below the required 1.125-inch minimum. Therefore, these limitations precluded sizing the combustor volume for peak loading at 45,000 feet, M = 0.85.

Several alternative approaches could be considered to provide for ignition at this 45,000-foot flight condition. Required cooling flow may be reduced by selecting a more exotic material (i.e., refractory metals or ceramics) or alternative cooling methods such that the allowable surface area can be increased. Another approach would be to maximize the combustor volume within the limitations imposed by the coolable surface area and increase the engine ignition speed to the level where acceptable combustor loading is achieved at the more stringent altitude ignition condition. As shown in Figure 6, 45,000 feet, M = 0.85 ignition could be achieved with a combustor sized for 25,000 feet, M = 0 by cranking the engine to $N/\sqrt{\theta}$ = 47 percent and thereby bypassing the high loading conditions where insufficient combustion efficiency occurs.

2.3 COMBUSTOR PRELIMINARY DESIGN

Based on the general geometric constraints discussed above and the dominating liner cooling requirements, the following overall combustor dimensions were selected:

Combustor length-to-height ratio	= 2.5
Combustor height (inches)	= 1.25
Combustor length (inches)	= 3.13
Inner wall radius (inches)	= 1.7
Combustor volume* (cubic inches)	= 56.5
Liner surface area* (square inches)	= 91.0
Cooling air (percent)	= 50
Heat release rate (Btu/hr-ft^3-atm)	= 9.96×10^6

The analytical models developed in Phase I and Phase II of the contract were used to refine the initial design of the combustor. For example, the annulus-pressure-loss model was used to assess airflow distribution. The liner-cooling model was used to substantiate empirically the cooling air requirements, which were later found to be conservative because of a even lower radiant heat loading than combustors using

*Excluding transition section.

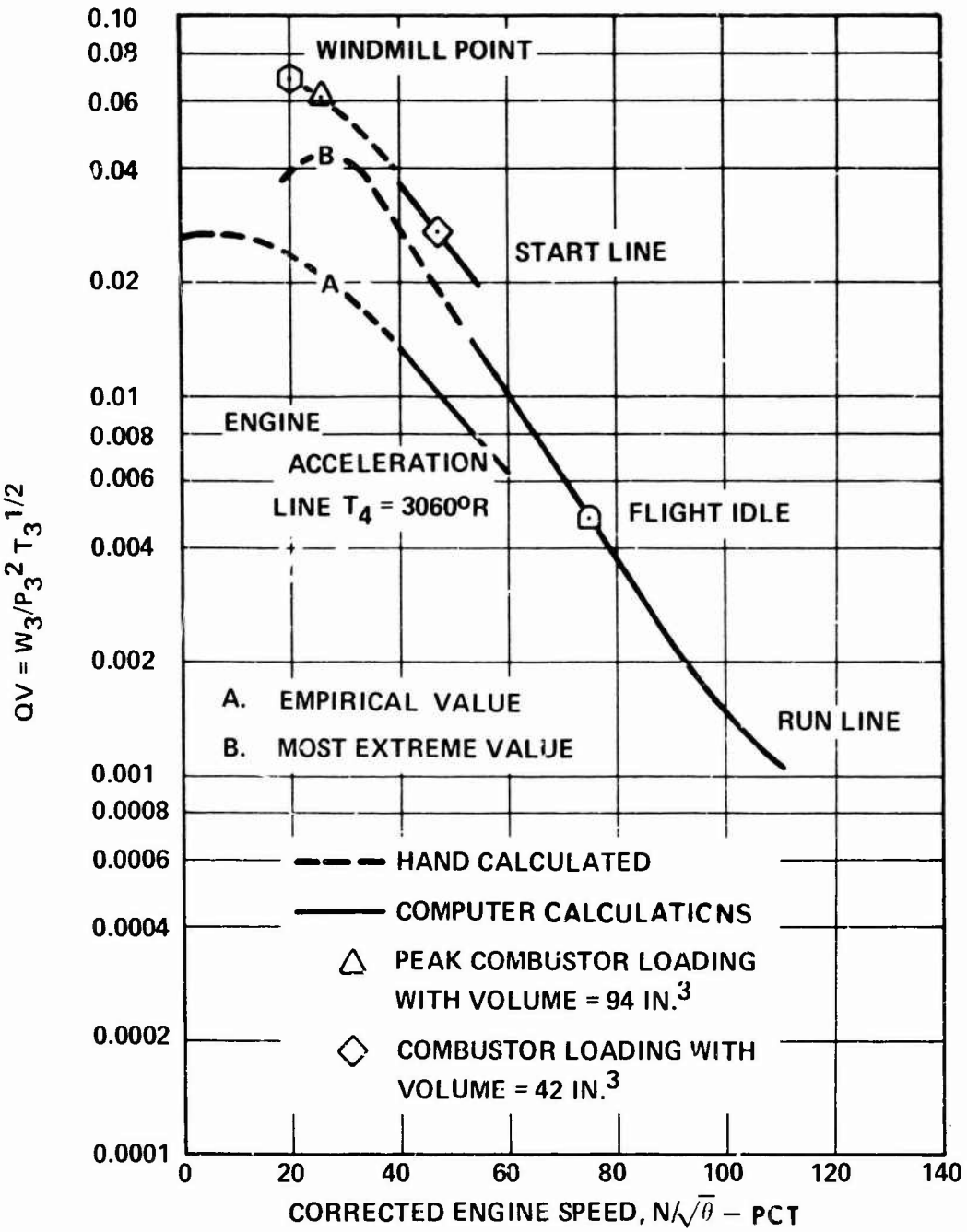

Figure 6. Aerodynamic Loading Number vs Gas Generator Speed (45,000 Feet and Mach 0.85).

vaporizers. The jet-trajectory analysis and air recirculation model were used to aid in sizing primary-zone orifices and amount of dilution air.

Two of the models were modified prior to application to the Phase III combustor. The fuel-insertion model was expanded to provide a means to predict SMD of the air-shear nozzle. The cooling model was extended to include a consideration of mainstream turbulence on the cooling air requirement.

A cross section of the resultant combustor is shown in Figure 7, and the fabricated combustor is shown in Figure 8. The film-cooled area is minimized, while the resultant volume, length, and height are adequate to provide the performance goals. Leakage control was considered critical; for this reason, both inner and outer liner seals are piston rings with the sealing mechanisms fabricated as an integral part of the combustor liner.

The following paragraphs present the detail design features of the selected configuration.

2.3.1 Film Cooling Design

The selected combustor has outer and inner liner surface areas of 58 square inches and 33 square inches, respectively. From Figure 3, the cooling air requirement is 0.0152 pounds per second per square inch. The air required for cooling a 1-inch length of the outer and inner walls is 0.282 pound per second and 0.161 pound per second respectively. Corresponding total cooling flow rates are 0.883 pound per second and 0.503 pound per second for the outer and inner liners. Because cooling skirt gap control is critical for a design life of 5000 hours, wiggle strips are included in all cooling slots to maintain slot spacing and skirt mechanical integrity. The four cooling slots on each wall are 0.050 inch high to accommodate the 50-percent blockage of the 0.025-inch-thick wiggle strips. The slot-discharge effective open areas on the outer and inner liners are 0.459 and 0.271 square inch respectively.

Based on an experimentally determined maximum cooling film length of 30 slot heights and a film effective height of 0.025 inch, the required distance between cooling slots is 0.75 inch. This necessitated four cooling skirts on both the inner and outer liners. The flow through each cooling slot is 0.221 pound per second on the outer liner and 0.126 pound per second on the inner liner. For the combustor inlet design conditions, the air velocities at the slot were calculated to be 140 feet per second for the outer liner and 136 feet per second for the inner liner.

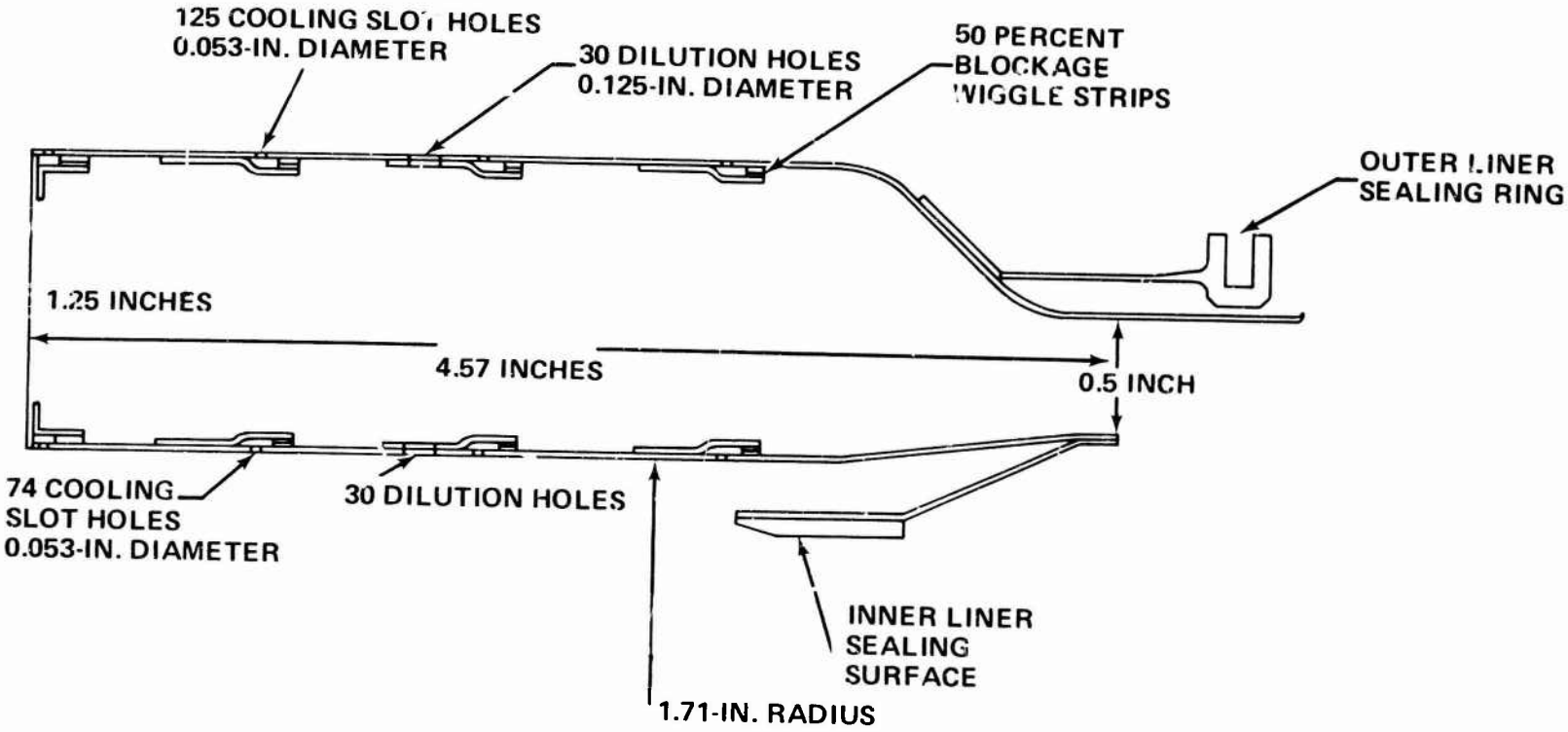

Figure 7. Combustor Schematic.

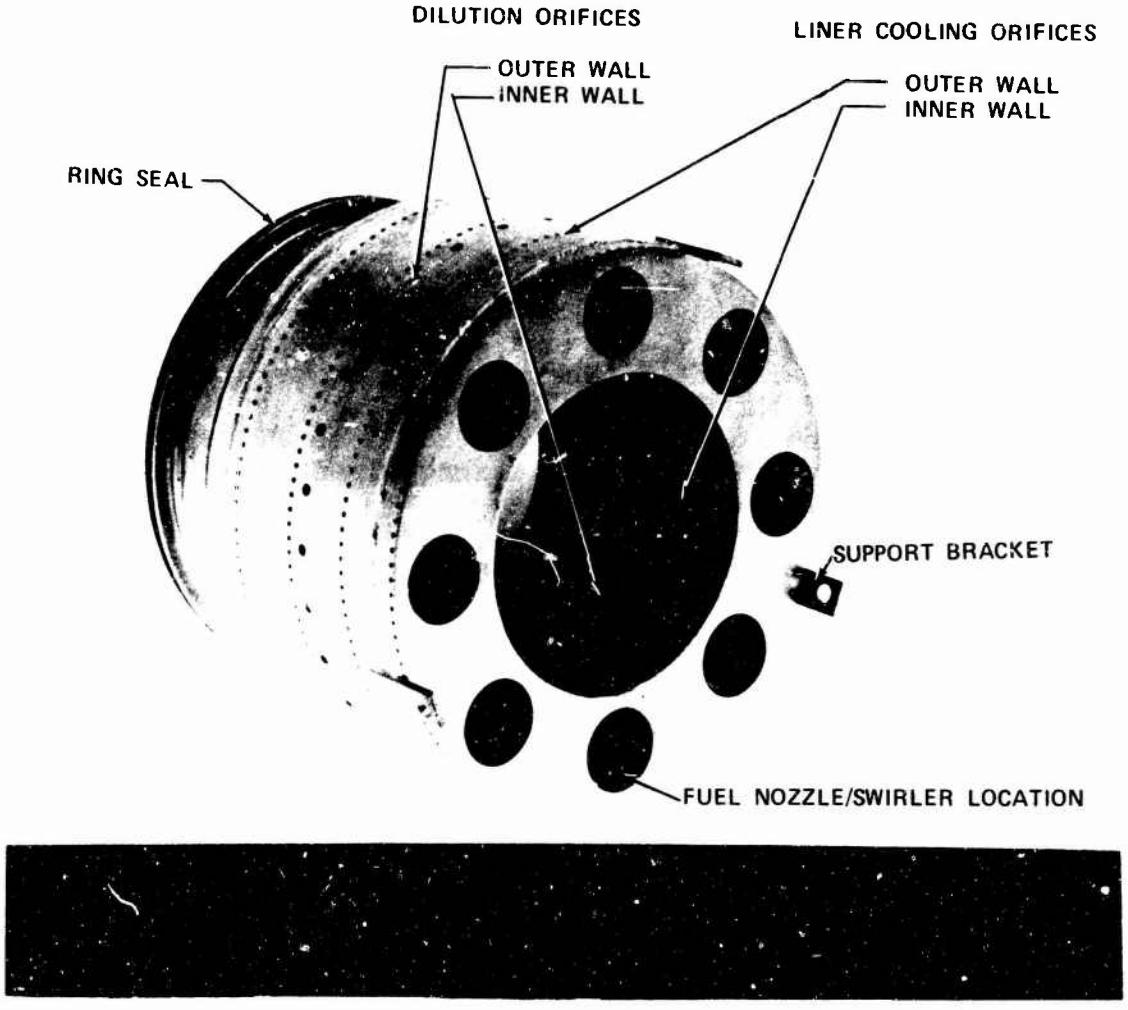

Figure 8. Combustor (AiResearch Part Number PAP211408-2).

Cooling air requirements were also determined by the mathematical model for comparison with those empirically derived values. For the mathematical model, the following assumptions were made:

Mainstream gas temperature = 3300°F (Ideal primary zone combustion temperature = 3870°F)

Cold-side hydraulic diameter = 0.4 inch

Outer feed annulus air velocity = 80 ft/sec

Experimentally determined cooling film velocity decay factor at x/s = 100 is 0.12 (discussed in Section 7.0 of Volume I of this report)

Mainstream gas velocity (V_M) = 60 and 120 ft/sec

Figure 9 presents the calculated liner temperature as a function of panel length and shows relatively small temperature variations over the range of assumed mainstream gas velocities. The calculated liner average temperature at 0.75 inch downstream of the slot is 1400°F for U_M = 60 feet per second. Corresponding hot spots of 1650°F to 1700°F may be encountered, and therefore these average levels should not be exceeded.

It is known that the film effectiveness coefficient is influenced by free-stream turbulence level and hot to cold stream temperature in addition to parameters studied in Phases I and II (refer to Volume I, Section 7.0). The liner-cooling model could not be updated to account for these variables. However, the effect of turbulence level in film effectiveness is briefly discussed.

Film effectiveness data obtained experimentally and successfully correlated by Equation (1) was compared with a semiempirical expression obtained by Juhasz and Market[2]:

$$\eta_{film} = \frac{1}{1 + 0.0069\ (\bar{W})^{-1.35}\ell/s} \qquad (1)$$

where η_{film} = film effectiveness

$\bar{W}$ = ratio of coolant mass velocity to the mainstream mass velocity

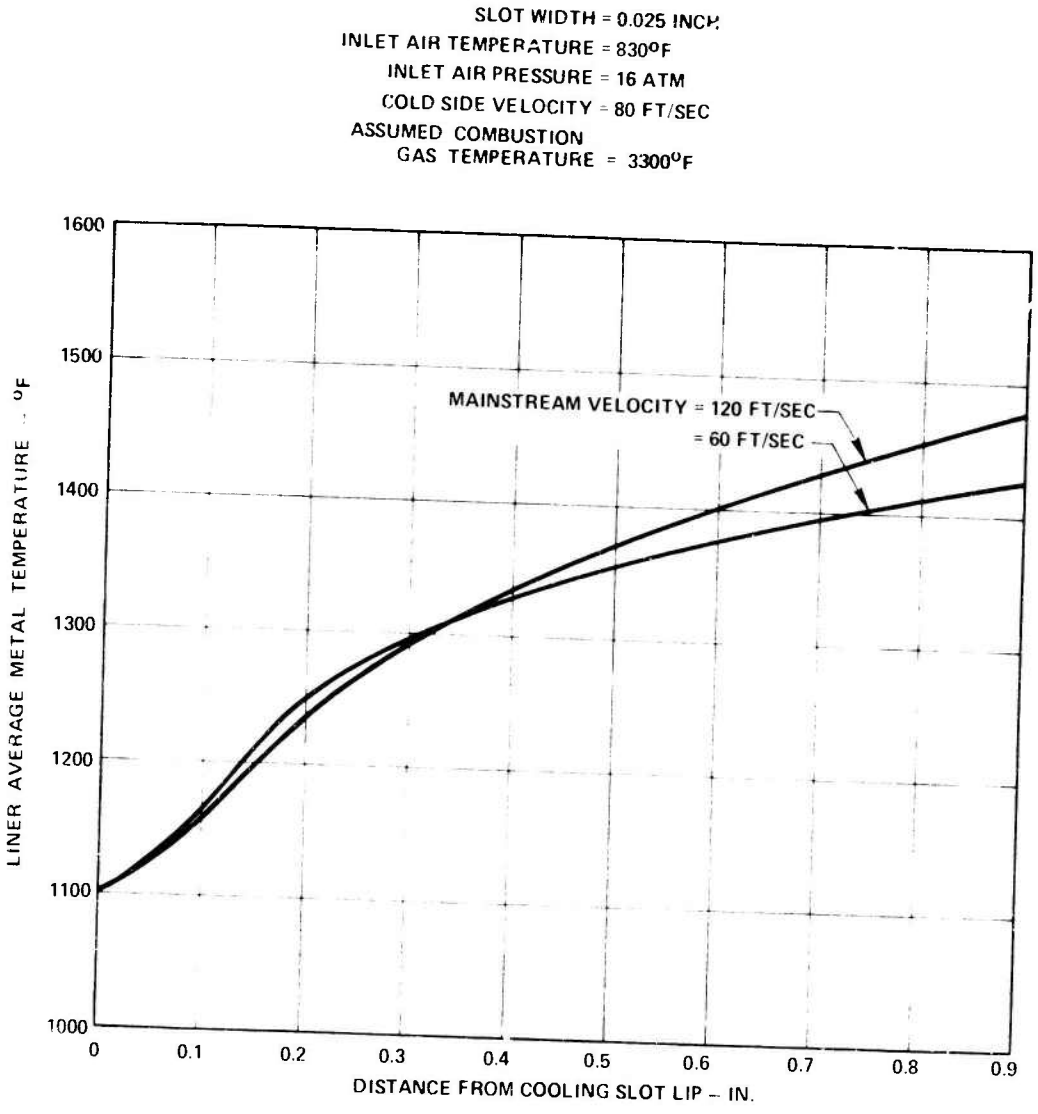

Figure 9. Calculated Liner Temperature as a Function of Panel Length for Two Assumed Mainstream Gas Velocities.

ℓ = axial length downstream of cooling slot

s = film cooling slot height

The expression given by Juhasz includes mainstream turbulence level considerations and is given in Equation (2):

$$\eta_{film} = \frac{1}{C_m} \bar{W} \frac{s}{\ell} \ln \left(1 + \frac{C_m}{\bar{W}} \frac{\ell}{s}\right) \qquad (2)$$

where C_m equals fraction turbulence level

Figure 10 is a plot of η_{film} against $\bar{W}$ using Equation (2) and turbulence levels (C_m) of 0.02, 0.05, and 0.15. This plot shows a significant reduction in film effectiveness with increasing mainstream turbulence.

Typical turbulence levels existing in the test section used to obtain Equation (1) could be expected to be of the order of 2 to 3 percent. A comparison of the curve obtained using Equation (1) with that obtained from Equation (2) for a 2-percent turbulence shows good agreement.

Levels of turbulence in an actual combustor may be as high as 15 percent, which would result in Equation (1) overpredicting film effectiveness. No work was undertaken to measure turbulence levels within a combustor. It should be noted, however, that this variable may have a significant effect on film-cooling requirements.

Because of the good agreement between the empirically and analytically derived panel length (0.75 inch), it was concluded that the selected film-cooling configuration will provide the required liner temperatures.

2.3.2 Fuel Injector Design

The ratio of fuel injector circumferential spacing to combustor dome height is typically on the order of 1.5 to 2.5 to provide required performance levels, particularly with regard to achieving the specified pattern factor and lean stability characteristics. These performance characteristics are more readily achieved as the number of injectors is increased. However, increasing the number of injectors increases combustion system cost; and more significantly, fuel contamination resistance (fuel orifice geometry) becomes an overriding constraint for small annular combustors. Since atomization by the pneumatic-impact injector is not dependent

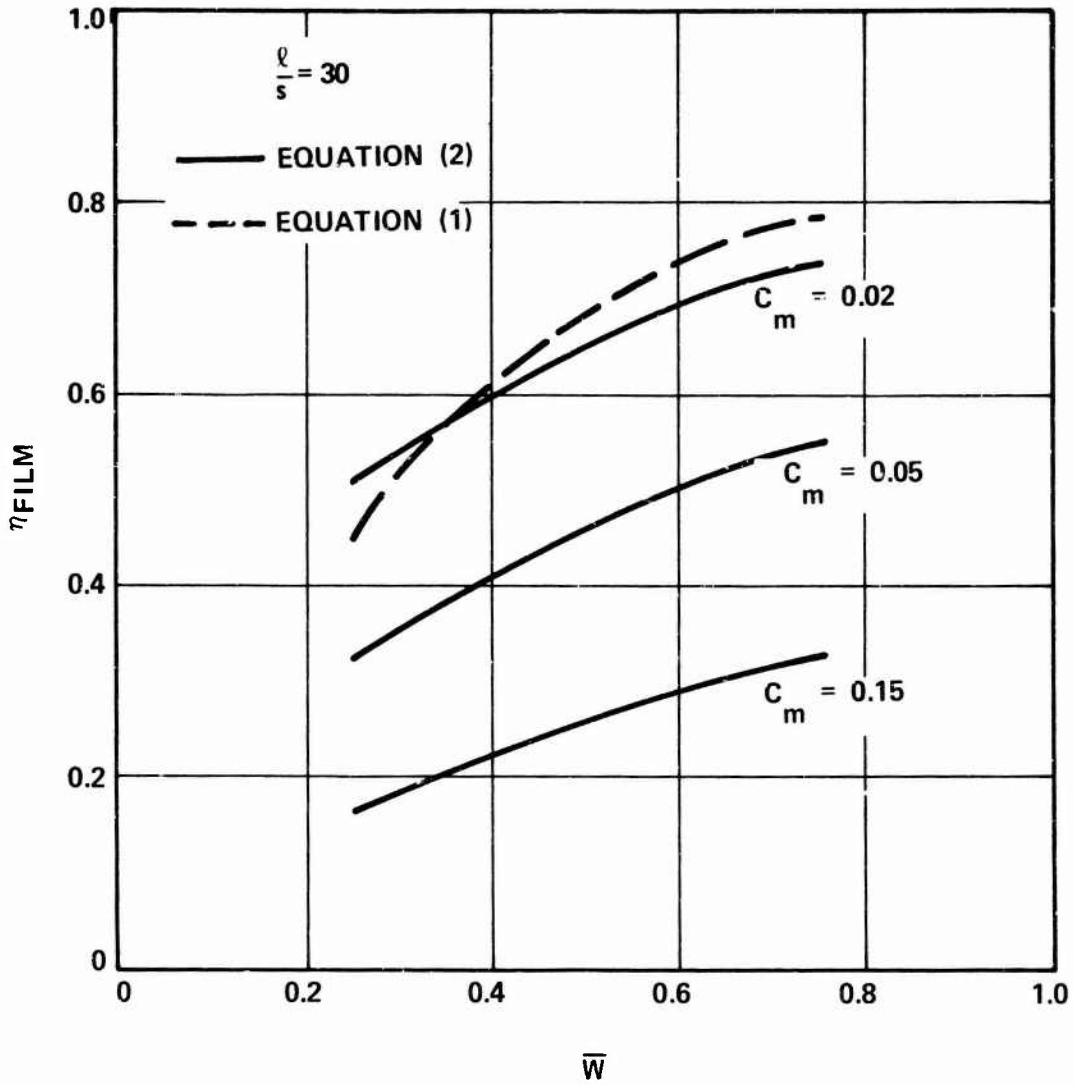

Figure 10. Influence of Mainstream Turbulence Level on Film Effectiveness.

upon fuel pressure, the fuel orifices are relatively large and therefore not limited by fuel contamination. Several fuel nozzle spacings were initially considered and eventually reduced to designs using 6 or 8 injectors, with spacing ratios of 1.94 and 1.46, respectively. The eight-nozzle configuration was selected for the basic design, as the larger number will afford the greater overall performance and not significantly affect fuel contamination tolerance levels. The minimum passage detriment for the fuel injectors was 0.035 inch and occurs in the metering section to achieve balanced circumferential flow rates. The SMD and the fuel jet trajectory were calculated by using fuel-injection models and the Spalding-Gosman program.

A schematic of the air-shear injector system is shown in Figure 11. The fuel-air mixture from the pneumatic-impact type nozzle impinges on the central cylindrical surface, causing some of the fuel to form a film on the cylinder (Zone B) and some to be entrained in the airflow through the cylinder (Zone A). Entrainment is dependent upon the surface structure of the interfacial region, air velocity, temperature, and pressure, and is therefore difficult to calculate. Work by Dukler and Moye[3] indicates that approximately 30 percent of the total fuel flow will be airborne at the exit plane of the inner cylinder. At the central cylinder lip, the balance of the fuel is discharged in the form of a liquid sheet and is subject to shearing action caused by the airflow in regions A and C.

A complete mathematical analysis of the shear injector entails modeling flows in the initial (transition) zone, regions A, B, and C, and correlating Sauter mean diameters of the fuel spray with sheet thickness s, velocities V_1, V_2, V_s, fuel flow W_f, and fuel and air properties. Such an analysis would be a highly complex mathematical problem, and even then exact quantitative correlations between theory and experiment could be obtained only through some kind of empiricism. Therefore, it was decided that the mathematical analysis used would be simplified using information previously available.

The analysis for predicting SMD is based on the following assumptions:

- Uniform annulus film is of thickness s.
- Fuel entrainment by the inflowing air is negligible.

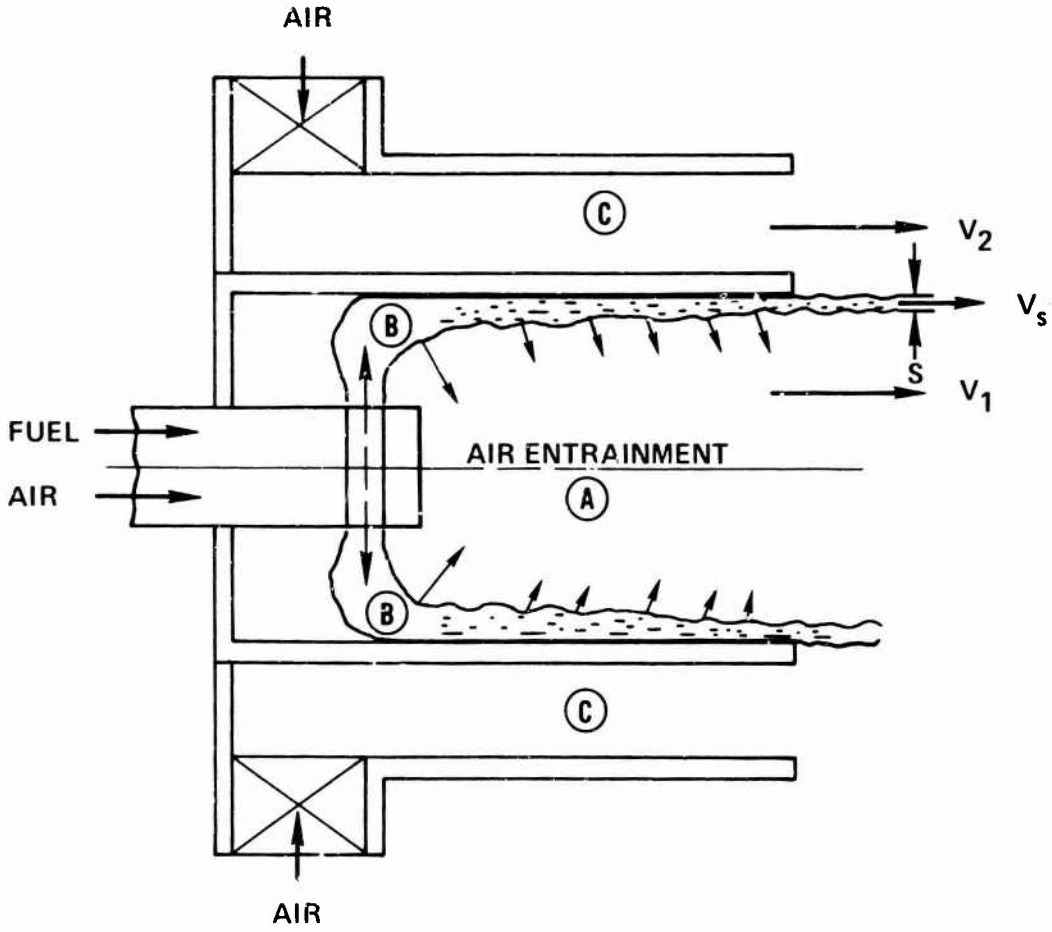

Figure 11. Schematic of the Air-Shear Injector.

- Velocities V_1 and V_2 are taken as equal to mass average velocities.
- Sheet thickness is small compared to the cylinder diameter, D.

The analysis can be divided into two parts:

- Dependence of SMD on V_s, V_1, V_2 and fuel and air properties
- Dependence of sheet thickness and velocity on W_{Al}, W_f, fuel and air properties, and diameter (D) of the central cylinder

The SMD can be correlated, according to Fraser, et al,[4] by the expression

$$SMD = K_1 + K_2 \nu^n \left[\frac{\sigma s}{\rho_g V_e^2}\right]^{1/2} \quad (3)$$

where

SMD = Sauter mean diameter, μ

ν = fuel viscosity, centistokes

σ = surface tension of fuel, dynes/cm

V_e^2 = mean square of relative fuel-air velocities on both sides of the fuel sheet, ft^2/sec^2

$$= \frac{(V_1-V_2)^2 + (V_2-V_s)^2}{2}$$

ρ_g = air density, lb_m/ft^3

s = fuel sheet thickness, μ

K_1 = constant

K_2 = constant

Equation (3) was best fit to the experimental data by Fraser and is shown in Figure 12, where $K_1 = 1.4$ and $K_2 = 44.3$.

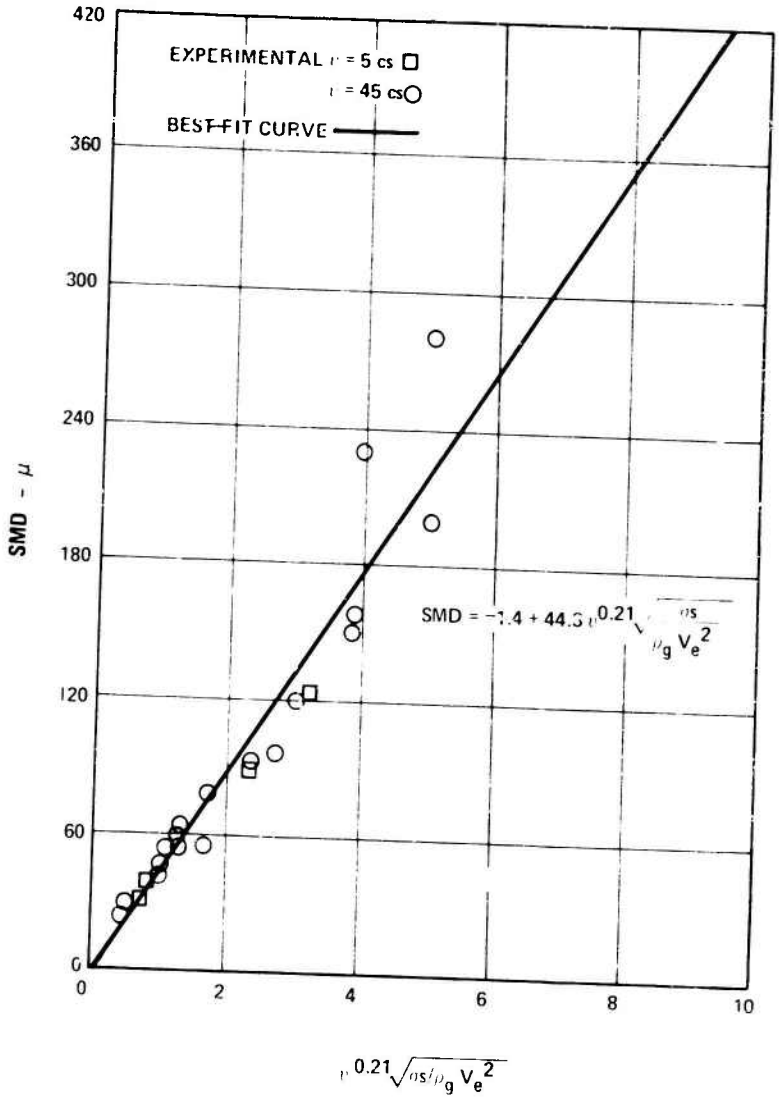

Figure 12. SMD Correlation, Experimental Data From Fraser, et al[4] (1963).

The sheet thickness, s, was calculated by using the work of Levy.[5] The following procedure was used:

- Calculate pressure drop (-dp/dz) for a two-phase annular flow.
- Compute left-hand side of Equation (4).
- Determine thickness, δ [cm], of the film by using Figure 13.

$$\sqrt{\frac{\left(\frac{dp}{dz}\right)\frac{D}{4}}{\rho_f}}\left(\frac{1}{V_1}\right) R\left(\frac{\rho_f}{\rho_A}\right) = F'\left(\frac{2\delta}{D}\right) \qquad (4)$$

where

$-\frac{dp}{dz}$ = pressure drop, dynes/cm^3

D = diameter of central cylinder, cm

ρ_f = density of fuel, gm/cm^3

V_1 = mass mean velocity of air in the central cylinder, cm/sec

δ = thickness of fuel sheet, cm

$R(\rho_f/\rho_A) = (\rho_f/\rho_A)^{1/3}$

From limited data on pressure drop in a two-phase annular flow, it can be assumed that

$$-\frac{dp}{dz} = 4\left(-\frac{dp}{dz}\right)_{S.P.} \qquad (5)$$

where $[-dp/dz]_{S.P.}$ is the pressure drop due to air flowing alone in the pipe, and is given by

$$\frac{-dp}{dz}_{S.P.} = \frac{f}{D}\left(\frac{\rho V_1^2}{2\, g_c}\right) \text{ lb}_f/\text{ft}^3 \qquad (6)$$

$f = 0.184/Rn_A^{0.2}$ $\quad 10{,}000 < Rn'_A < 120{,}000$

where Rn'_A = superficial air Reynolds number

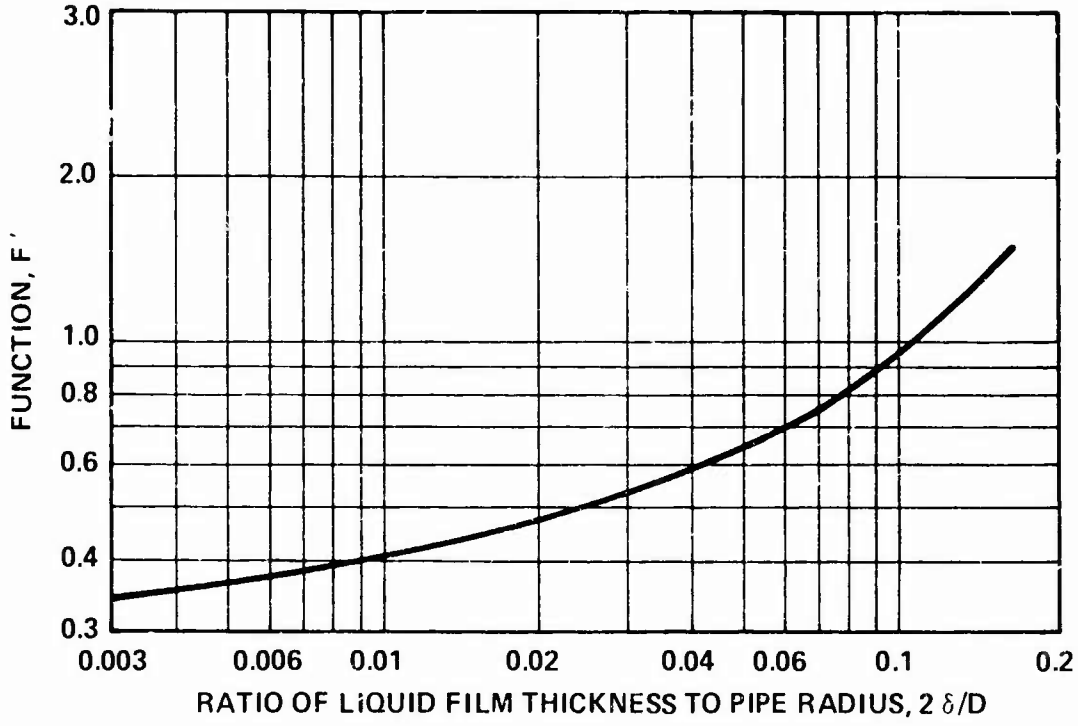

Figure 13. Dependence of Liquid Film Thickness in Two-Phase Annular Flow-Function, F' (Figure 9 From Levy[5]).

$$R'_{n_A} = 4\ mW_{A1}/\pi\ D\ \mu_A \qquad (7)$$

By using Equations (3) through (6), the SMD of the fuel spray from air-shear injector can be calculated as a function of the following:

- Air split between outer and inner cylinder
- Fuel flow rate
- Pressure and temperature
- Diameters of the inner and outer cylinders
- Fuel-to-air ratio, $W_f/W_{A1} + W_{A2})$

Calculations were performed for the sea-level design point, the sea-level light-off, and the 25,000-ft light-off conditions. The numerical values for different variables are:

Inner cylinder diameter = 0.64 in.

Outer cylinder diameter = 0.86 in.

Airflow ratio, W_{A2}/W_{A1} = 2.0

W_{A1} = 0.03416, 0.005, 0.00175 lb_m/sec per nozzle

W_f = 0.009753, 0.000833, 0.000833 lb_m/sec per nozzle

P_3 = 235.7, 20.6, 7.9 psia

T_3 = 1290, 630, 495°R

Fuel= JP-4

Figure 14 shows calculated SMD as a function of fuel temperature. As expected, SMD increases with decreasing fuel temperatures; SMD at sea-level light-off is higher than that at sea-level design conditions. SMD at 25,000-ft altitude light-off is the highest.

From these approximate calculations it appeared that the proposed air-shear atomizer would be acceptable for initial checkout tests.

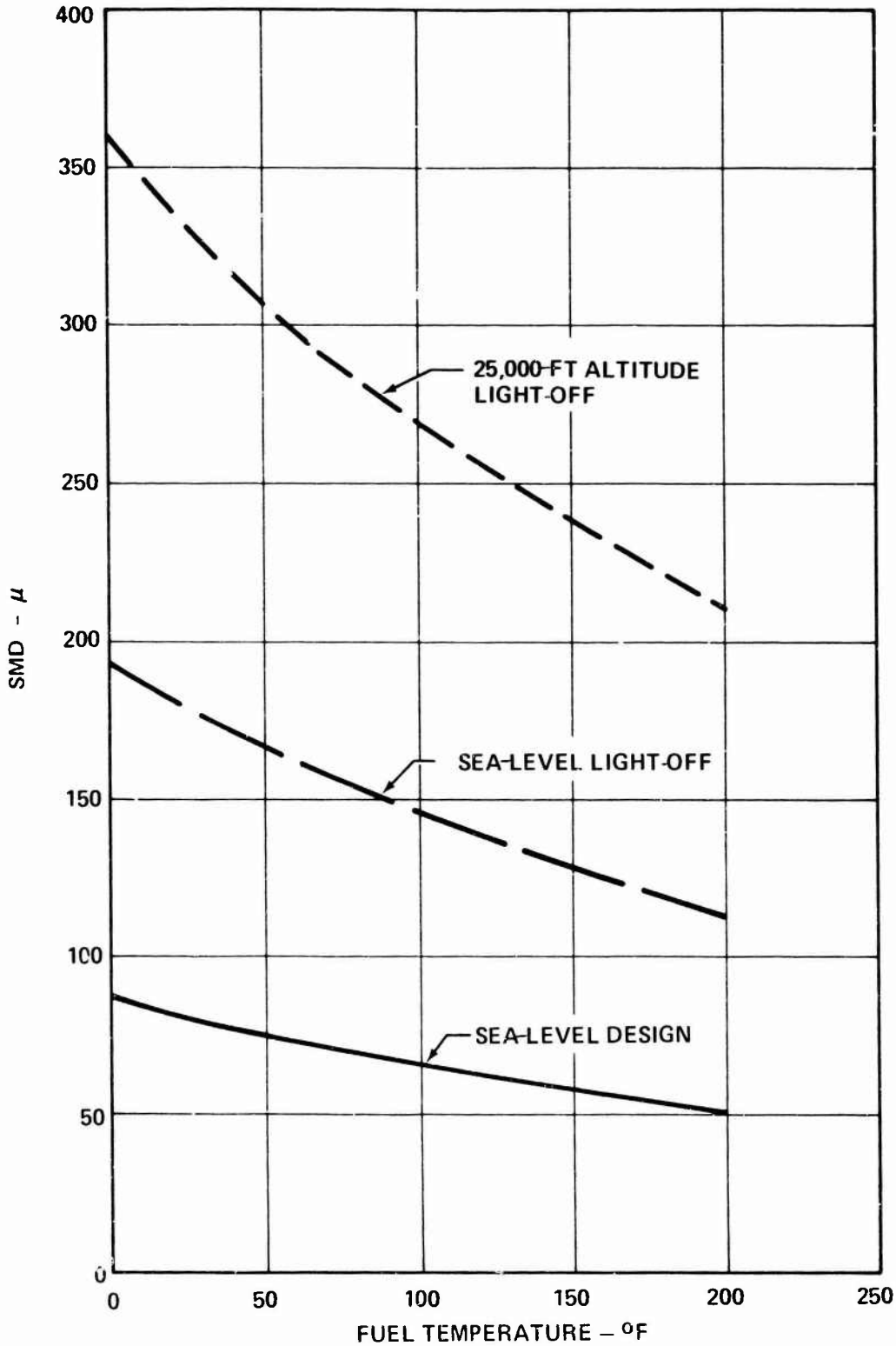

Figure 14. Predicted SMD From Air-Shear Atomizer.

2.3.3 Primary-Zone Design

For eight fuel nozzles, the pneumatic impact venturi (throat) area is 0.232 square inch (0.029 square inch per nozzle), which constitutes 10.6 percent of the total combustor effective open area. The airflow through the nozzles was calculated to be 0.273 pound per second.

The primary zone design fuel-air ratio (f/a), based on design practice, was 0.057 (ϕ pz = 0.85) and therefore required 50 percent of the total combustor air. This percentage requires dual utilization of part of the cooling air and dilution air within the primary zone combustion process. All of the air from the first cooling skirts of the inner and outer liner and approximately half of the flow from the second skirts, plus air from the dilution zone, are utilized in the primary zone reaction. This flow, combined with that through the fuel nozzle, is approximately 30 percent of the total airflow. The remaining primary flow is provided by the air swirlers. The primary zone flow model calculations assured stable behavior of the combustor over the entire range of operation.

2.3.4 Dilution-Zone Design

Twenty percent of the airflow was allocated for dilution. This was based upon the predictions of primary-flow model and air-recirculation model. Geometric open area of the dilution orifices is 0.438 square inch. Iterative calculations for sizing and spacing considerations show that thick-walled opposed ($d_h/t \leq 4$) or opposed plunged orifices with 0.125 inch diameter would be optimum, assuming

Discharge Coefficient (C_D) = 0.6

Efflux Angle (β = 80° to 90°

Area (actual geometric) = 0.0073 sq in.

One row consisting of 30 dilution orifices was located on both the inner and outer liners. The resulting orifice spacing-to-diameter ratios are 4.1 and 2.8 for the outer and inner liners respectively.

The dilution jet velocity at the design-point conditions is 361 feet per second. This would be the initial cross-stream velocity for a 90-degree efflux angle. Assuming a cross-stream velocity of 300 feet per second to allow for variation in efflux angle and that the penetration is a function of the hole diameter and jet-to-mainstream flow, then the jet

penetration can be calculated from empirical correlations recently presented by Aiba and Inove[6] as

$$\frac{\text{Jet penetration}}{\text{Jet diameter}} = 2.2\left(\frac{\rho_{Jet}\ V_{Jet}}{\rho_{Main}\ V_{Main}} - 0.10\right)^{0.68} \qquad (8)$$

Therefore,

Jet penetration = 0.973 inch

Since the combustor height is 1.25 inches, these opposing jets should penetrate more than halfway across the combustor, and thus impinge as desired for good dilution-zone mixing and primary-zone recirculation. The recirculation model for impinging jets described in Volume I was used to calculate the dilution flow which will recirculate to the primary zone. These calculations indicated that 20 percent of the dilution flow (4 percent of the combustor airflow) will be recirculated. An initial design objective was 6.8 percent of the total airflow, but since some of the second cooling slot flow was also entrained for recirculation, the calculated values are considered adequate.

2.4 ENGINE CONCEPTUAL LAYOUT

A conceptual engine layout was prepared to insure mechanical feasibility of the selected combustor configuration. The turboshaft engine layout is presented in Figure 15. The adjacent engine components were defined earlier in the program (Volume I, Section 2.0).

Minor variations from the referenced engine layout have been incorporated. For example, the engine length has been increased from 28.75 inches to 29.4 to adequately provide for bearings, inlet, accessory drive, etc. The axial straight-through configuration was necessary to minimize combustor surface area.

A shaft dynamics analysis was conducted to establish the feasibility of the configuration shown. This analysis demonstrated that an inner shaft bearing is required between the coaxial gas generator and power turbine shafts to eliminate critical speed problems for the power takeoff at the front of the engine. The shaft size, speed, and bearing arrangement were selected to maintain operation below the third (bending) critical speed of the power turbine shaft. Since the inner-shaft bearing is functional only during transition through the critical speeds, an air bearing was selected, as depicted, to preclude provisions for bearing lubrication.

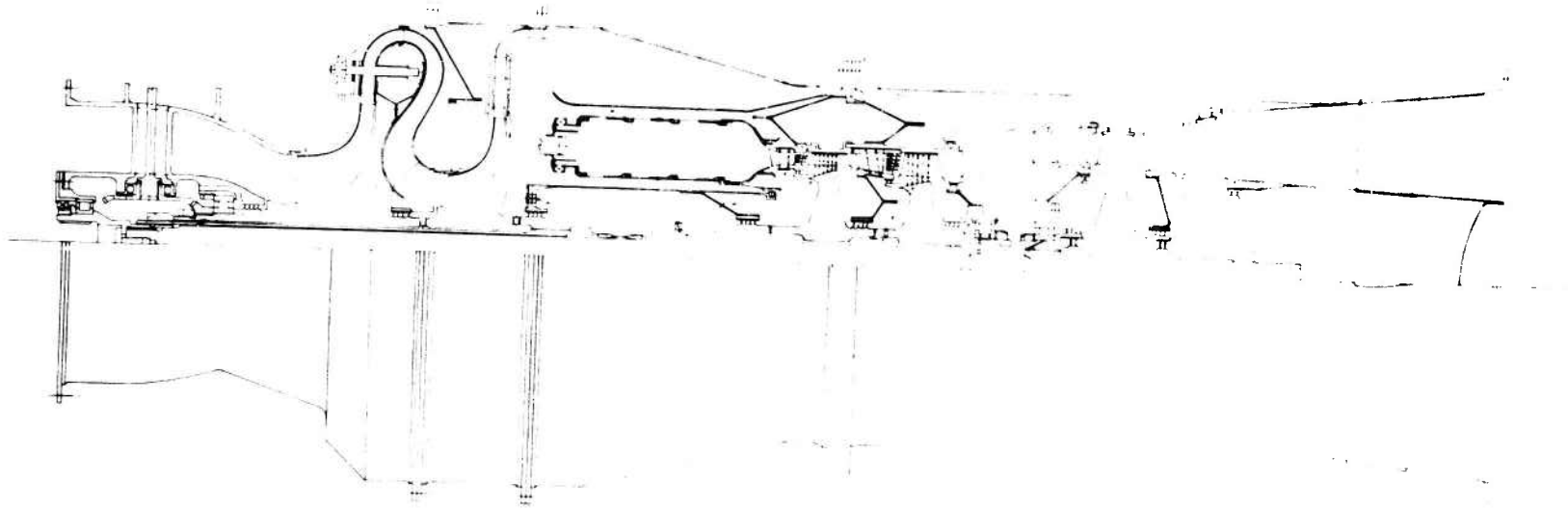

ENGINE CYCLE:

W_A = 3.0 LB/SEC

P/P = 16.0

TIT = 2500°F

ENGINE DIAMETER = 10.70 INCHES

ENGINE LENGTH = 29.40 INCHES

ENGINE PERFORMANCE (CALCULATED):

MAXIMUM POWER = 610 SHP

S.F.C. = 0.443 LB/HP-HR

Figure 15. Conceptual Turboshaft Engine Layout.

3.0 RIG TEST PROGRAM

A fuel nozzle and swirler unit was tested in a fuel spray rig to visually assess fuel atomization and distribution. Subsequently, the entire combustor (as well as individual fuel atomizer/swirler units) was tested in a discharge coefficient rig to determine the system effective open area and pressure drop.

Velocity profiles within the combustor were obtained during cold-flow mapping tests in an atmospheric rig to provide data for comparison with analytical predictions. Extensive combustion tests in both the atmospheric rig and the high-pressure rig were conducted to obtain combustor performance and gaseous emissions data. Combustor operating conditions for the rig tests were determined from the turboshaft engine cycle calculations. (Refer to Table II, Volume I of the report). A plot of combustor overall fuel-air ratio (f/a) versus engine power is presented in Figure 16.

3.1 FUEL NOZZLE/SWIRLER SPRAY TESTING

The pneumatic-impact/swirler system shown in Figure 11 was tested using the fuel distribution test rig shown in Figure 17. The results indicated poor fuel atomization and distribution for pressure drops of less than 4 percent (16.0 inches of water) across the system. The distribution was particularly poor with low fuel flows. In all cases the fuel deposited on the filming cylinders was successfully atomized, but a large percentage of the fuel remained attached to the nozzle impact plate and formed large drops on the downstream surface of this plate. These drops were then discharged either as large unatomized drops or in a continuous stream, resulting in poor overall atomization and distribution. The spray half-angle with the system (downstream of the swirler) was found to lie between 70 and 85 degrees; such a wide angle is undesirable since the fuel would impinge on the combustor walls before evaporation and combustion could take place on the wall, thus resulting in the strong possibility of combustor wall burnout.

Several modified nozzle designs were tested in attempts to overcome the above problems [Figure 18(a) through (d)]. The most satisfactory of these designs in terms of spray quality subsequently was modification (d). Figure 19 shows the resulting configuration. A set of these nozzles was fabricated for full-scale combustor testing.

It is essential with this design that the central plug be concentric with the swirler filming cylinder. To ensure that the combustor did not move radially once the nozzles were centered,

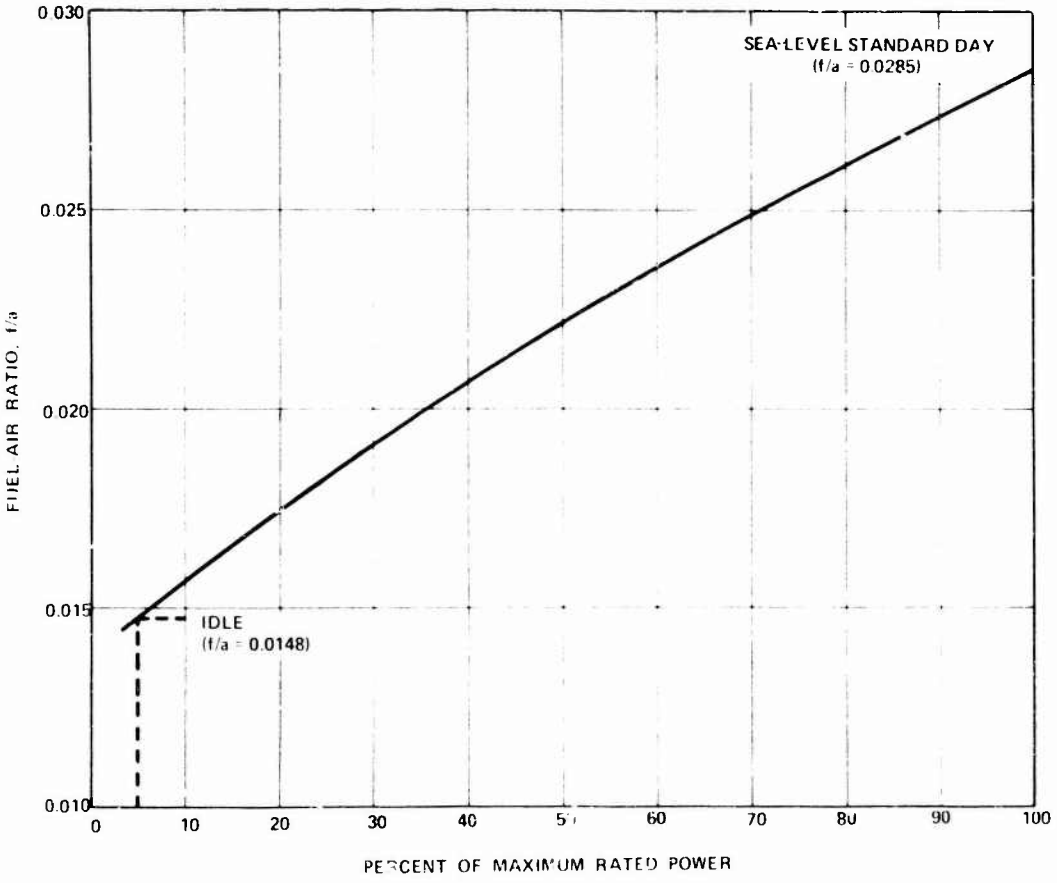

Figure 16. Combustor Fuel-Air Ratio as a Function of Maximum Rated Power.

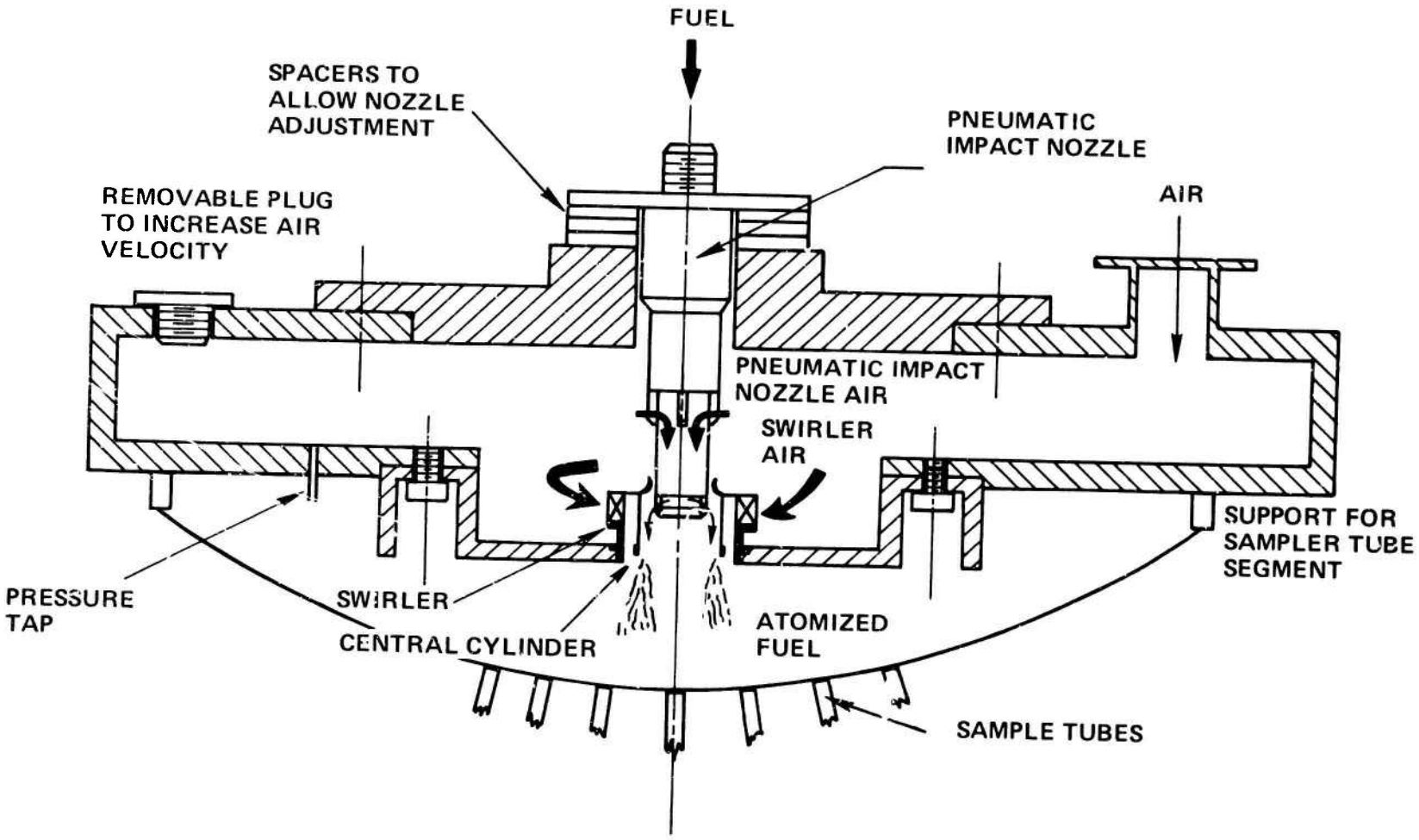

Figure 17. Pneumatic Impact/Swirler Test Rig.

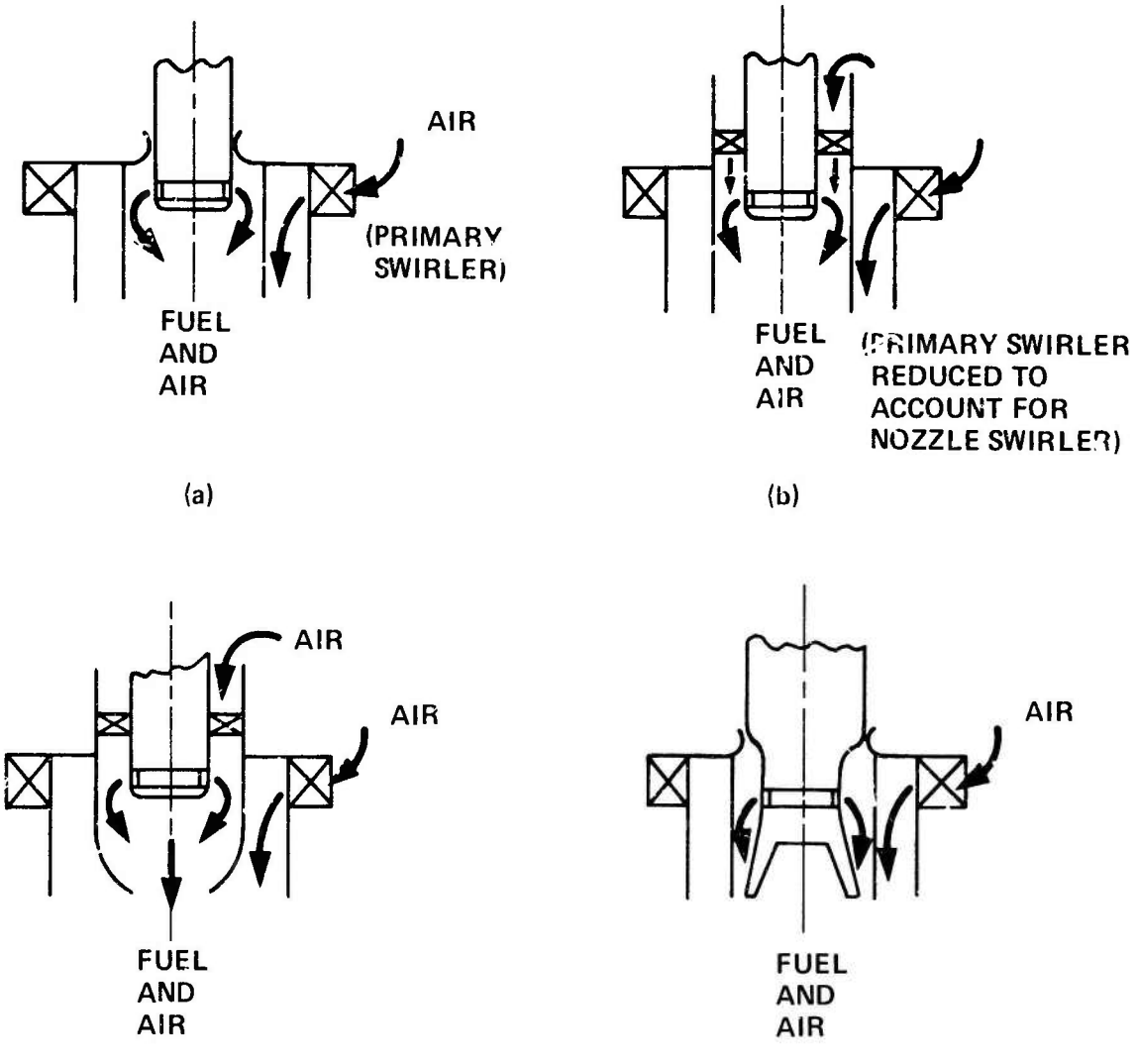

Figure 18. Modified Nozzle Designs for Fuel Nozzle/Swirler Assembly.

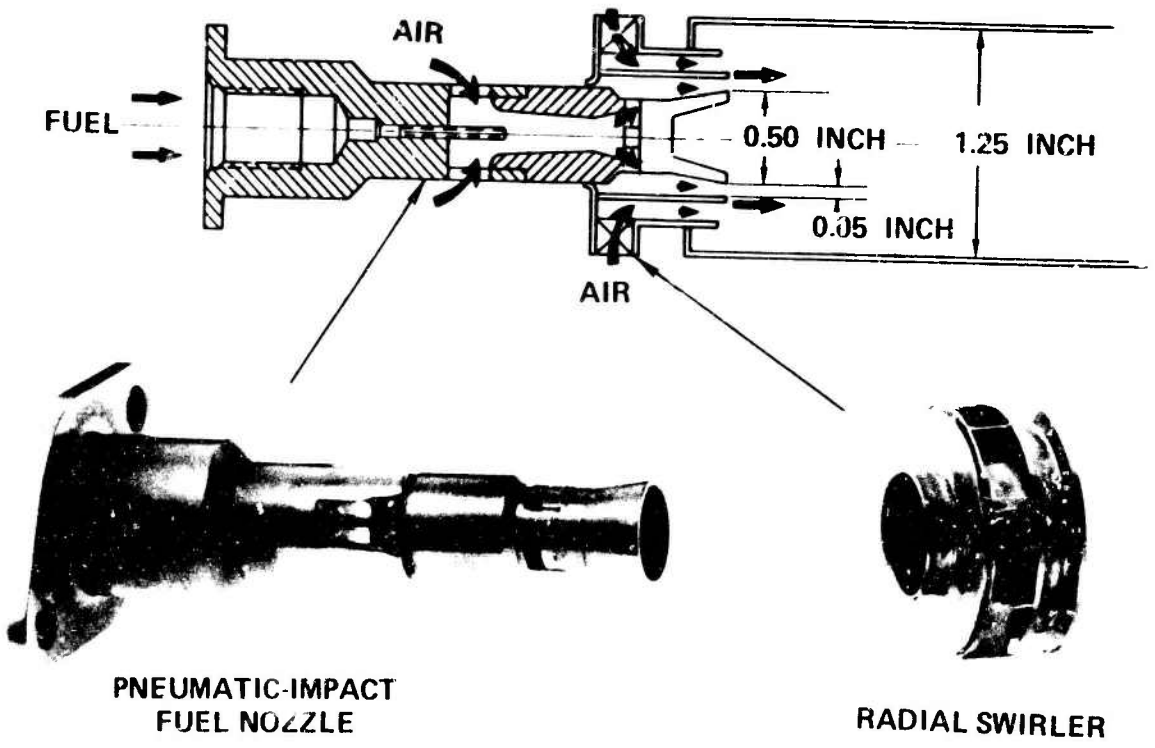

Figure 19. Fuel Injection System.

support tabs were included on the inner liner circumference. These support tabs were in addition to the three originally attached to the outer liner circumference.

Fuel manifold pressure versus fuel flow rate characteristics were determined experimentally with a single restrictor* and two restrictors in series; the results are shown in Figure 20. Following this test a flow check of the manifold and all eight nozzles at 20 pounds per hour total flow, and at manifold pressure of 1.55 psig, showed only a 3-percent flow variation. (A variation of 6 percent is considered to be acceptable.)

Figure 20 also shows the results of a contaminated fuel test that was conducted with the fuel nozzle system. A single restrictor was placed between the fuel manifold and each nozzle for this test. A 40-micron filter was used upstream of the manifold to simulate a fuel control filter similar to an engine installation. A continuous 20-hour test was conducted at a flow rate of 255 pounds per hour using JP-4 fuel which was contaminated with the debris defined in MIL-E-5007C.

A flow check, conducted after the 20-hour test, indicated that the fuel pressure/flow rate characteristics had not been affected by the contaminated fuel (see data point on Figure 20). This was expected since the particles that would pass through the 40-micron filter were significantly smaller than the minimum passage (0.035) in the fuel system.

3.2 DISCHARGE COEFFICIENT TESTING

Combustor open-to-plenum discharge coefficient tests were conducted without the fuel nozzles or swirlers in position. The purpose of these tests was to determine effective open areas for the cooling bands and dilution holes. Results of these tests are shown in Table II for the individual elements open and for all elements open. Also given is a comparison of the percentage of total combustor air based on the measured effective open areas and that predicted by means of the annulus loss program.

---

*Lee Axial Visco Jet, Lee Company Part Number 19XVL330DKO.

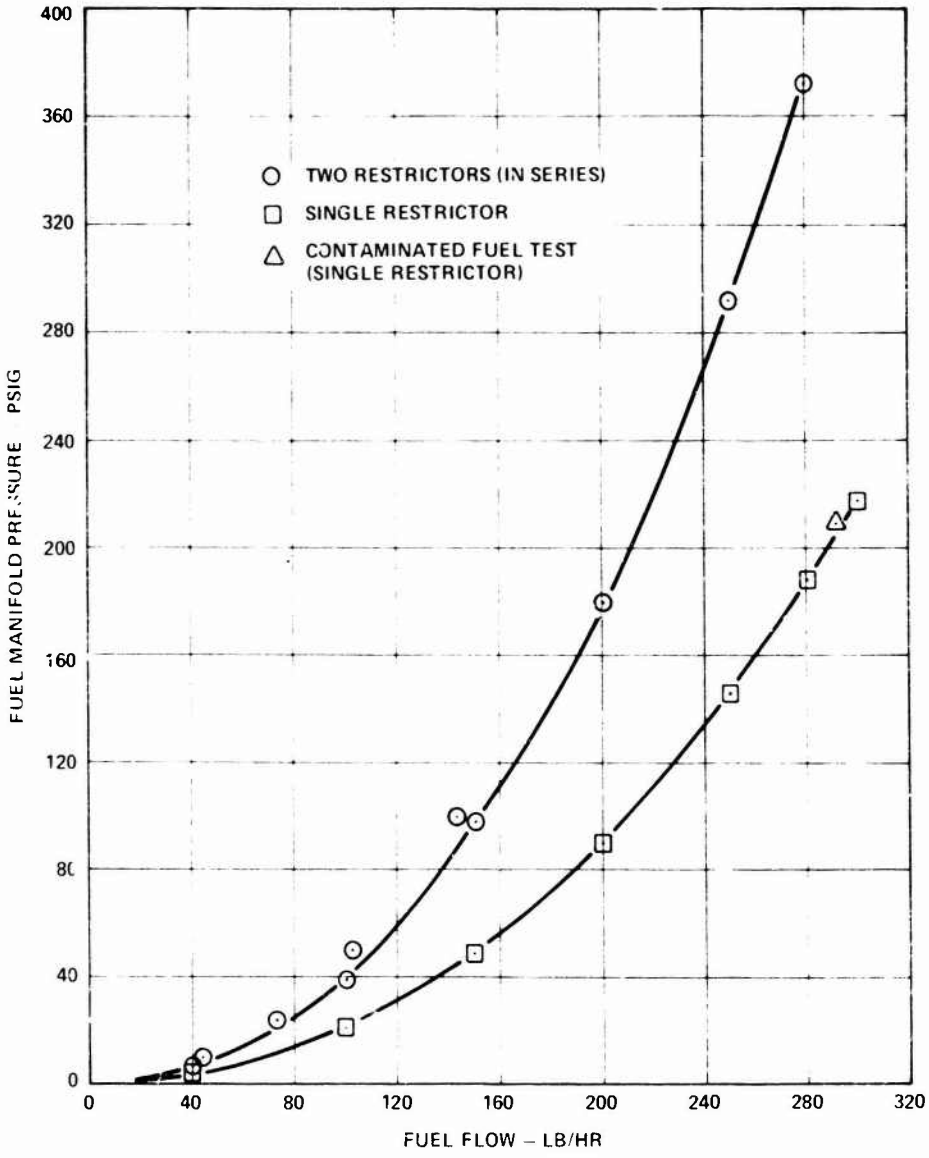

Figure 20. Fuel Manifold Pressure vs Fuel Flow Characteristics.

TABLE II. COMBUSTOR LINER EFFECTIVE OPEN AREA (SWIRLER AND NOZZLE NOT INCLUDED)

Open Elements	Measured		Predicted
	C_DA	Percentage of Total Air	Percentage of Total Air
Inner Dilution Holes	0.301	13.7	10.56
Outer Dilution Holes	0.320	14.6	11.03
Inner Cooling Bands (4)	0.412	18.8	17.44
Outer Cooling Bands (4)	0.736	33.6	30.99
Total (Summed)	1.769	80.7	70.02
Total (Measured)	1.58	72	

When the elements were run separately and the airflow from each element summed to determine the total airflow was calculated to be 10 percent greater than that predicted. When all elements excluding fuel atomizer and swirler were open, the total measured airflow was 72 percent, in close comparison to the 70 percent predicted. The above results indicate that when all elements are open, each feels some influence from the others and a reduction in effective open area results. Similar tests were conducted to determine the discharge coefficient of the swirler and swirler/fuel nozzle assembly. This data, combined with the combustor cooling bands and dilution orifices coefficient data, was used to determine the effective open area of the total system.

Test data indicated that each swirler had an effective open area of 0.089 square inch. Therefore, at the design point, the eight swirlers would pass 32.5 percent of the inlet airflow compared to a design objective of 20 percent. The design equivalence ratio was regained by closing the first row of cooling holes. This is discussed later in this report.

The fuel nozzle effective area was determined to be 0.033 square inch, which corresponds to 12 percent of the inlet airflow compared to the design objective of 10 percent. No modifications were made prior to installing the swirlers and nozzles in the combustor and running the atmospheric tests. This approach was selected since it was theorized (and later substantiated) that the additional primary airflow would enhance flame stability by strengthening the recirculation. It was

also verified at a later date that the airflow from the swirlers would provide sufficient cooling for the first panels. By eliminating the first inner and outer cooling bands, the required reduction in orifice area and attendant increase in pressure drop to the design objective levels were chieved.

3.3 ATMOSPHERIC RIG TESTS

The combustor was installed in the atmospheric rig, and pressure drop test data, cold flow mapping, and hot performance survey information were obtained for initial testing and for comparison with primary-zone flow modeling predictions.

3.3.1 Pressure Drop Measurement

The combustor isothermal pressure drop characteristics were determined by measuring the differences between the total pressure probes at location A (refer to Figure 21) and atmospheric discharge over a range of inlet airflow rates. Pressure instrumentation at locations B, C, D and E was also monitored throughout this testing. Figure 22 shows a summary of the results obtained plotted against corrected airflow, with the design requirement included for comparison. The results showed a pressure drop 1 percentage point below the 3 percent required at design conditions, confirming discharge coefficient rig data which indicated that the combustor open area was greater than required or that there were leaks in the system. Pressure checks were conducted which indicated that rig leakage was at an acceptable level. It was therefore confirmed that the combustor open area was too great.

As previously indicated, no modification to the combustor was made until some indication of the combustion characteristics, liner metal temperatures and required cooling modifications had been determined. Based on this indication, the decision was made to raise the pressure drop and to provide the design equivalence ratio by eliminating the first inner and outer cooling bands.

3.3.2 Cold-Flow Mapping

The cold-flow mapping was conducted to determine the axial and tangential velocity profiles within the combustor. The main purpose of these tests was to provide data for the verification of the analytical predictions. A secondary purpose was to give some indication of possible flow instabilities which could cause unstable combustion and resonance within the burner.

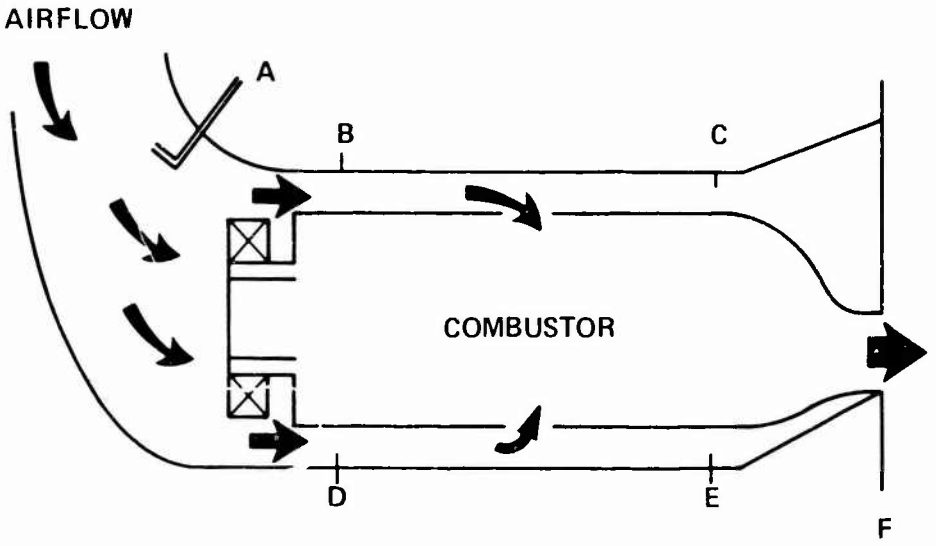

LEGEND	
SYMBOL	INSTRUMENTATION
A	TOTAL PRESSURE AT 3 CIRCUMFERENTIAL LOCATIONS TOTAL TEMPERATURE AT 3 CIRCUMFERENTIAL LOCATIONS
B	TOTAL PRESSURE AT 3 CIRCUMFERENTIAL LOCATIONS STATIC PRESSURE AT 3 CIRCUMFERENTIAL LOCATIONS
C	STATIC PRESSURE AT 2 CIRCUMFERENTIAL LOCATIONS
D	TOTAL PRESSURE AT 3 CIRCUMFERENTIAL LOCATIONS STATIC PRESSURE AT 3 CIRCUMFERENTIAL LOCATIONS
E	STATIC PRESSURE AT 2 CIRCUMFERENTIAL LOCATIONS
F	4-ELEMENT TOTAL PRESSURE RAKE AT 2 CIRCUMFERENTIAL LOCATIONS 3-ELEMENT TOTAL TEMPERATURE RAKE AT 2 CIRCUMFERENTIAL LOCATIONS

Figure 21. Combustor Rig Instrumentation Schematic.

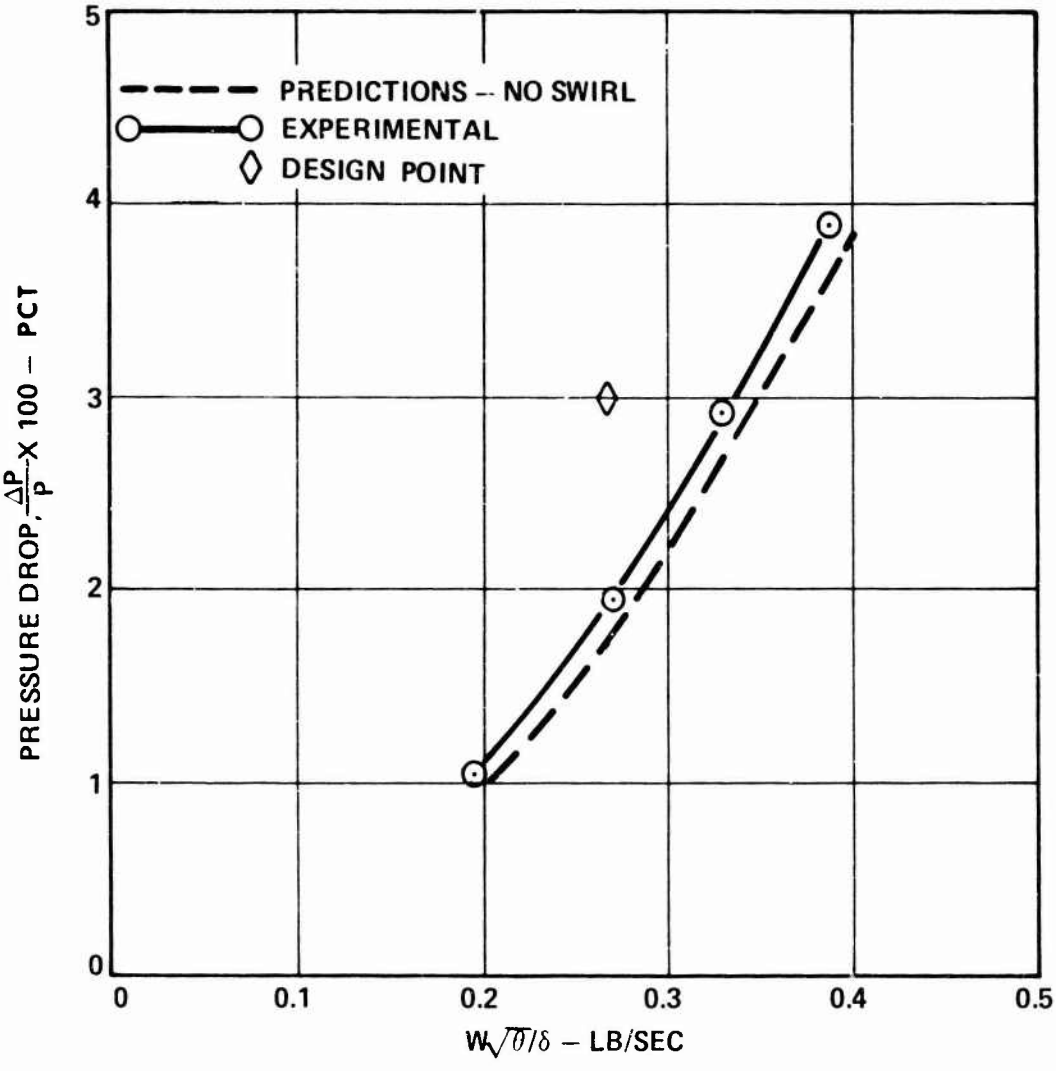

Figure 22. Combustor Isothermal Pressure Drop.

Axial and tangential velocity profiles were measured at four axial positions along the length of the combustor for each of two different circumferential positions by using a wedge probe and liquid micromanometer. The circumferential positions (shown in Figure 23) were (a) directly in line with one swirler and (b) between two swirlers. Resultant plots of axial and tangential velocities in line with the swirler are shown in Figures 24 and 25 for pressure drops of approximately 2 and 4 percent. Similar plots were also made for between-swirler locations. Figures 24(a) and 24(b) are axial velocity profiles upstream of the dilution holes, and these clearly show the recirculation zone for both the 2- and 4-percent pressure drop conditions. Figures 24(c) and (d) show axial velocity profiles downstream of the dilution holes where no recirculation exists.

Corresponding tangential components are given in Figure 25. These plots show that swirl exists up to the dilution hole location (refer to Figures 25(a) and (b)) and is then destroyed by the dilution air entry (refer to Figures 25(c) and (d).

Based on these measurements, it was concluded that there is a strong recirculation pattern in the primary zone and that the overall combustor flow field exhibits the basic requirements for stable combustion.

Figures 26, 27, and 28 show several comparisons of the cold-flow data and predictions of the Gosman-Spalding program. Exact modeling of the combustor geometry was not possible due to limitations (outlined below) in the computer program. Figure 29 shows a comparison of the experimental and analytical geometries. The analytical model has only a single entry, no cooling slots, and an effective two-dimensional dilution flow compared with the experimental geometry of two primary entries (one with swirl, one without swirl), four inner- and four outer-cooling bands, and discrete impinging dilution jets.

The present analytical model appears to be incapable of handling more than one primary entry. Attempts to do this resulted in instability in the solution and the solution convergence to incorrect values. Convergence was also found to be sensitive to grid size even though all increments were within those suggested in the Gosman text. Based on the above limitations, the experimental and predicted velocity profiles showed fair agreement but indicate that the model still requires more refinement to obtain unconditional convergence before it is capable of accurately describing a complete combustion system configuration with strong swirling flow.

PORTS 1 THRU 4 – IN LINE WITH SWIRLER
PORTS 5 THRU 8 – BETWEEN SWIRLERS
X – DIMENSIONS INDICATE AXIAL DISTANCE FROM COMBUSTOR DOME

Figure 23. Combustor Cold-Flow Mapping Ports (After Weld Repair).

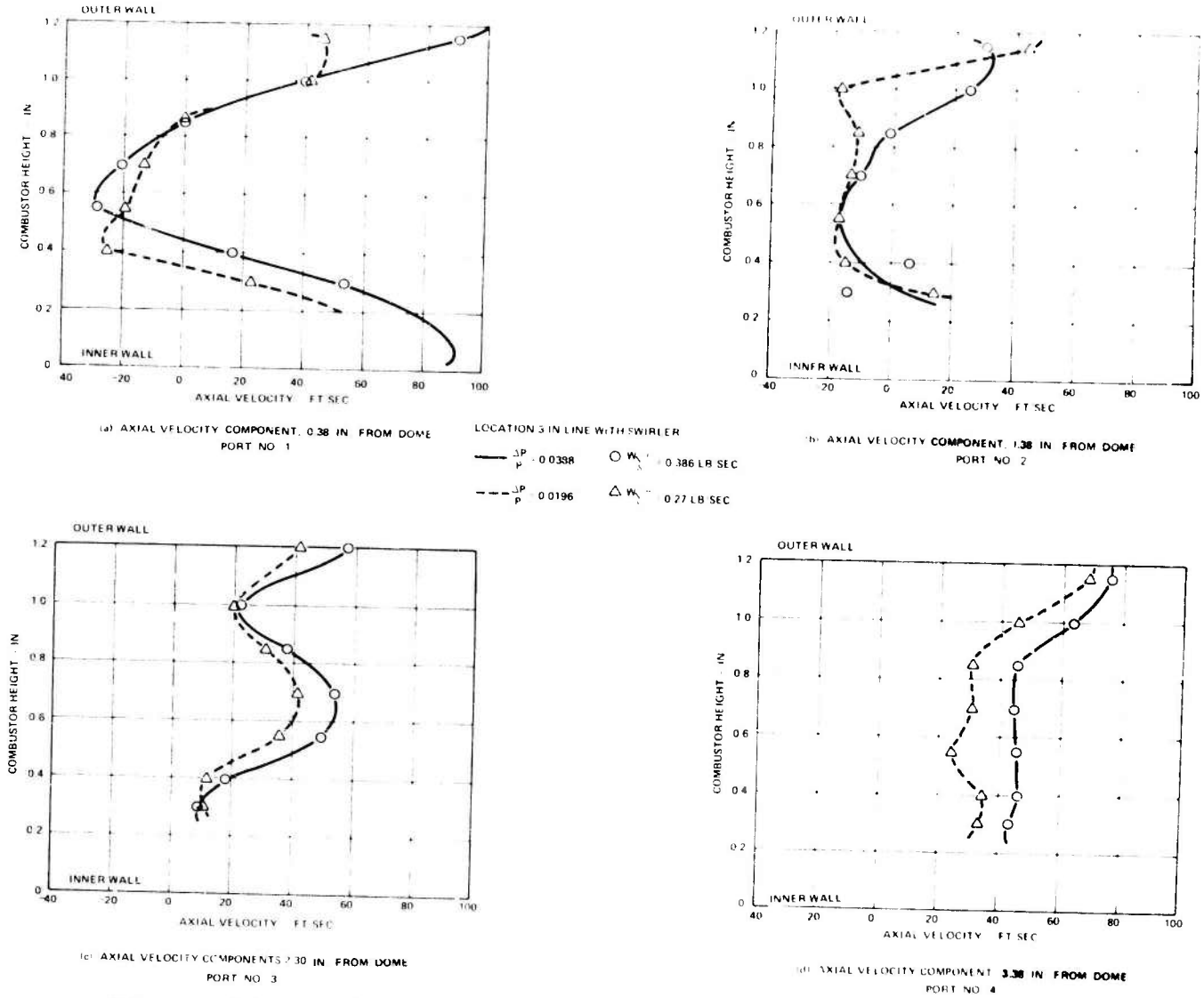

(a) AXIAL VELOCITY COMPONENT, 0.38 IN. FROM DOME PORT NO. 1

(b) AXIAL VELOCITY COMPONENT, 1.38 IN. FROM DOME PORT NO. 2

(c) AXIAL VELOCITY COMPONENTS 2.30 IN. FROM DOME PORT NO. 3

(d) AXIAL VELOCITY COMPONENT, 3.38 IN. FROM DOME PORT NO. 4

Figure 24. Axial Velocity Profiles In Line With Swirler.

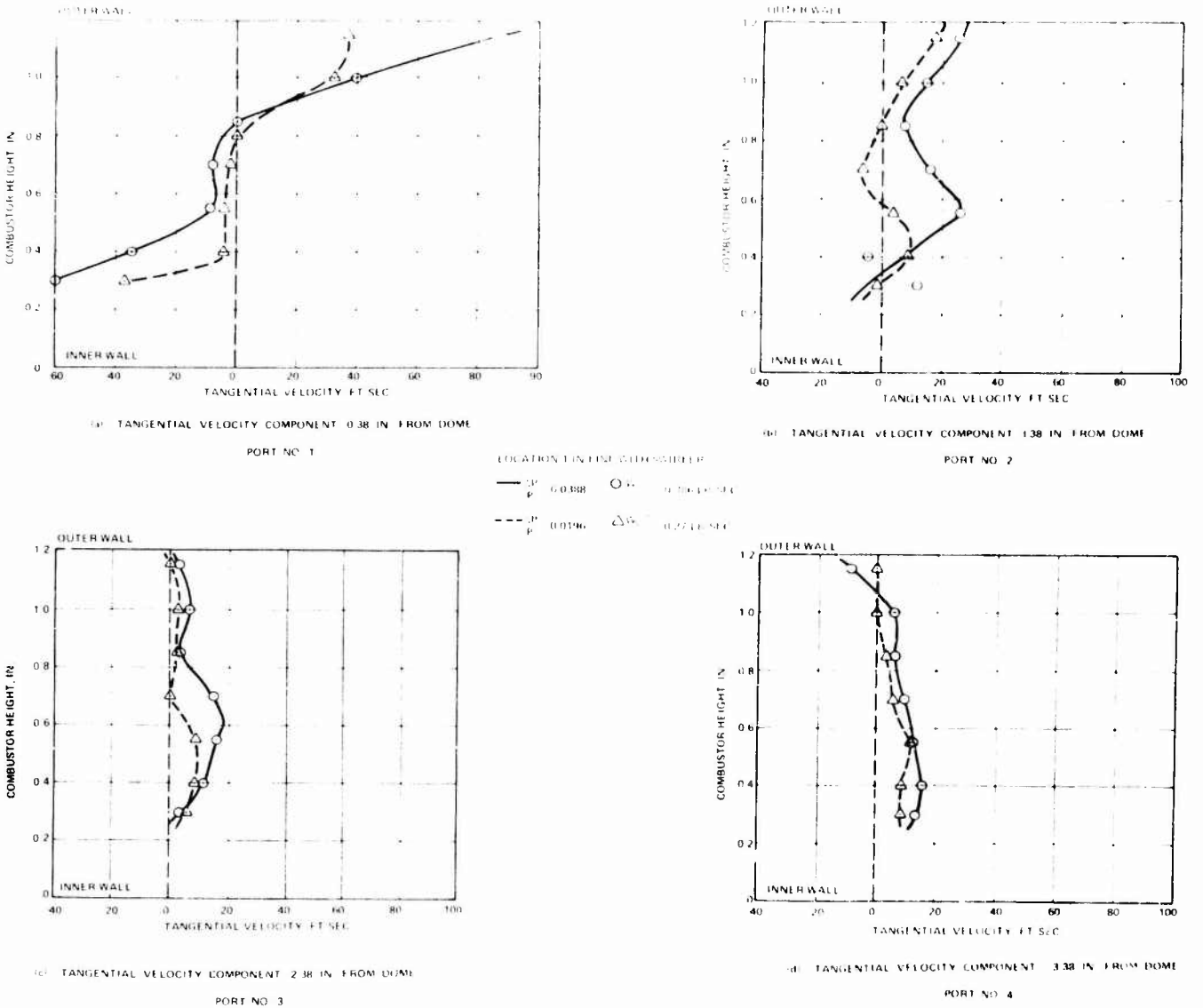

(a) TANGENTIAL VELOCITY COMPONENT 0.38 IN FROM DOME PORT NO 1

(b) TANGENTIAL VELOCITY COMPONENT 1.38 IN FROM DOME PORT NO 2

(c) TANGENTIAL VELOCITY COMPONENT 2.38 IN FROM DOME PORT NO 3

(d) TANGENTIAL VELOCITY COMPONENT 3.38 IN FROM DOME PORT NO 4

Figure 25. Tangential Velocity Profiles in Line With Swirler.

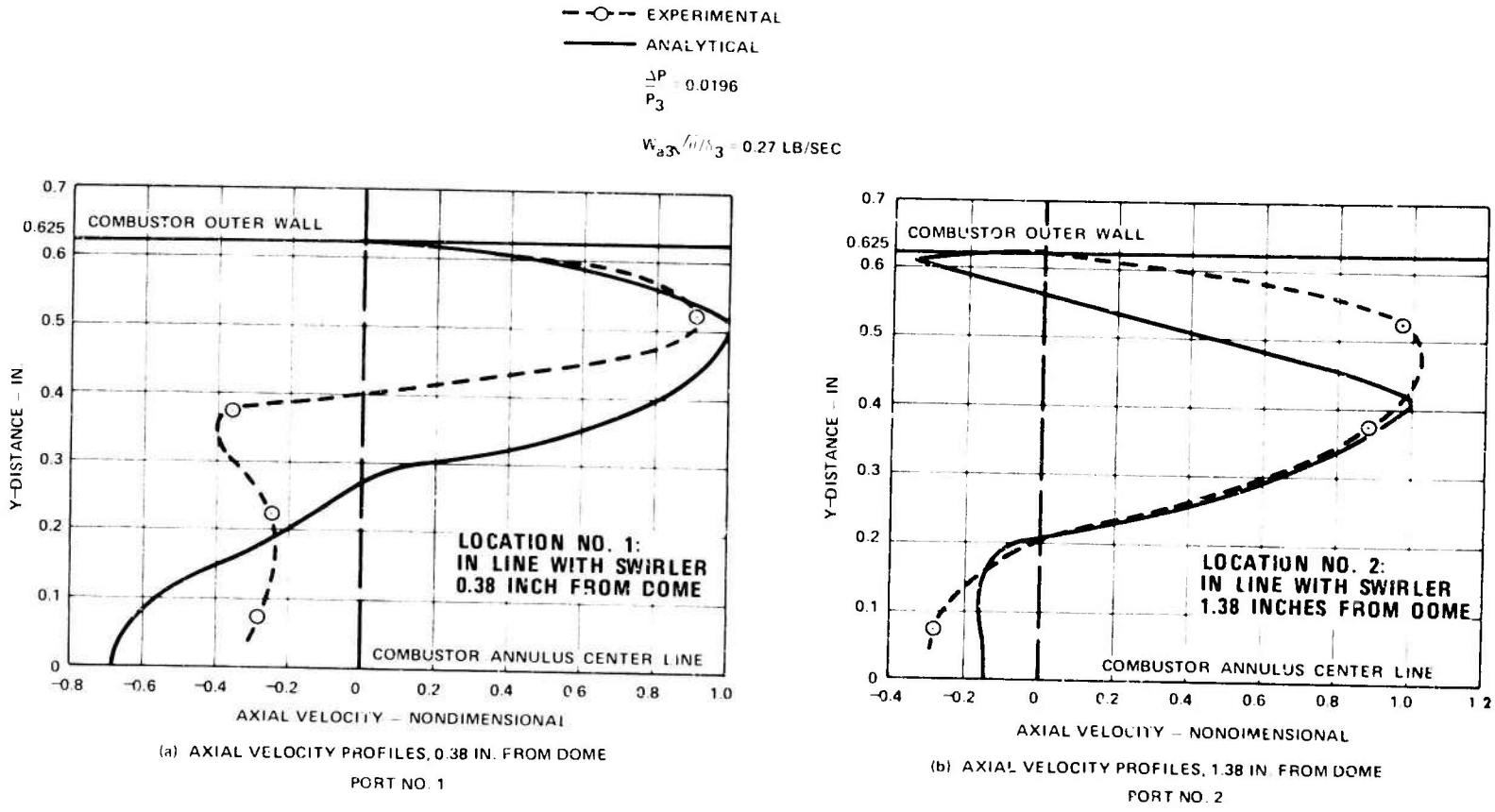

(a) AXIAL VELOCITY PROFILES, 0.38 IN. FROM DOME PORT NO. 1

(b) AXIAL VELOCITY PROFILES, 1.38 IN. FROM DOME PORT NO. 2

Figure 26. Combustor Velocity Profiles Comparing Experimental Data and Predictions From Gosman-Spalding Program.

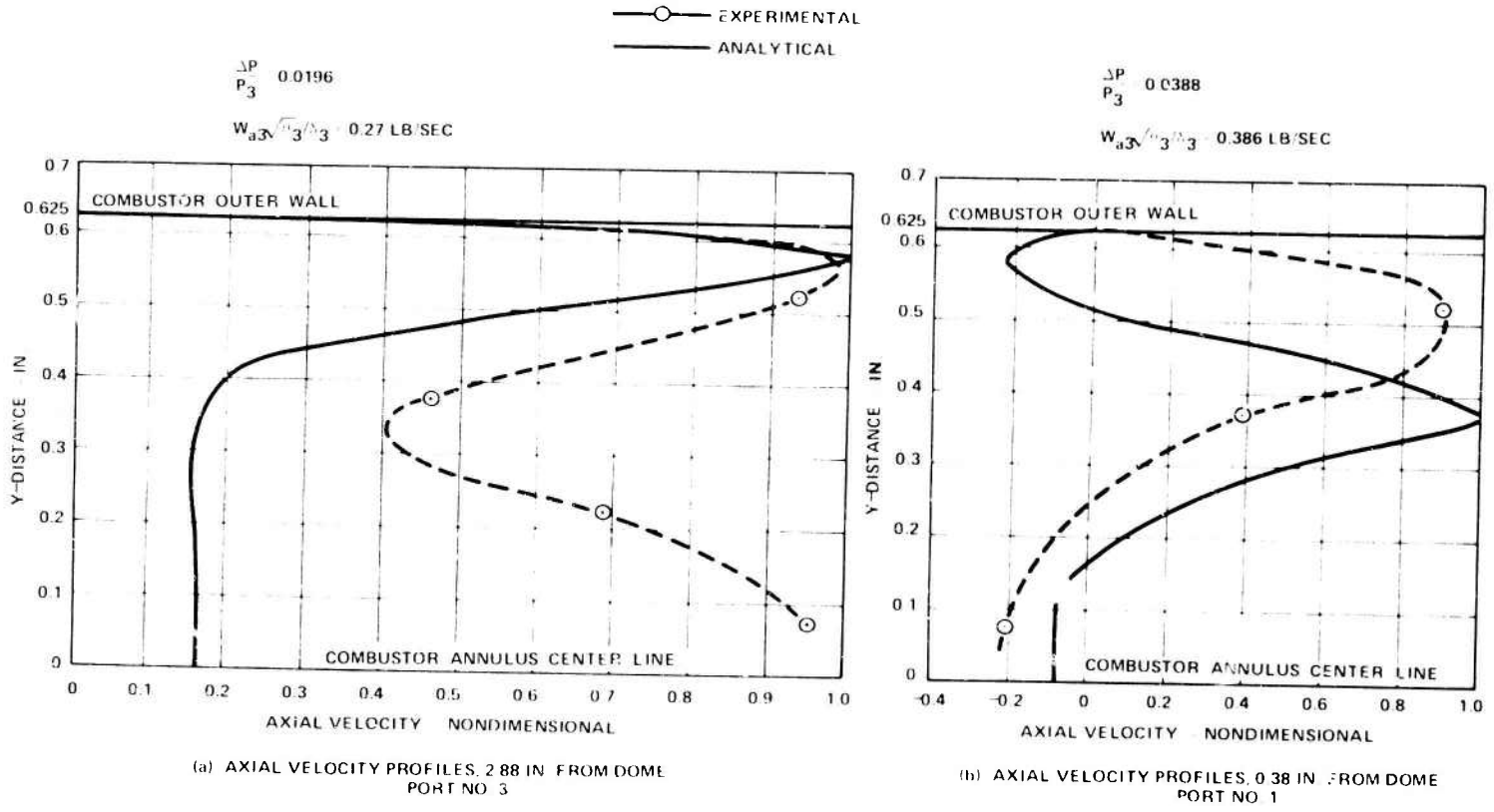

(a) AXIAL VELOCITY PROFILES, 2.88 IN. FROM DOME PORT NO. 3

(b) AXIAL VELOCITY PROFILES, 0.38 IN. FROM DOME PORT NO. 1

Figure 27. Combustor Axial Velocity Profiles Comparing Experimental Data and Predictions From Gosman-Spalding Program.

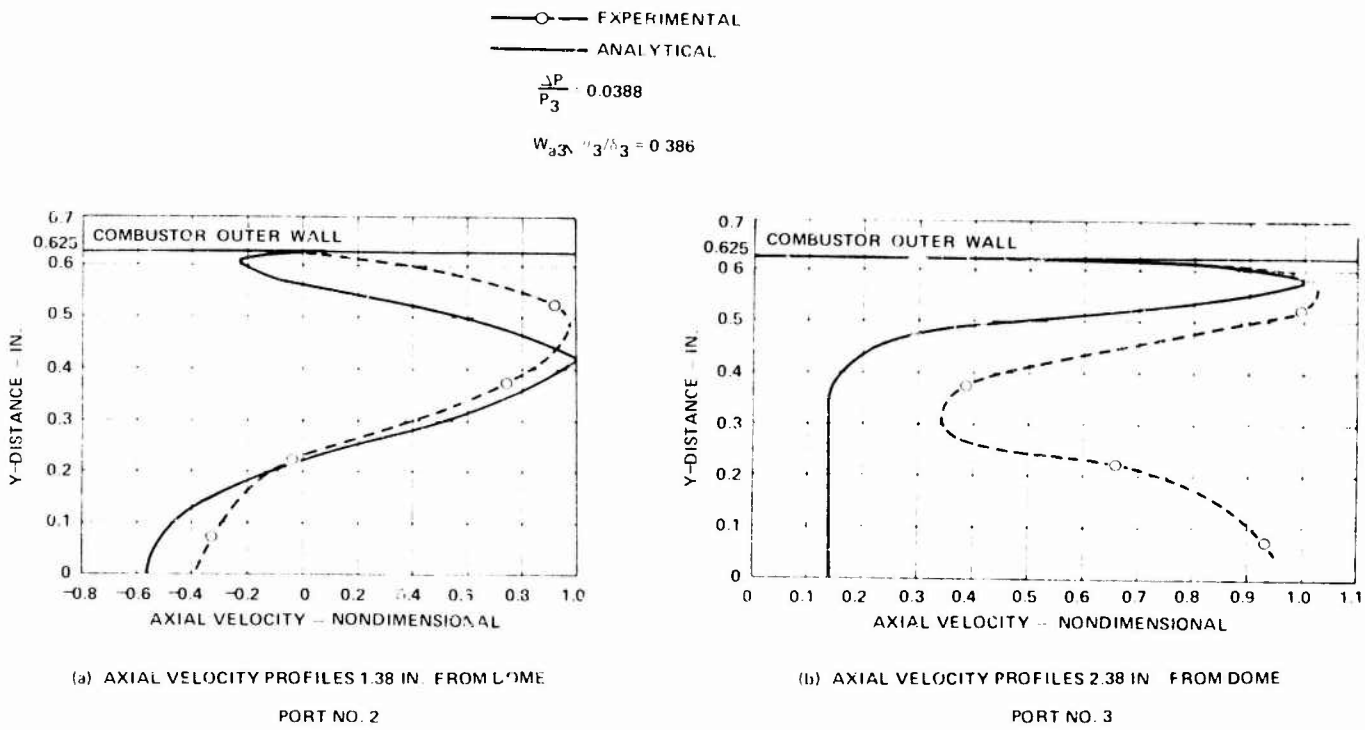

(a) AXIAL VELOCITY PROFILES 1.38 IN. FROM DOME PORT NO. 2

(b) AXIAL VELOCITY PROFILES 2.38 IN. FROM DOME PORT NO. 3

Figure 28. Combustor Axial Velocity Profiles Comparing Experimental Data and Predictions From Gosman-Spalding Program.

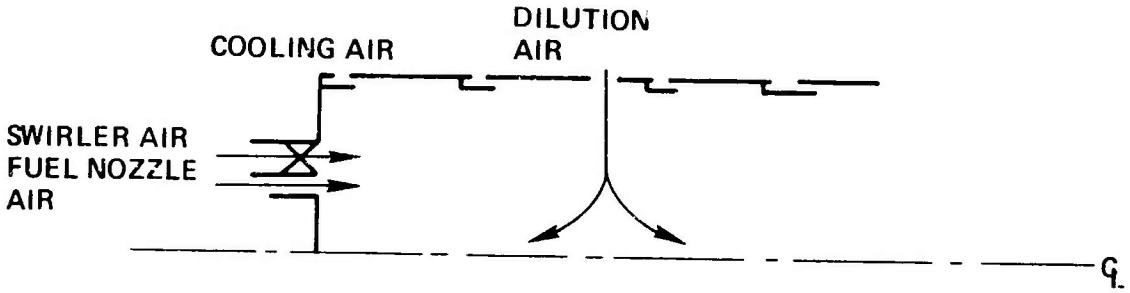

(a) EXPERIMENTAL MODEL (2 PRIMARY OPENINGS)

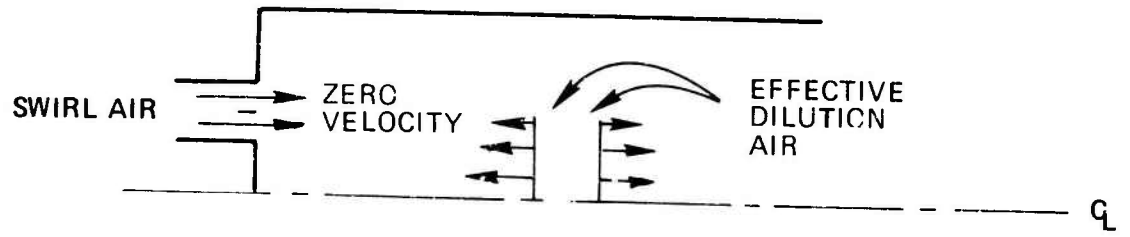

(b) ANALYTICAL MODEL (SINGLE PRIMARY OPENING WITH ZERO VELOCITY POINT)

Figure 29. Comparison of Experimental and Analytical Models.

3.3.3 Combustion Tests

Atmospheric tests were conducted to observe flame characteristics prior to pressure rig testing. It was necessary to use preheated inlet air to obtain light-off at pressure drop values of 1.0, 2.0, and 3.0 percent, indicating the need for better atomization at start conditions. Once light-off was obtained, the flame showed good coverage and was retained within the primary zone. With the exception of one small luminous streak, the flame was blue. This one luminous streak was attributed to a misaligned fuel nozzle.

No efficiency or exit temperature distributions were measured initially due to incorrect temperature rake assembly. It was determined that contamination of the thermocouple insulation (MgO) had occurred by high-temperature brazing during rake assembly. Revised assembly procedures were used to eliminate this problem. Observation of the liner walls during the tests and subsequent inspection following rig disassembly showed no indication of hot regions.

Based on the above observations and the low-pressure-drop values, it was determined that the effective open area could be reduced by eliminating the cooling bands near the dome on the inner and outer walls. It was theorized that sufficient cooling protection to this first panel would be provided by the primary air from the swirlers.

A thermal paint test was conducted with this modified configuration, with an inlet air temperature of 512°F (maximum available from facility), $\Delta P/P = 0.03$ and an overall fuel-air ratio of 0.023. The average wall temperature was less than 700°F with a peak temperature of 900°F. Exit plane temperature data was not available due to instrumentation problems as discussed previously. The calculated ideal exit temperature was 1992°F.

Conclusions drawn from the results obtained in the above atmospheric tests were:

- Pressure drop of the modified combustor with combustion was approximately 3 percent at the design-point conditions.
- Flame location, coverage, and color showed that the initial combustor design was suitable for pressure testing and performance mapping.

- Liner cooling should be sufficient at the 16-atmosphere, design-point conditions to keep wall temperatures within acceptable limits (hot-spot temperature $\leq$ 1650°F).

- Ignition without preheat was a problem with the undeveloped fuel nozzle configuration. This problem could be overcome by reduction of the fuel droplet SMD, but because of time and cost considerations, no further development was undertaken.

3.3.4 Rich Limit Blowout Tests

Rich limit blowout tests were conducted at 1 atmosphere at a remote test site due to safety considerations. The tests were conducted with 2- and 3-percent pressure drop and inlet air temperatures between 200° and 450°F. During the tests, the airflow conditions were set, a low fuel flow was provided to permit ignition, and then fuel flow was increased to attempt a rich limit blowout.

Overall fuel-air ratios of approximately two times stoichiometric (f/a >0.12) were achieved for all test conditions without producing a blowout. At the high fuel-air ratios, the flame moved downstream of the primary zone. Since the flame would not propagate back into the primary zone when the fuel-air ratio was reduced, it was decided that rich limit blowout would be defined at the fuel-air ratio at which the flame began to move downstream of the primary zone (as indicated by thermocouples mounted on the combustor dome). However, subsequent tests to obtain this ratio were not valid because of erratic data. It was determined that the difficulty was the result of fuel coking within the fuel manifold and fuel nozzles during the rig preheat, since the manifold purge air had not been used. Based on the initial tests where it had been observed that good stability had been achieved at fuel-air ratios well above the stoichiometric overall fuel-air ratio (well in excess of the design point of 0.0285), it was concluded that rich limit stability would pose no problem for this combustor/fuel system design.

3.4 PRESSURE RIG TESTS

The high-pressure primary-zone combustion rig used in Phase II was modified such that it could be utilized for testing the combustor configuration. Figures 30 and 31 show the basic rig layout. Appropriate instrumentation to measure the following parameters was included:

(a) Inlet airflow - The inlet airflow was measured (±1% accuracy) by means of standard regularly calibrated orifice measuring sections upstream of the test rig. Test rig inlet air temperature and static and total pressure were measured at three circumferential locations around the inlet annulus.

Static pressures were measured by means of wall taps, total pressures by means of shielded total pressure probes, and temperatures by means of iron-constantan thermocouples.

(b) Fuel flow - The fuel flow rate was measured (±0.5% accuracy) by means of rotometers calibrated for high and low flow ranges. Delivery pressure was also measured for each flow rate.

(c) Discharge conditions - Temperatures were measured by means of two Pt/Pt10% Rh thermocouple rakes capable of rotation through 360 degrees.

Figure 32 shows the rake instrumentation head. The two rakes of three thermocouples were arrayed 112.5° apart such that when one set of three thermocouples was directly in line with one fuel nozzle, the second rake was between two fuel nozzles. The thermocouples were aspirated, and these aspiration tubes were also used to obtain averaged discharge emission samples. Temperature output was displayed on Brown recorders:

0 to 1000°F with ±2° accuracy for iron constantan,
0 to 2400°F with ±5° accuracy for chromel-alumel,
0 to 3000°F with ±2° accuracy for PtPt10% Rh.

Traverse data was also recorded automatically by means of a digital data acquisition system.

(d) Emissions - Gaseous emissions were measured with the AiResearch mobile emission unit. A schematic of the analyzer flow system is depicted in Figure 33.

Total hydrocarbon content of the gas sample was determined by means of a heated hydrocarbon analyzer, Beckman Instrument Model 402, which consists of the following:

- Heated, temperature-controlled sample line

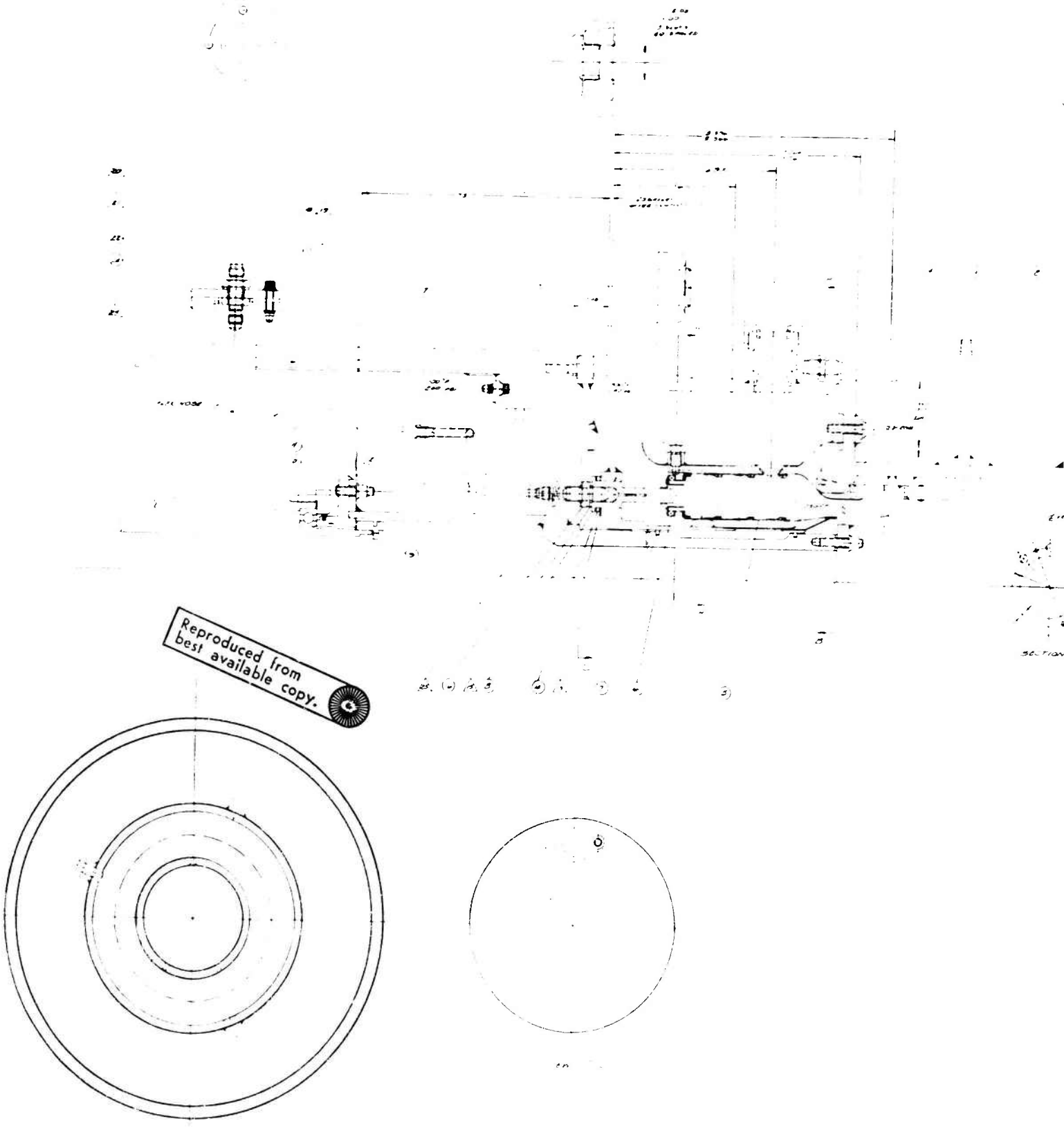

Figure 30. Combustor Rig Schematic.

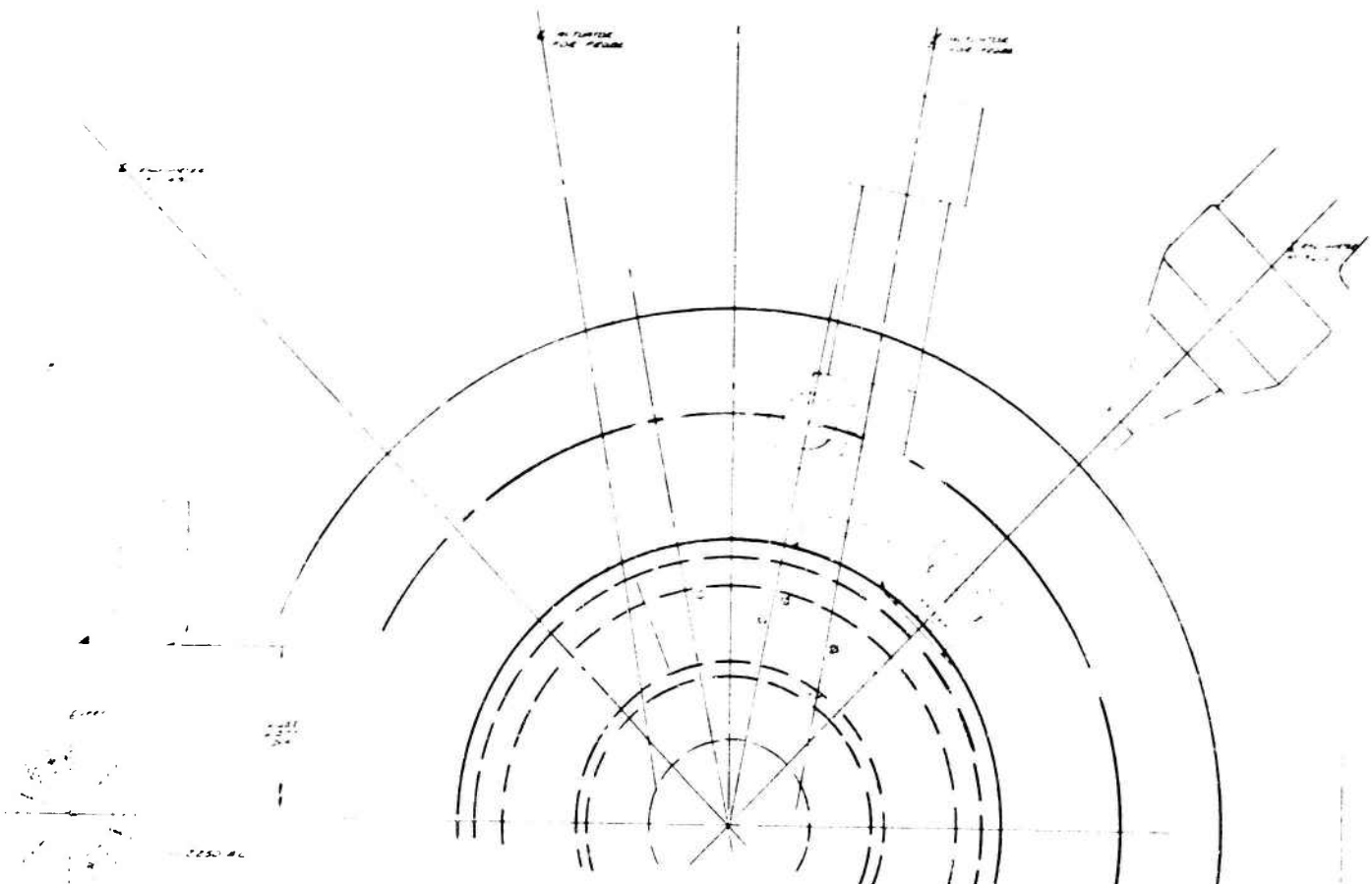

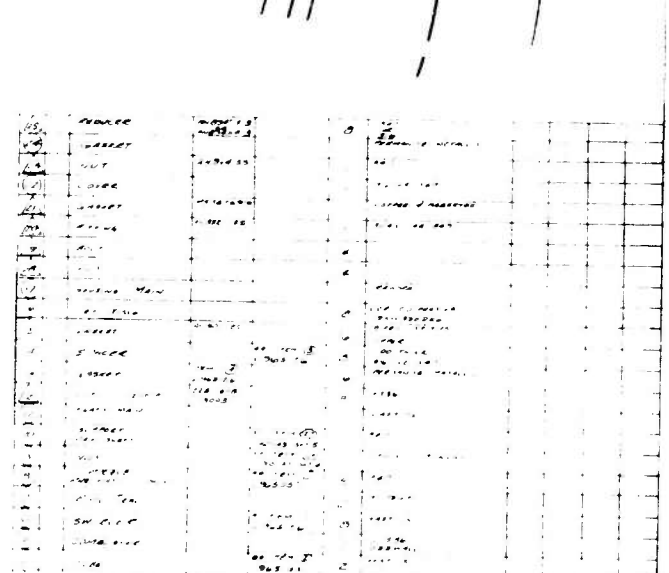

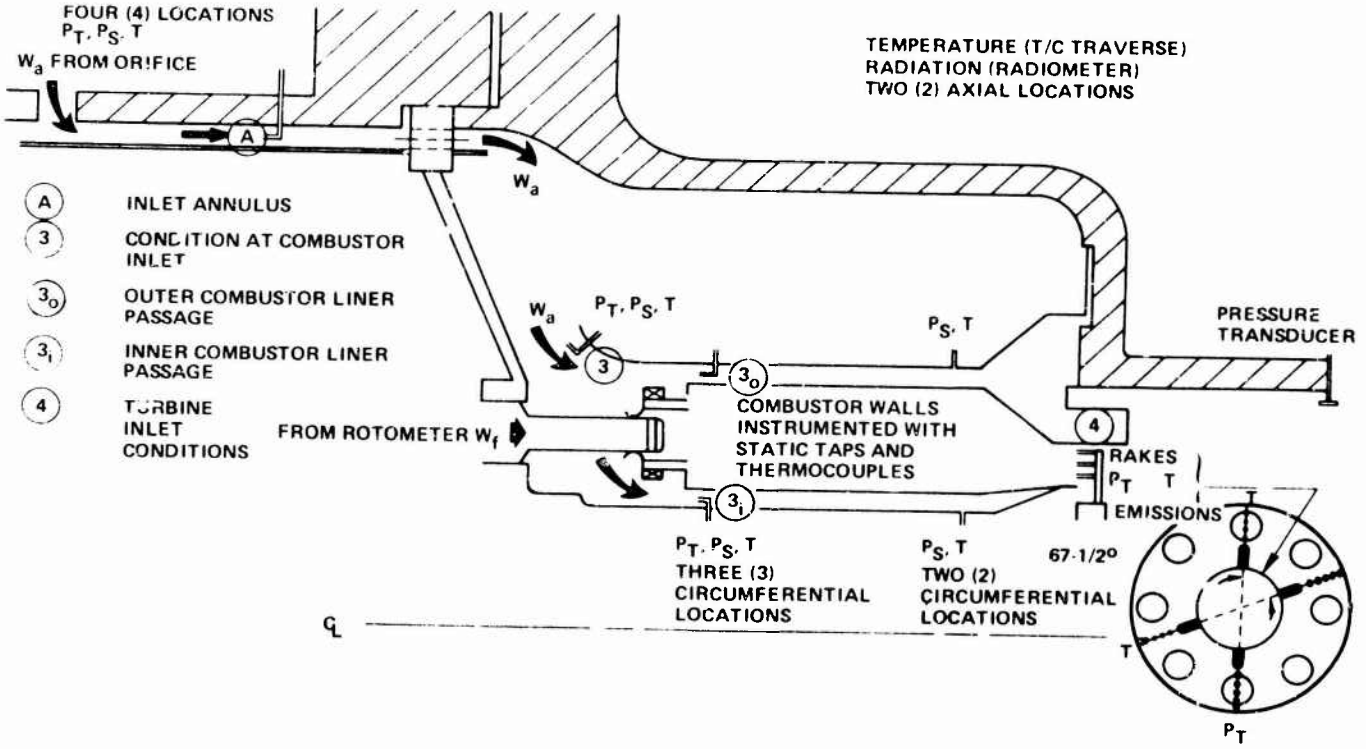

Figure 31. Test Rig Instrumentation Layout.

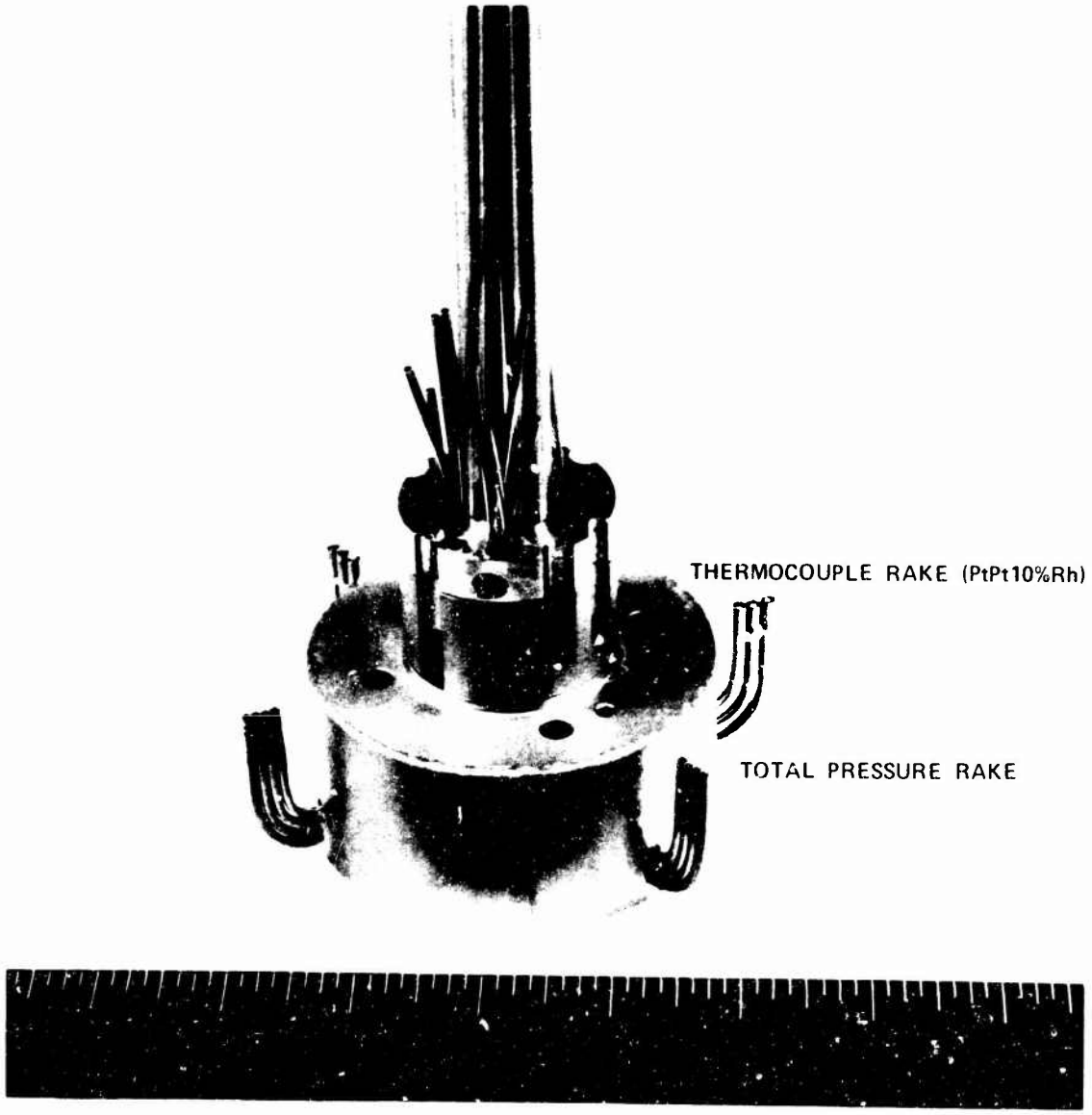

Figure 32. Combustor Exit Plane Instrumentation (Front Three-Quarter View).

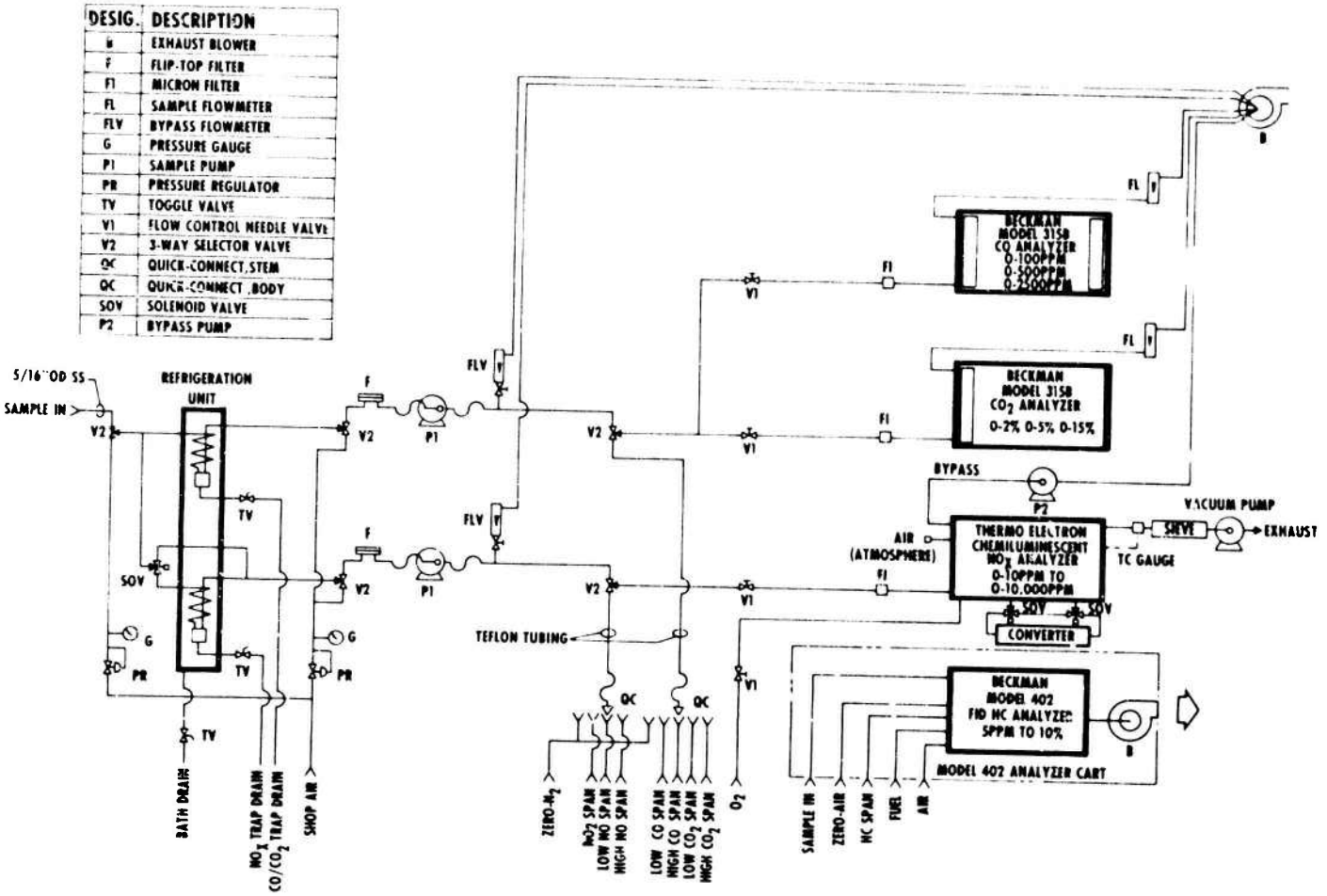

Figure 33. Exhaust Gas Analyzer Flow System.

- Analyzer unit, incorporating a flame-ionization detector and associated sample-handling system, with critical sample-handling components contained within a temperature-controlled oven

- Electronics unit, containing an electrometer amplifier and associated circuitry, readout meter, and recorder output provisions.

The NO and NO_x content was determined by the chemiluminescent NO-NO_x analyzer, Thermo Electron Corporation Model 10A.

The CO and CO_2 content was measured by the non-dispersive infrared (NDIR) analyzer, which consists of:

- Two infrared, energy beam sources

- Two flow-through-cell tubes, one containing a constant flow of sample gas and the other a gas selected for its negligible absorption of infrared energy of the wavelengths absorbed by the sample component

- A two-chambered detector, each chamber of which contains vapor of the same sample

Smoke was measured using the standard ARP1179 SAE millipore filter procedure.

The system analyzes wet samples of HC and NO_x and dry samples of NO, CO and CO_2. The emissions sampling and analyzing equipment conforms to the recommendations of SAE committee E31 (as outlined in ARP 1256 and ARP 1175 for gaseous and particular emissions, respectively). The equipment was calibrated and operated according to the SAE committee recommendations.

3.4.1 Perfor ance Survey

Initially, cold-pressure-drop tests were conducted in the pressure rig facility to determine cold pressure drop values and to ensure that there were no significant leaks.

Figure 34 shows a plot of combustor pressure drop against inlet corrected airflow. Pressure drop repeatability was within ±0.25 percent, and this variation was primarily due to leakage through the piston ring seals in the rig.

A preliminary evaluation test was conducted to provide some indication of rig and combustor performance at inlet pressures up to 16 atomspheres. Instrumentation included:

- Four liner wall thermocouples plus two dome thermocouples (refer to Figure 35)
- Outer and inner annulus total and static pressures
- Inlet airflow, pressure, and temperature
- Fuel flow and atomizer supply pressure
- Combustor discharge temperature and pressure rake

A summary of inlet conditions and the results obtained during the preliminary test are shown in Table III (Tests 5(2) through 5(4)). Circumferential and radial temperature profiles obtained during this test are shown in Figure 36 and 37 respectively. Calculated efficiency, based on the average temperature rise and overall fuel-air ratio determined by rake rotation through 360° at 22-1/2° increments, was 99 percent with a pattern factor of 0.239.

Disassembly following the 16-atmosphere pressure run revealed that one of the fuel nozzle centerbody cones had been damaged. This damage was apparently the reason for a hot streak visible on the combustor liner in line with the damaged nozzle and a corresponding increase in pattern factor due to a hot peak occurring at the same circumferential location. No absolute explanation can be given for this single nozzle failure, but it is believed that it was caused by severe misalignment of this one nozzle. Following nozzle repair, a more secure method of mounting the nozzles was adopted in an attempt to preclude misalignment in subsequent tests.

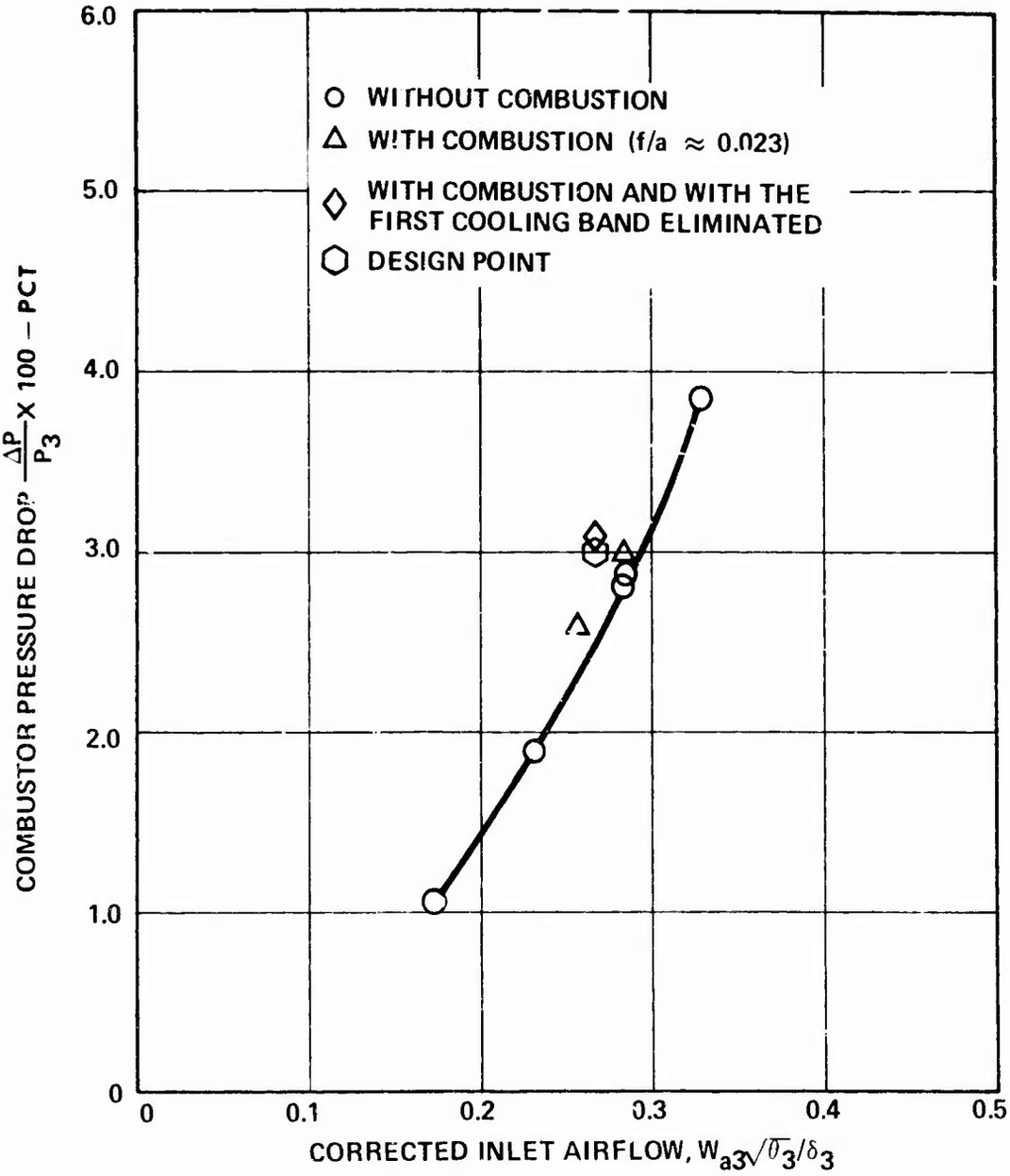

Figure 34. Combustor Pressure Drop vs Corrected Inlet Airflow in Pressure Rig.

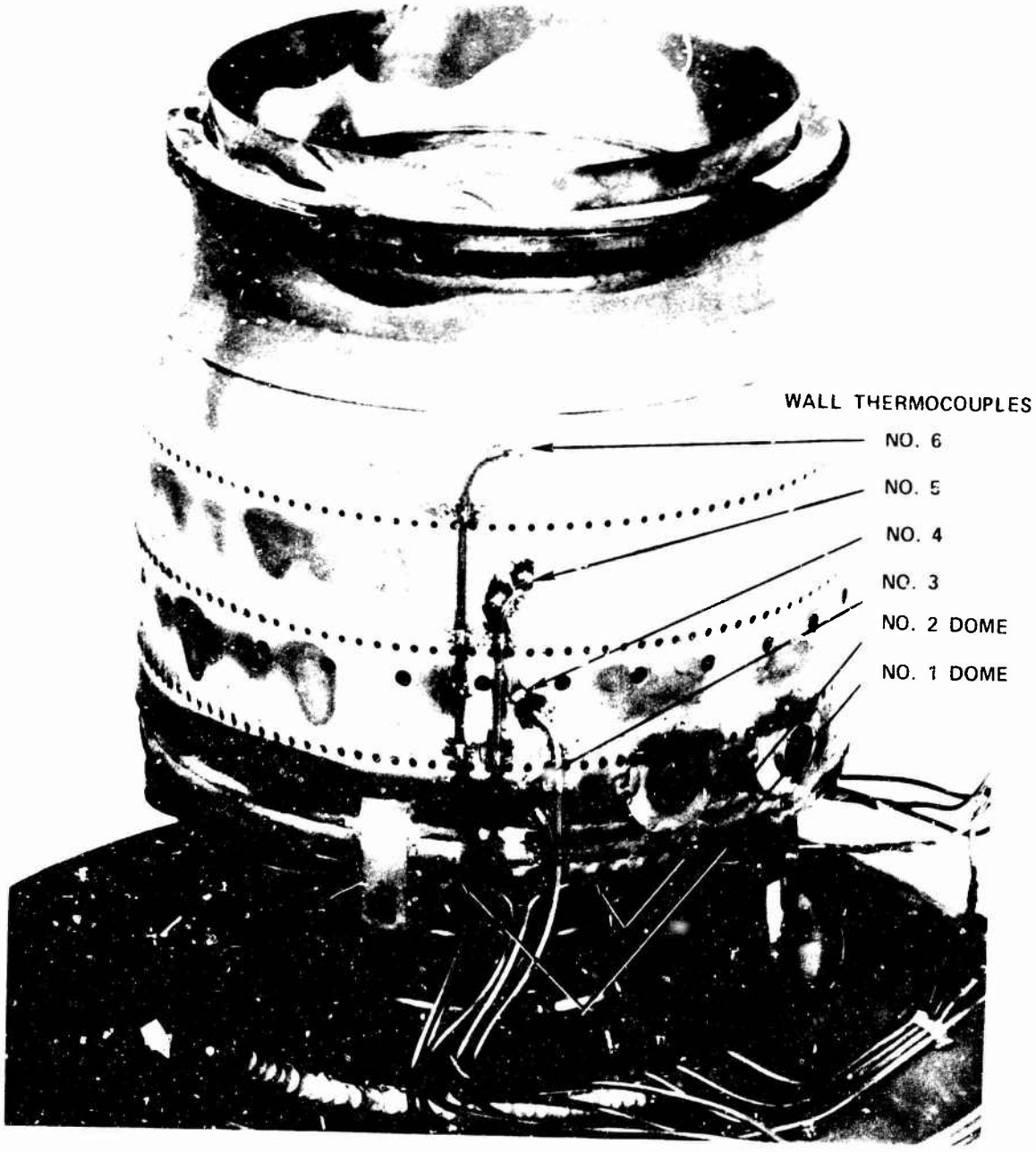

Figure 35. Combustor Wall Thermocouples.

TABLE III. PRESSURE RIG PERFORMANCE DATA

Test (Run) Number	Combustor Inlet Conditions						Combustor Wall Temperatures (Thermocouple Data) (1) (°F)						Combustor Performance					
	P_3 (psia)	T_3 (°F)	W_a (lb/sec)	W_f (4) (lb/hr)	$\frac{\Delta P}{P_3}$ (%)	f/a	T/C No. 1	T/C No. 2	T/C No. 3	T/C No. 4	T/C No. 5	T/C No. 6	T_4 (°F)	T_4 (°R)	Pattern Factor (2)	η_b Efficiency (%)	Blow-Out f/a	Blow-Out f/a
5 (2)	1	237	0.234	24.5	3.1	0.0292	360	520	360	390	445	510	1909	2439	0.317	69.4	0.032	0.017
5 (3)	6	600	1.078	80.0	2.6	0.0210	745	970	975	940	815	875	2183	2643	0.160	100 (3)	0.0087	0.0079
5 (4)	16	775	3.020	245.5	2.7	0.0226	915	1090	1150	1043	980	1045	2383	2923	0.330	100 (3)	-	0.0094
5 (5)	16	750	2.860	253.0	3.1	0.0260	-	1050	860 (5)	825 (5)	-	-	2363	2743	0.239	99.0	-	-

NOTES:

(1) Thermocouple locations shown on Figure 32.

(2) Pattern Factor = $\frac{T_{max} - T_{avg}}{T_{avg} - T_3}$

(3) Indicated efficiency is greater than 100 percent due to air leakage in the rig, and therefore the calculated fuel-air ratio is incorrect.

(4) JP-4 fuel.

(5) Thermocouple readings believed to be incorrect.

(6) Combustor efficiency = Actual Temperature Rise / Ideal Temperature Rise.

NOTES: 1. COMBUSTOR INLET CONDITIONS AND PERFORMANCE ARE DEFINED IN TABLE III (TEST 5(5))

2. RADIAL POSITION OF THERMOCOUPLES
   - □ – INSIDE
   - ○ – CENTER
   - △ – OUTSIDE

3. ↑ INDICATES RADIAL POSITION OF FUEL NOZZLES
4. ↑ INDICATES RADIAL POSITION OF IGNITORS

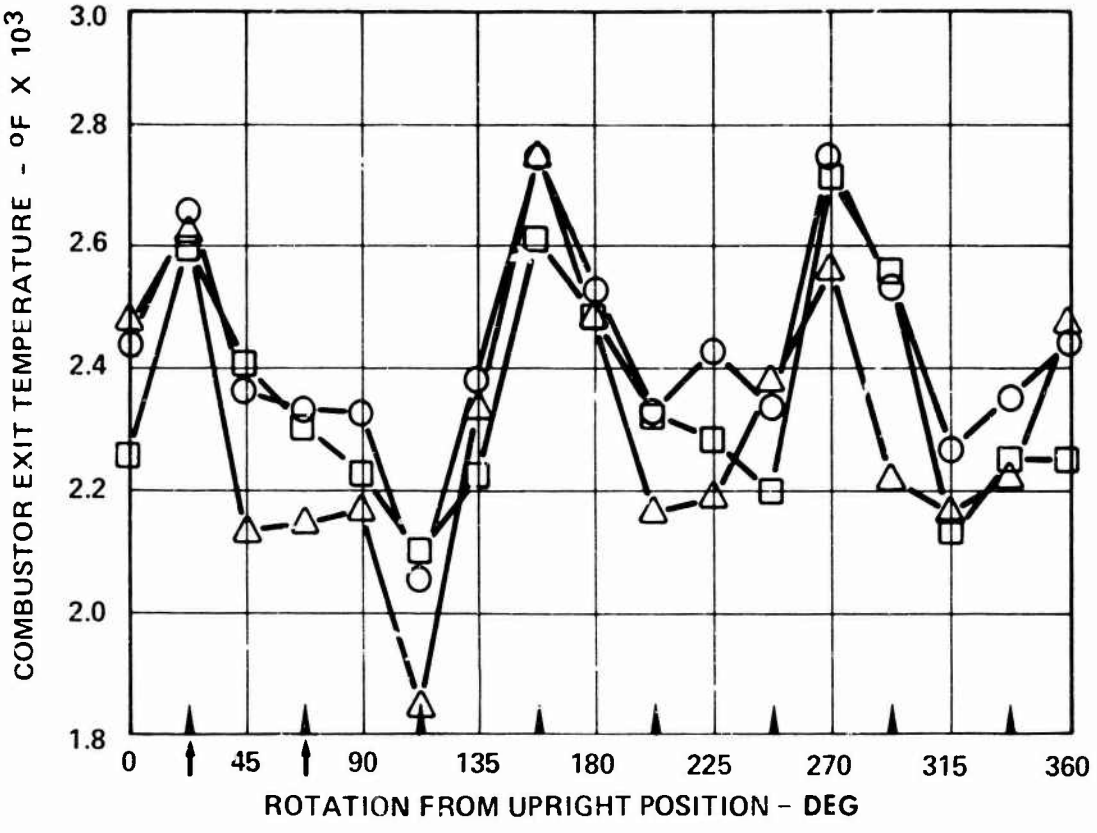

Figure 36. Combustor Exit Circumferential Temperature Distribution (P_3 = 16.0 ATM).

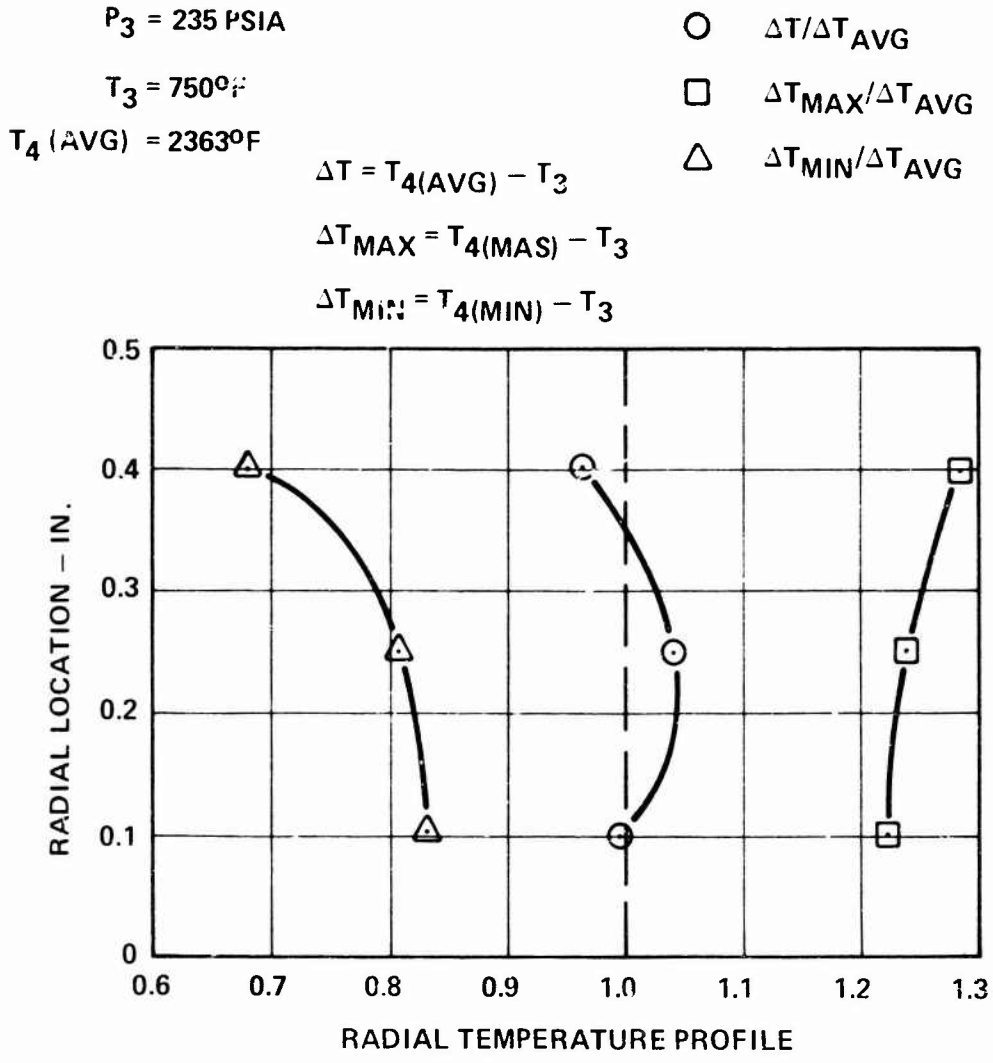

Figure 37. Radial Temperature Profile for Test 5 (5).

3.4.2 Wall Temperature Measurement

Testing was conducted at conditions near the design point to determine the combustor surface temperature gradients. The combustor was painted with thermopaint, OG-6, temperature-sensitive coating and run for the coating calibration time of 5 minutes. Facility limitations restricted the inlet air temperature to 750°F. A discharge temperature of 2500°F was set based on stationary discharge thermocouples. Subsequent analysis of the more complete exit temperature data. 48 thermocouple readings, obtained from the 360° rake rotation during the test (Test 5(5) from Table III) indicated that the actual average temperature was 2363°F. Maximum liner hot spots were 1600°F located in the first inner and outer panel. The average liner temperature was less than 1200°F.

3.4.3 Performance Mapping Tests

The previously described atmospheric rig tests, performance survey and thermopaint tests were conducted with the combustor fabricated from Hastelloy-X. These tests indicated that the performance characteristics of the initial combustor design were acceptable (by comparison to the contracted performance goals and within the current schedule and budgetary constraints).

A second combustor of identical geometry was fabricated from IN-586 (refer to Volume I, Section 3.0) for the following tests. The performance mapping tests were conducted over the operating range to determine

- Combustion efficiency
- Pattern factor (PF)
- Light-off and lean-blowout characteristics

The inlet conditions (temperature, pressure and airflow rate) were selected to adequately cover the combustor operating range. The effects of T_3 and the overall fuel-air ratio on PF and combustion efficiency were studied at the conditions outlined in Table IV. A summary of the results is shown in Table V.

The temperature readings at the exit plane were taken at 10-degree intervals around the circumference at each of the three thermocouple radii. Typical temperature traverse results are shown in Figures 38 and 39.

TABLE IV. INLET CONDITIONS FOR PERFORMANCE MAPPING TEST

Simulated Altitude (feet)	N_{GG} (%)	P_3 (psia)	T_3 (°F)	W_{a3} (lb/sec)
Sea level (Design)	100	235.7	830	2.733
Sea level	80	119.1	594	1.632
Sea level*	75	101.5	548	1.42
Sea level*	70	83.64	493	1.228
6000	100	197.4	807	2.294
15000	100	147.3	776	1.709
20000	100	123.3	755	1.434
25000	100	101.9	734	1.186
25000	70	39.62	393	0.612
-	-	14.7	-	0.23
S.L. Light-off Point	-	20.6	170	0.4
25,000 feet, M = 0 Light-off Point	-	7.9	76	0.14
45,000 feet, M = 0.85 Light-Off Point	-	4.2	72	0.11

*Idle condition defined at 5% power, N_{GG} = 75% (Test not conducted at this point)

TABLE V. TESTING RESULTS SUMMARY

Run Number	P_3 (psi)	T_3 (°R)	W_{a3} (lb/sec)	$W_{a3}\sqrt{\theta_3}/\delta_3$ (lb/sec)	$\frac{\Delta P}{P} \times 100$ (%)	f/a	T_4 (°R)	PF	$\eta_b^{(4)}$
1	14.72	717.3	0.239	0.28	2.91	0.0287	2460	0.255	0.928
2	14.68	712.0	0.239	0.2797	2.94	0.0207	1887	0.406	0.83
3	14.74	806.3	0.223	0.277	3.15	0.0289	2548	0.225	0.94
4	14.7	795.0	0.223	0.276	3.2	0.0221	2226	0.266	0.982
5	14.78	891.0	0.2125	0.28	3.3	0.0288	2655	0.217	0.962
6	14.77	887.0	0.2125	0.273	3.3	0.0216	2341	0.378	1.0
7	40.8	857.3	0.612	0.283	2.76	0.0150(1)	2006	0.365	1.0
8	40.8	844.0	0.612	0.286	2.84	0.020	2304	0.317	1.0
9	39.9	848.7	0.612	0.287	2.92	0.0273	2828	0.258	1.0
10	78.2	951.7	1.228	0.313	3.12	0.015	2166	0.359	1.0
11	78.1	956.3	1.228	0.313	3.04	0.02	2520	0.289	1.0
12	78.0	950.3	1.228	0.313	3.18	0.0251	2841	0.307	1.0
13	81.4	950.3	1.228	0.3		0 to 10	1546	0.4	0.948
14	152.4	1161.7	1.183	0.254	1.92	0.015	2343	0.353	1.0
15	152.6	1166.7	1.183	0.254	2.09	0.02	2672	0.328	1.0
16	153.0	1170.3	1.183	0.253	1.98	0.025	2984	0.24	1.0
17	152.9	1171.7	1.183	0.254	1.88	0.010	1945	0.328	1.0
18	153.7	1171.7	1.433	0.2576	2.11	0.014	2201	0.299	1.0
19	153.9	1166.7	1.433	0.2569	2.12	0.019	2618	0.273	1.0
20	153.9	1176.7	1.433	0.2576	2.22	0.024	2742	0.217(2)	1.0
21	152.9	1178.3	1.433	0.2582	2.33	0.0098	1838	0.318(2)	1.0
22	147.16	1168.3	1.708	0.2545	2.36	0.0141	2085	0.203(2)	1.0
22(3)	148.96	1149.7	1.708	0.2504	2.74	0.0141	2265	0.318	1.0
23	147.4	1150.7	1.708	0.2532	2.03	0.0190	2612	0.308	1.0
24	147.2	1153.7	1.708	0.2537	2.06	0.0097	1881	0.416	1.0
25	147.2	1154.7	1.708	0.254	2.28	0.0228	2794	0.271	1.0
26	196.6	1173.3	2.293	0.2574	2.05	0.015	2347	0.315	1.0
27	196.7	1171.7	2.293	0.257	2.06	0.0185	2543	0.365	1.0
28	196.9	1181.7	2.293	0.2593	2.09	0.0094	1903	0.380	1.0
29	197.8	1195	2.298	0.2581	2.17	0.0232	2940	0.337(4)	1.0
30	233.6	1205.0	2.733	0.2595	2.20	0.0095	1916	0.260	1.0
31	234.4	1210.0	2.733	0.2607	2.31	0.0143	2430	0.262(2)	1.0
32	236.4	1208.3	2.733	0.2589	-	0.0191	2675	0.2825(2)	1.0
33	237.4	1210	2.733	0.258	2.33	0.0243	2937	0.295(2)	1.0
5(5)	235.0	1210	2.617	0.268	3.1	0.026	2823	0.239	1.0

(1) Because of leakage, true f/a is higher than indicated f/a and pressure drop is lower also.

(2) P.F. extrapolated by using two thermocouple readings

(3) P.F. at design point with design pressure drop

(4) η_b from thermocouple traverse

(5) Data from Test 5(5) presented here for comparison

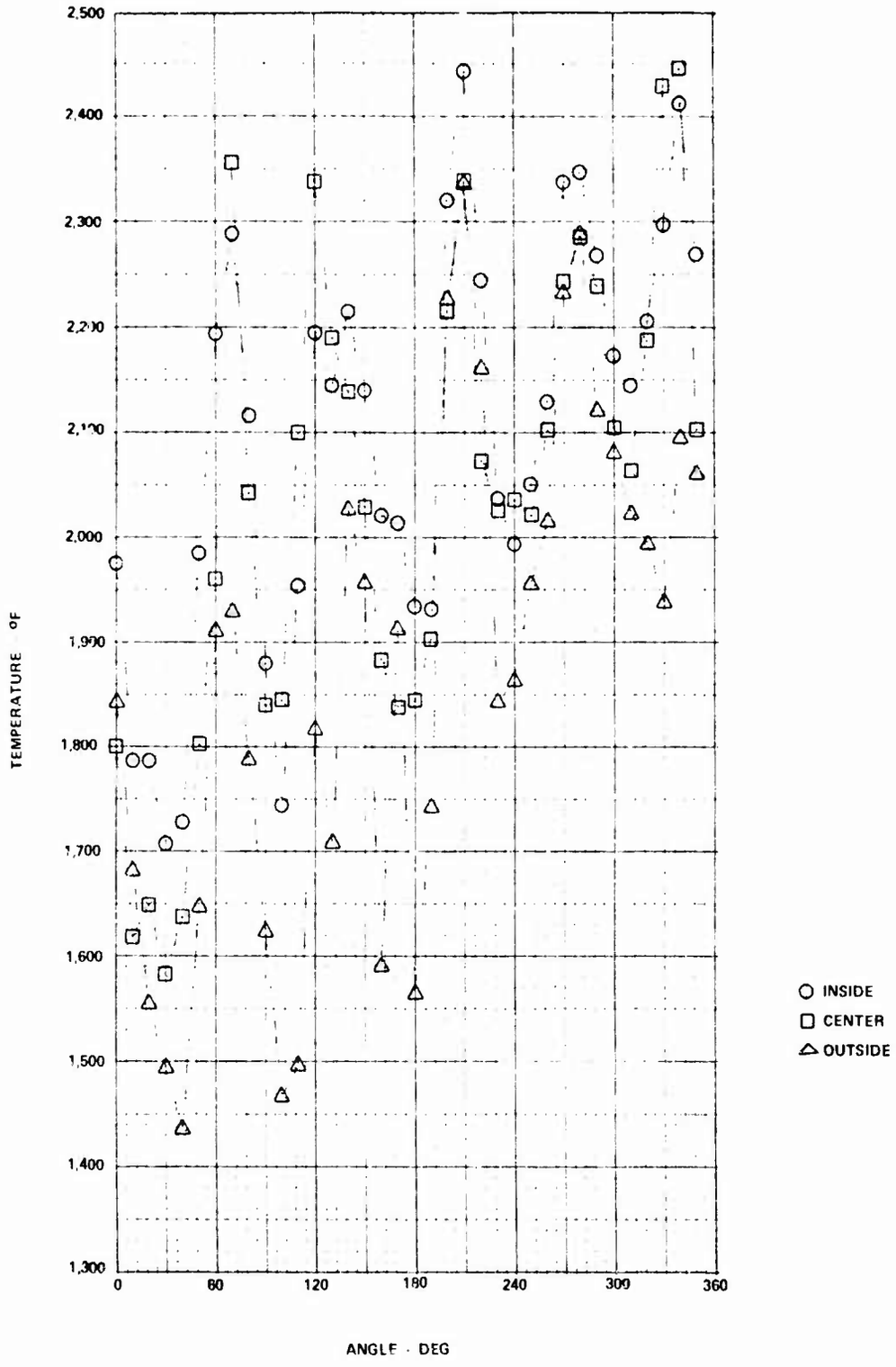

Figure 38. Temperature Traverse of USAAMRDL Combustor, (P_3 = 14.7 psi, W_{a3} = 0.239 lb/sec, T_3 = 717°R, f/a = 0.0287).

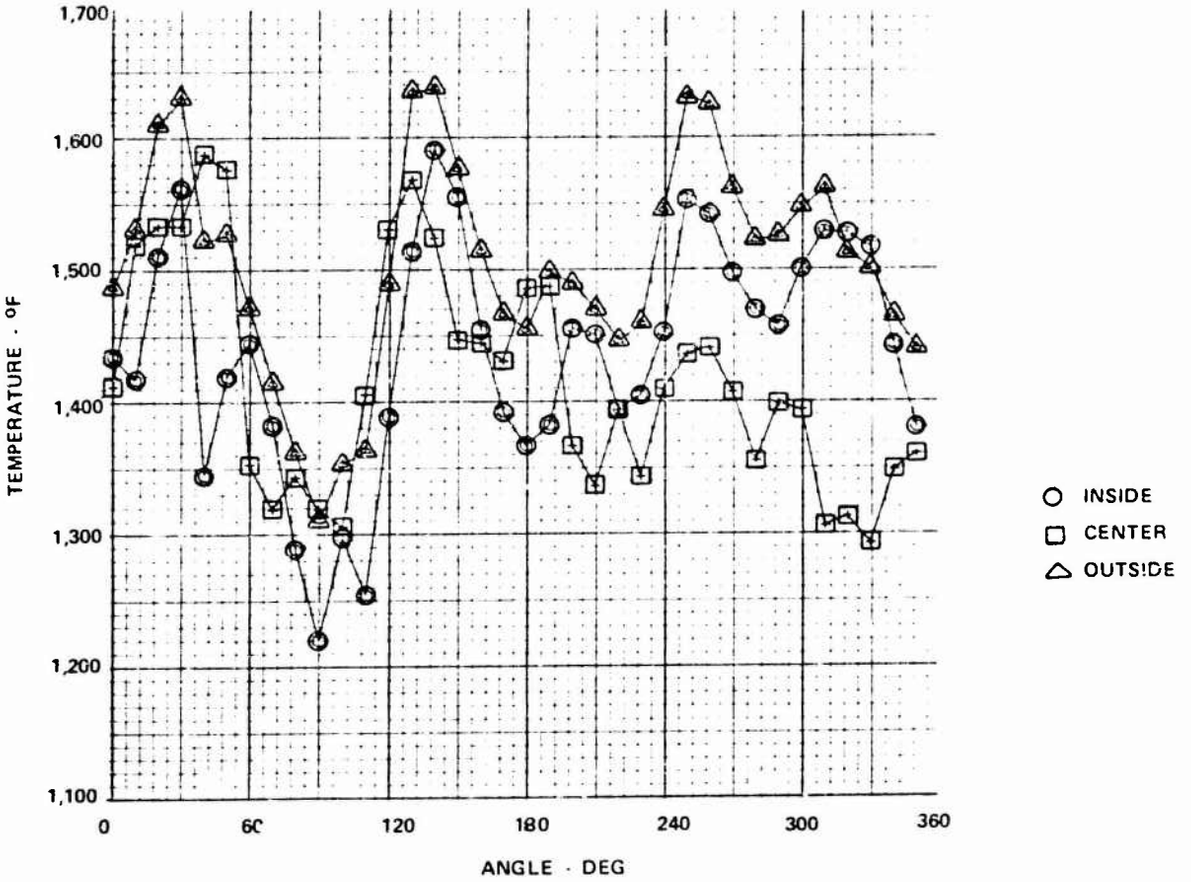

Figure 39. Temperature Traverse of USAAMRDL Combustor (P_3 = 235.5 psi, W_{a3} = 2.733 lb/sec, T_3 = 1205°R, f/a = 0.0095).

The PF and combustion efficiency (calculated by the ratio of actual temperature rise to ideal temperature) for different conditions are also listed in Table V. The calculated combustion efficiency in most of the runs is more than 100 percent (up to 115 percent in some cases). This could be attributed either to leakage (resulting in actual fuel-air ratio higher than calculated) or to error in thermocouple readings. A simple analysis taking into account convection, conduction and radiation losses from thermocouples showed that thermocouple readings were 20° to 50°F lower than actual values. Hence, the major factor in the error was attributed to leakage. By comparing measured fuel-air ratios with those calculated from the gas sampling analysis, it was possible to obtain a correction factor for the measured fuel-air ratios taken in the T_4 survey tests. The efficiencies calculated using the corrected fuel-air ratios were then found to be closer to 100 percent (up to 105 percent against 115 percent for uncorrected fuel-air ratio cases).

To provide as much performance data as possible, the design point test (Run number 33) was conducted last, because of the possibility of a failure occurring at the high-temperature, high-pressure conditions. A review of the data, subsequent to the test, indicated that the pressure drop was low (indicating system leaks) and that only two exit-plane thermocouples were functioning for the measurement of the exit temperature, efficiency, and pattern factor. Therefore, the best indication of design-point performance is Run number 5(5) from the performance survey tests (Table III).

The computed combustion efficiency (η_B) from the performance mapping tests was plotted against three of the most common aerodynamic loading parameters. Results using the loading parameter in Equation (9) over a limited range, such as operating at simulated sea-level conditions, are shown in Figure 40.

$$\text{Loading Parameter} = Q = W_{a3} K^{1/2} / V \delta_3^2 T_3^{1/2} \qquad (9)$$

where W_{a3} = combustor airflow, lb/sec

V = combustor volume, ft^3

δ_3 = combustor inlet pressure, atm

T_3 = combustor inlet temperature, °R

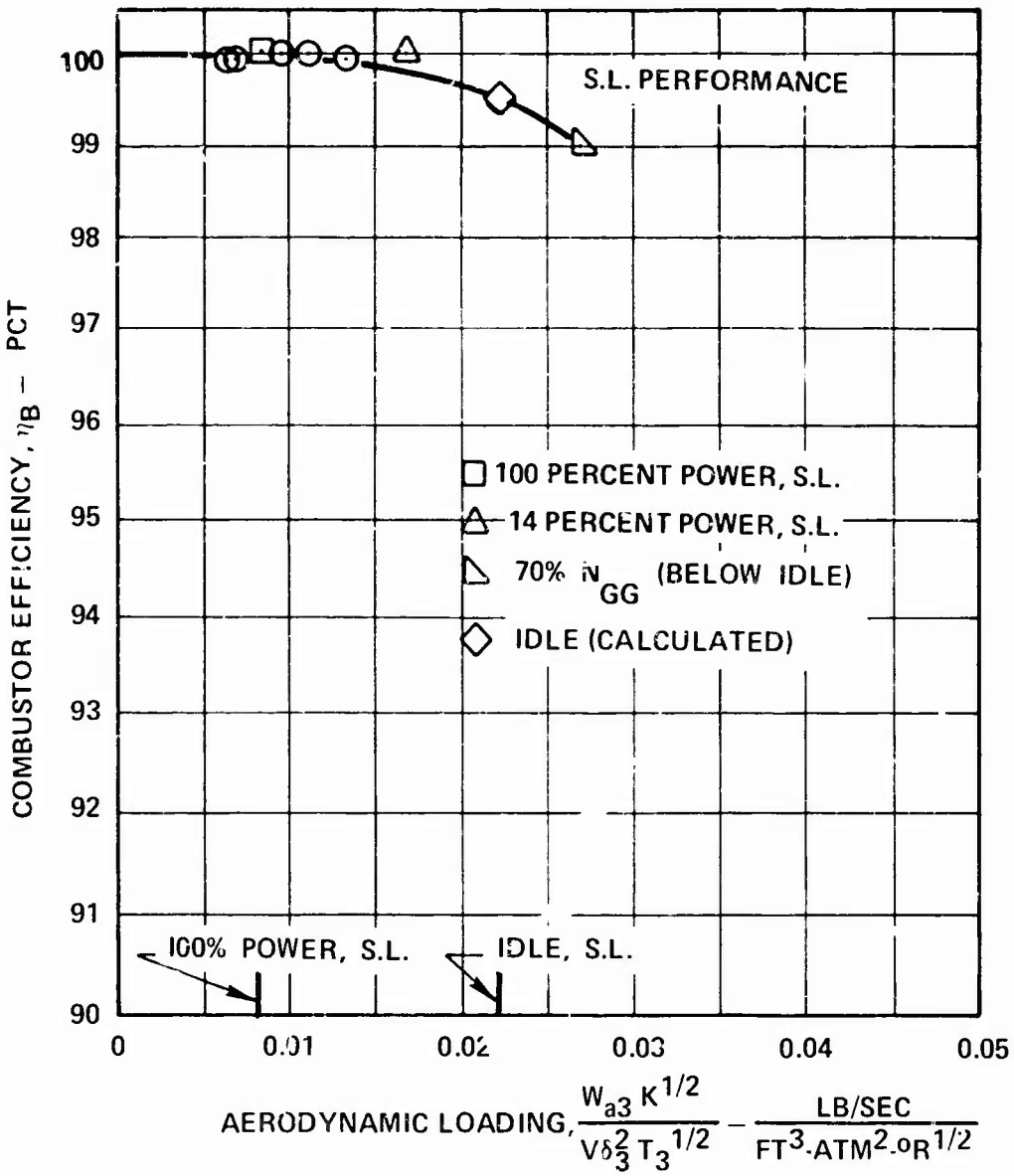

Figure 40. Correlation of Combustor Efficiency With Aerodynamic Loading for a Limited Range.

$$k = \begin{cases} (f/a)/0.02 \text{ if } f/a > 0.02 \\ 1.0 \text{ if } 0.012 < f/a > 0.02 \\ 0.012/(f/a) \text{ if } f/a \leq .012 \end{cases}$$

A sample calculation of Q [see Equation (9)] at the idle (sea level, static) condition is presented here for clarification:

$$Q = W_{a3} K^{1/2} / V \delta_3^2 T_3^{1/2}$$

At idle,

$W_{a3} = 1.42$ lb/sec

$V = 0.044$ ft^3

$\delta_3 = \frac{101.5}{14.7} = 6.9$ atm

$T_3 = 1007°R$

$f/a = 85/(1.42 \times 3600) = 0.0166$

Therefore, $K = 1.0$

$$Q = \frac{1.42 \times (1.0)^{1/2}}{0.044 \times (6.9)^2 \times (1007)^{1/2}} = 0.021 \text{ lb/sec ft}^3 \text{ atm}^2 - °R^{1/2}$$

When this parameter was used over the entire range of combustor operation, as shown in Figure 41, a satisfactory correlation was not obtained. This may be partially explained by the following:

The combustion efficiency could not be well correlated by P_3^2/W_{a3} (which is proportional to $P_3 T_3 / V_{REF}$).
Lefebvre's parameter,

$$Q = W_{a3}/(\delta_3)^{1.75} V \exp(T_3/b) \qquad (10)$$

where $b = 540°R$

was found to more adequately correlate the combustion efficiency data. This parameter, which can be derived by applying turbulent flame theory, has been useful in correlating combustion efficiencies of different combustors. The most significant drawback is that the empirical constant "b" is not a unique function of f/a and may also depend upon different

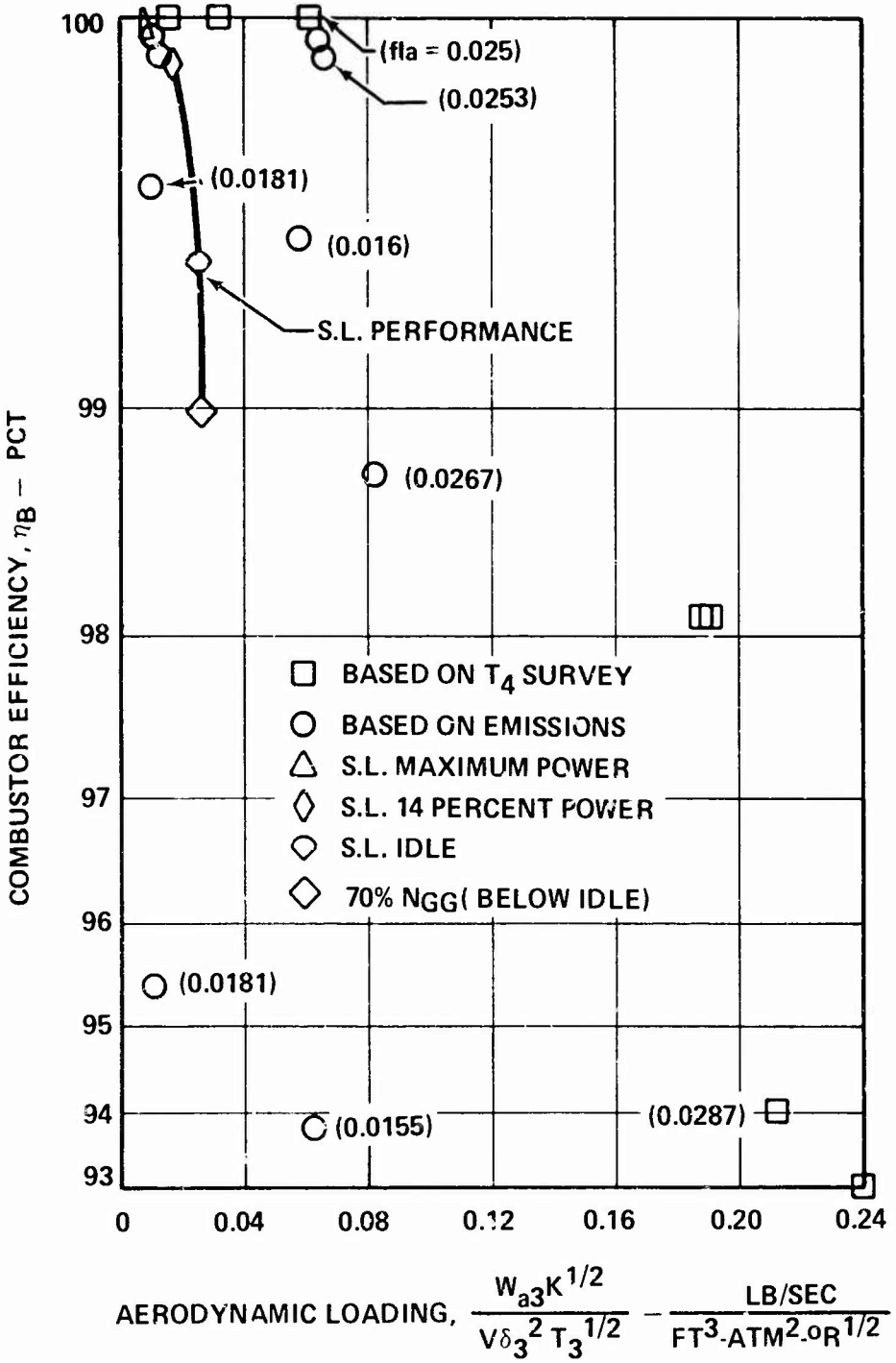

Figure 41. Combustor Efficiency of Designed Combustor.

combustor parameters. However, a reasonable correlation was obtained as shown in Figure 42. The combustion efficiency for most of the points shown is based upon the gas sampling analysis. These points are indicated by the symbols for sea level power ratings. The other symbols represent data from a T_4 survey taken at 1 atmosphere where the air leakage was minimum. It may be noted (Figure 42) that combustion efficiency over the entire range of operation (sea level and 25,000 feet, maximum power to idle) is never less than 99 percent and is approximately 99.5 percent at the idle point (75% N_{GG}, 5% power).

Effect of T_3 on PF is shown in Figure 43. As expected, PF improved with increase in inlet temperature due to higher evaporation rate and lower SMD with increasing T_3 as shown previously in Figure 14. It can be concluded from Figure 43 that PF also improves with fuel-air ratio at 1 atmosphere. This trend is also followed at higher P_3, as shown by runs 7 through 17 (refer to Table V).

The minimum value of PF at 1 atmosphere, T_3 = 891°R, and f/a = 0.0288 was 0.217 (run No. 5 in Table V). It can be expected that PF of the present combustor should improve with increasing P_3 for the same equivalent flow rate, T_3 and fuel-air ratio. This is because of better atomization characteristics of the air-shear system at higher pressures in addition to other variables. However, most of the values of PF in runs at higher pressures are in excess of 0.217. This can be explained as follows.

It has been shown that PF improves with increasing combustor pressure drop when equivalent flow rate, P_3, T_3 and fuel-air ratio are kept constant[8]. (Note that, due to leakage, the pressure drop in Runs 14 to 33 was as much as 1.0 percent lower than expected.) Therefore, it appears that PF for the conditions shown in Runs 13 through 19 and 23 through 28 (where all three radially located thermocouples were functioning properly) could be lower than the rig calculated values shown in Table V.

In some of the runs (superscripted 2), one of the three radially located thermocouples was not functioning. For these runs, PF was extrapolated. For runs with all three thermocouples working, it was observed that the ratio of the central thermocouple average reading to the inner or outer thermocouple average reading was relatively constant. Therefore, if averages of two radial thermocouples were known, it was possible to calculate the average reading of the third thermocouple and hence average T_4, then PF could be calculated.

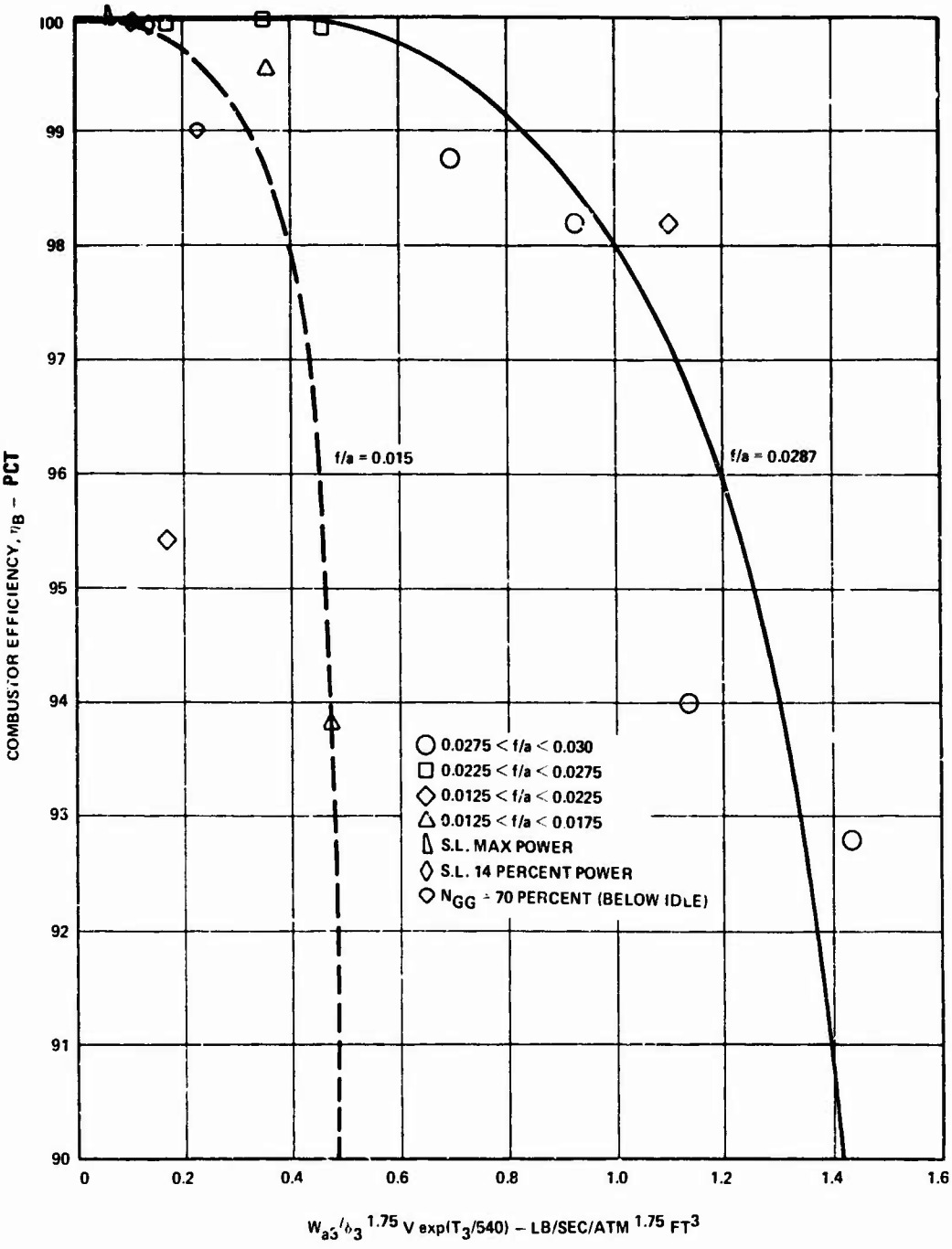

Figure 42. Combustion Efficiency Correlation With Lefebvre's Parameter.

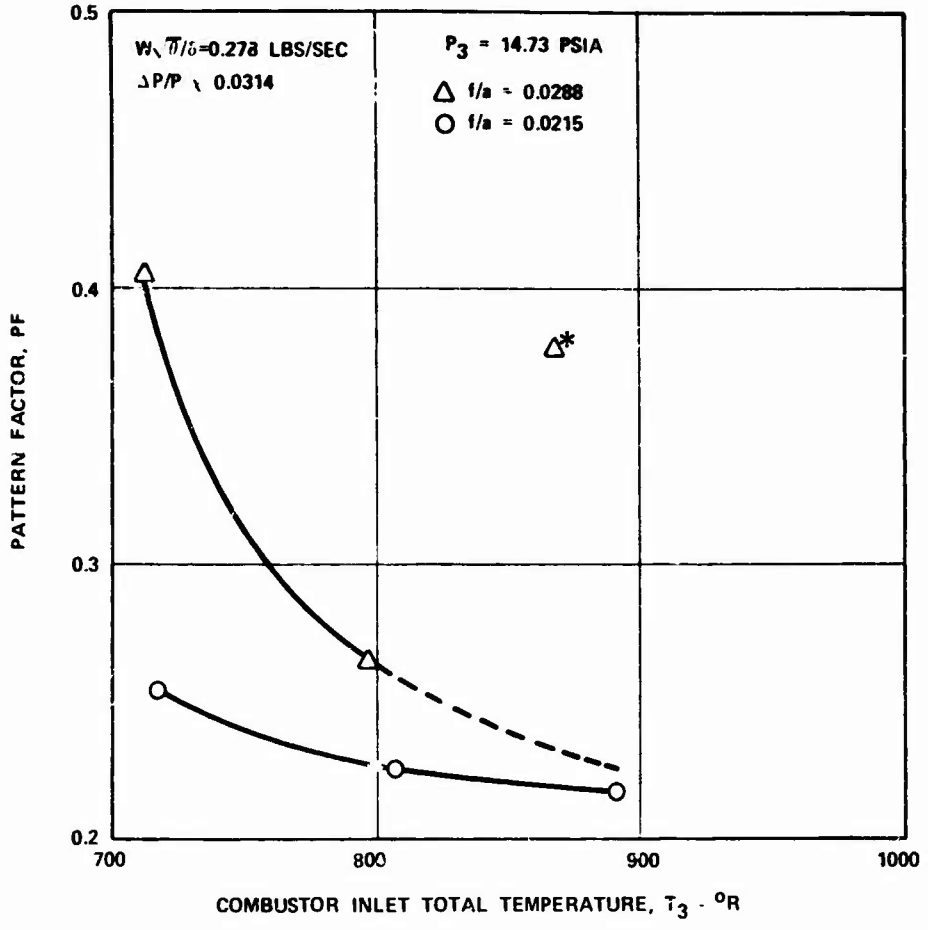

*THIS POINT WAS RERUN BUT PF WAS STILL HIGHER DUE TO ONE FUEL NOZZLE'S BURNED-OUT TIP.

Figure 43. Effect of Combustor Inlet Temperature on Pattern Factor.

The effect of combustor pressure drop on PF at S.L. design point is illustrated by Runs 33 and 5(5), pressure drops being 2.33 and 3.1 percent, respectively. Thus, at S.L. design condition, a 0.77-percent decrease in pressure drop increased PF by 0.056, or about 20 percent of PF of Run 33. With this observation, it can be concluded that PF values for runs listed in Table V at the high fuel-air ratios lie in the range of 0.217 to 0.334, and most of them are less than 0.25.

The light-off (LO) and lean blowout (LBO) fuel-air ratios with JP-4, -5 and -8 fuel were obtained for the runs listed in Table V. For these tests, the fuel temperature was not conditioned to correspond to the simulated test condition. The LO and LBO fuel-air ratios are generally represented as a function of airflow (W_{a3}) or reference velocity and combustor pressure. However, by noting that ignition energy is proportional to $e^{-T_3} V_{REF}/P_3^2(f/a)$, it can be shown that

$$f/a_{(LO)} = F(e^{-\theta_3} V_{REF}/\delta_3^2) \qquad (11)$$

where F = "function"

$\theta_3 = T_3/520$

V_{REF} = mass mean velocity at the combustor exit area at the combustor inlet conditions = $W_{a3}/P_3 A_{REF}$

$\delta_3 = P_{t3}/14.69$

Therefore, all the data points for LO fuel-air ratio at different values of inlet pressure, temperature and airflow should fall on the same curve of LO fuel-air ratio versus $e^{-\theta_3} V_{REF}/\delta_3^2$. This is shown by the correlations in Figure 44. From these correlations, a plot of LO fuel-air ratio versus altitude was prepared (Figure 45). Except at lower power settings and high-altitude conditions, LO fuel-air ratio variations with fuels JP-4, -5, and -8 are within the experimental uncertainties. At lower values of T_3 and P_3, LO fuel-air ratio is higher with JP-5 and JP-8 as compared to JP-4. Light-off with JP-4 at 25,000 feet, M = 0, and 45,000 feet, M = 0.85, could not be obtained. This was as expected due to coarse droplet size and low T_3.

The LBO fuel-air ratio can be explained by considering the balance of heat generation due to chemical reaction and heat loss due to convection. From dimensional arguments, LBO fuel-air

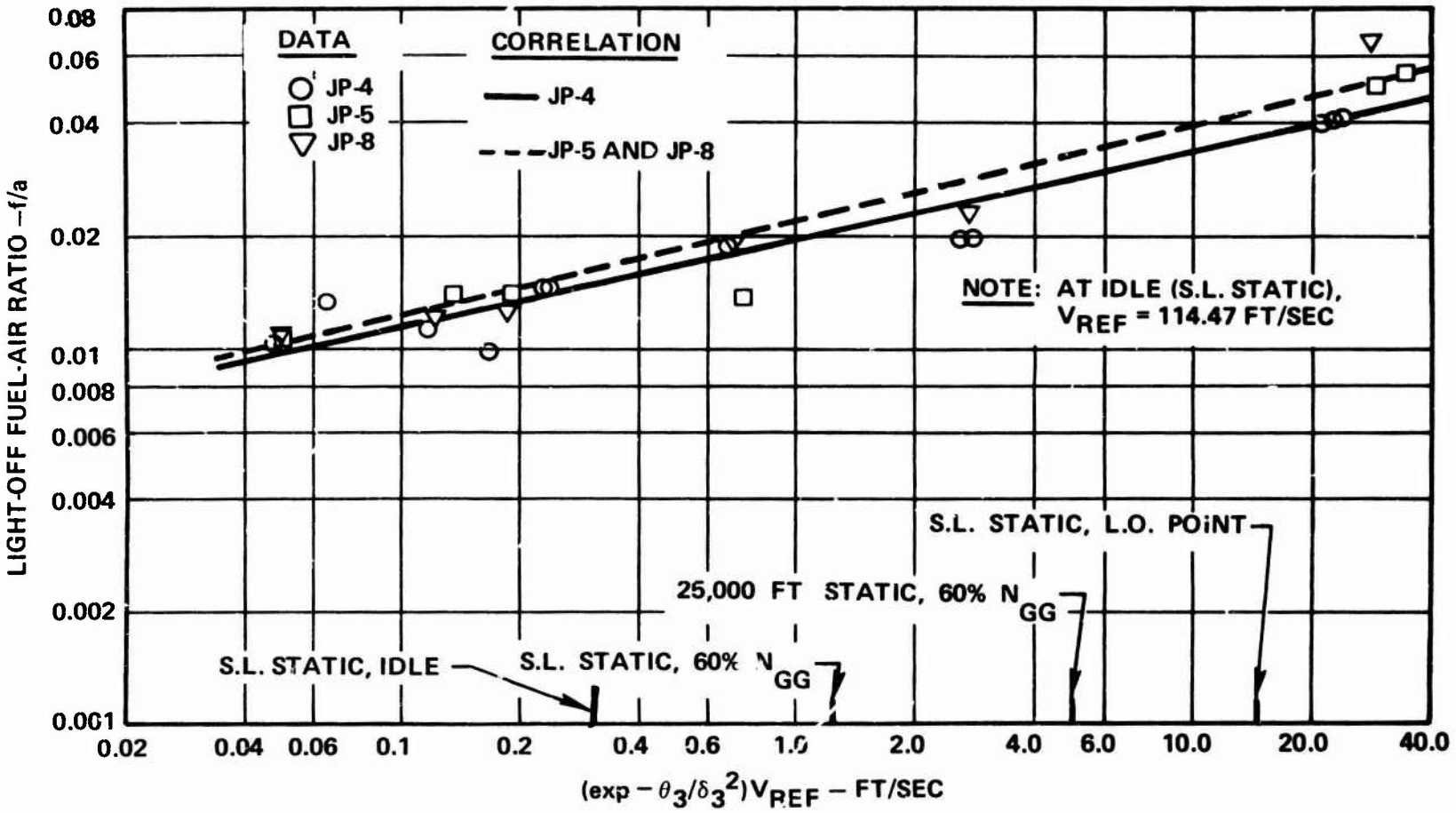

Figure 44. Light-Off Fuel-Air Ratio of Combustor With Different Fuels.

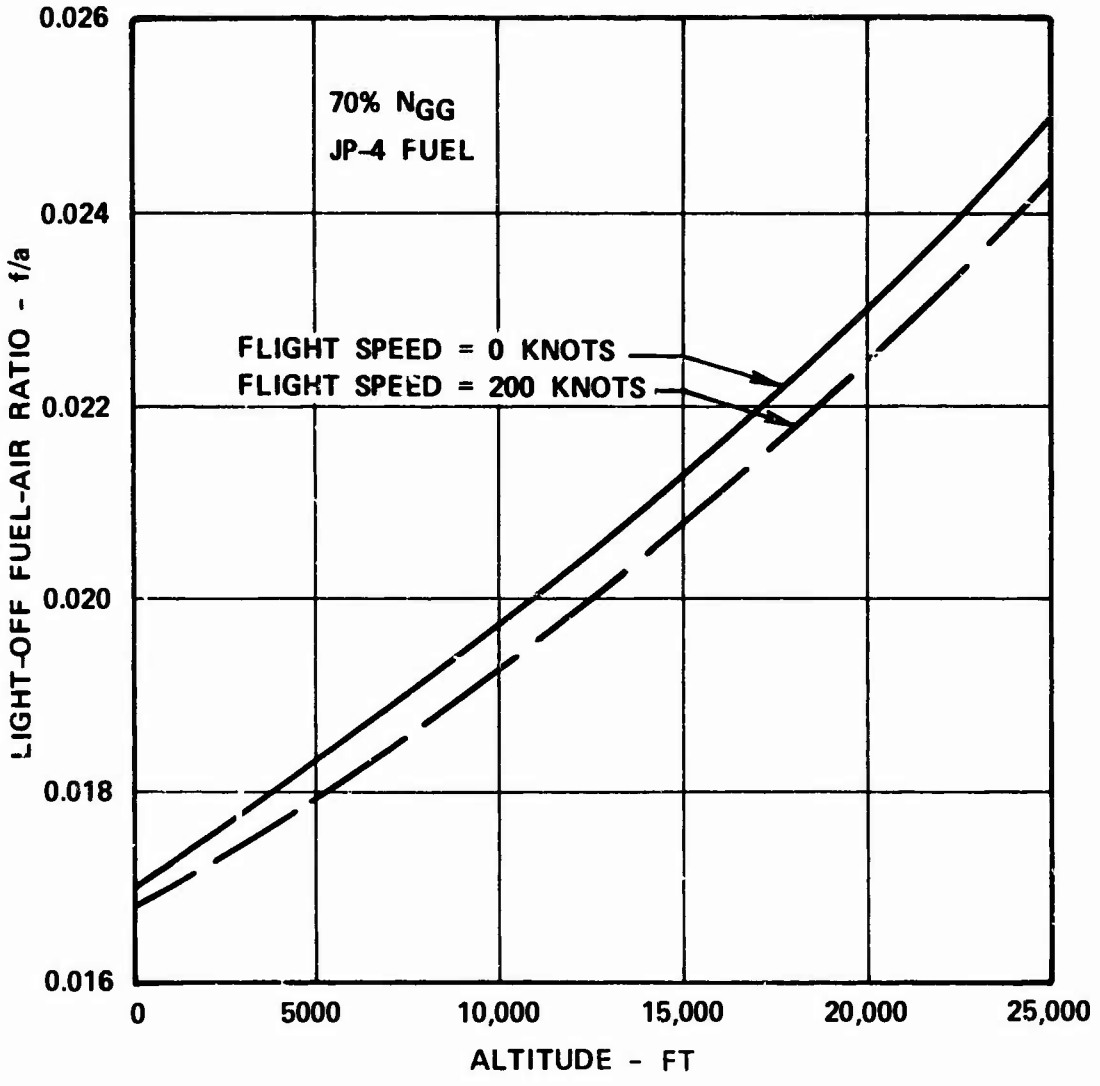

Figure 45. Light-off Fuel-Air Ratio vs Altitude (Based on Data Correlation From Figure 44).

ratio should be a function of $e^{1/\theta_3} V_{REF}/\delta_3\theta_3$, or

$$f/a_{(LBO)} = F(e^{1/\theta_3} V_{REF}/\delta_3\theta_3) \quad (12)$$

The different data points for (f/a) LBO fall on a straight line on the logarithmic scale illustrated in Figure 44.

The LBO data can be correlated by the parameter $e^{1/\theta_3} V_{REF}/\delta_3\theta_3$ as shown in Figure 46. It appears that JP-4, -5, and -8 have similar LBO characteristics except at low P_3 and T_3, where JP-5 had considerably higher LBO fuel-air ratio [$(f/a)_{LBO} = 0.052$ $e^{1/\theta_3} V_{REF}/\delta_3\theta_3 = 230$ ft/sec.] It can be assumed that the LO and LBO characteristics could be improved with some fuel system and combustor development.

3.4.4 Emission Tests

The concentrations of carbon monoxide (CO), unburned hydrocarbons (UHC), and nitrogen oxides (NO_x) are influenced to varying degrees by T_3, P_3, overall fuel-air ratio, and combustor residence time. Therefore, two types of emission tests were conducted:

- Runs in which all variables except one are kept constant
- Runs at different simulated engine power settings where most of the variables change simultaneously

Emission samples were taken with the use of the six thermocouple aspiration tubes manifolded to give an average sample for three evenly spaced radial locations and two circumferential locations, rotated through 360°. The probes were positioned such that when three points were along the centerline of one fuel nozzle, the other three points were between two other nozzles, with the rakes 112.5° apart. Sample line temperatures were kept at 300° to 350°F by means of electrical heating tapes. The mobile emissions unit provided on-line analysis. The results are tabulated in Table VI and shown graphically in Figures 47, 48, and 49. From the data from Runs 1 through 14 (Table VI, Figures 47 and 48), the effect of P_3, T_3 and T_4 on gaseous emissions was assessed. The results shown are statistical averages of gas samples obtained by the six-point averaging probe traversed through 16 circumferential positions.

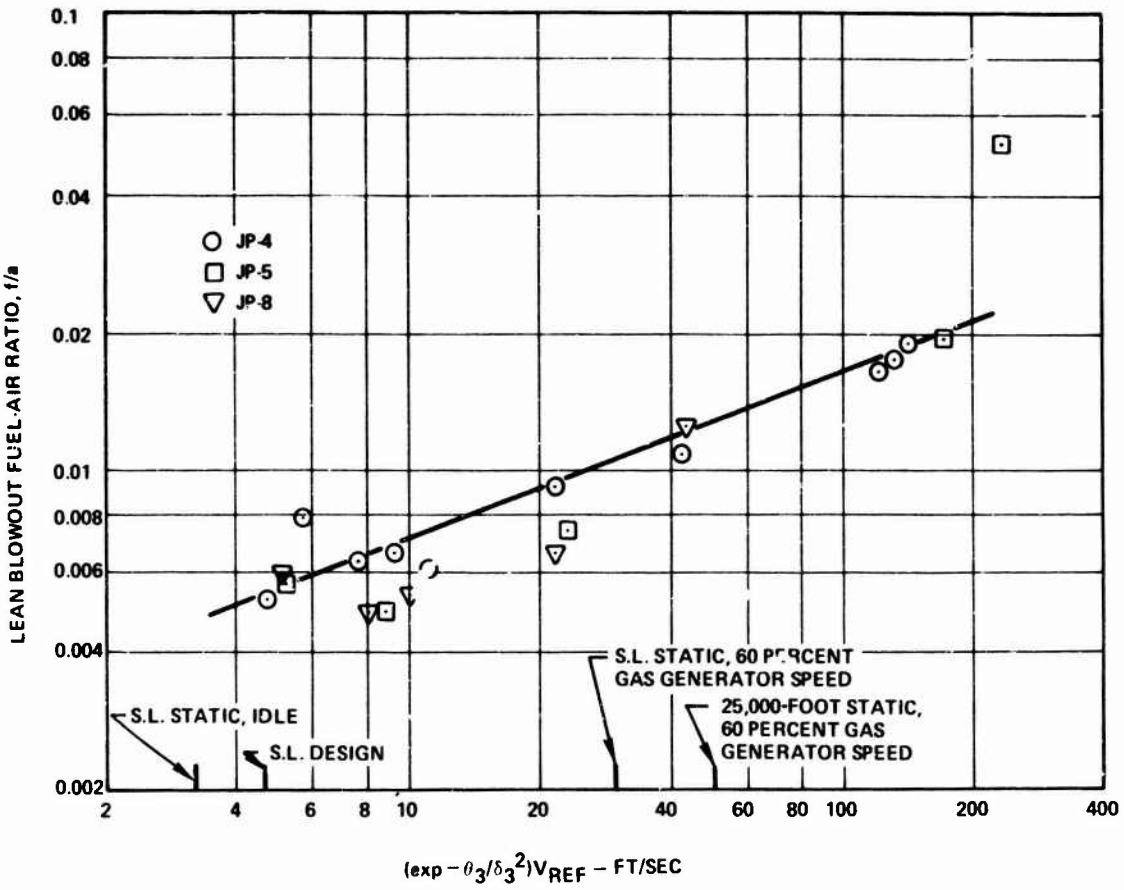

Figure 46. Lean Blowout Fuel-Air Ratio of Combustor With Different Fuels.

TABLE VI. EXHAUST EMISSIONS OF USAAMRDL COMBUSTOR

Run No.	P_3 (psia)	T_3 (°F)	T_4 (°F)	W_{a3} (lb/sec)	f/a	η_B (1) (%)	CO (lb/1000 lb fuel)	UHC (lb/1000 lb fuel)	NO (lb/1000 lb fuel)	Smoke (2) Number SAE ARP 1179
1	40.1	210	633	0.61	0.0144	41.46	80.27	643.1	0.579	-
2	40.6	210	2029	0.61	0.0296	92.79	12.766	78.4	2.108	-
4	40.2	215	1978	0.61	0.0267	98.75	15.834	9.98	2.761	-
5	40.2	430	2184	0.61	0.155	93.81	72.383	51.383	2.146	-
6	40.2	447	2076	0.61	0.0253	99.93	0.943	0.524	4.091	-
7	40.1	580	1665	0.61	0.0163	99.53	7.024	3.511	3.414	-
8	40.1	585	2124	0.61	0.0244	99.96	0.664	0.276	4.792	-
9	196.2	210	1336	2.29	0.0181	95.42	27.224	44.693	3.021	-
10	196.2	205	1994	2.30	0.0273	99.94	1.221	0.4	4.83	-
11	196.3	456	1672	2.28	0.0181	99.65	8.077	1.858	5.391	-
12	196.3	440	2170	2.27	0.0269	99.97	1.083	0.07	7.004	-
13	196.3	680	1859	2.31	0.0182	99.87	4.5	0.332	9.894	-
14	196.3	715	2325	2.28	0.0259	99.98	0.481	0.073	13.444	-
16 (3)	224.2	725	2205	2.71	0.0237	99.99	0.425	0.06	13.859	0
17 (4)	120.7	594	1833	1.63	0.0191	99.92	2.004	0.425	7.05	0
18 (5)	85.2	491	1460	1.23	0.0138	98.91	13.377	8.836	4.055	0

(1) Combustor efficiency computed by methods described in Federal Register Vol. 37, No. 239, dated 12 December 1972.

(2) Smoke data obtained only for Runs 16, 17, and 18.

(3) Conditions for this run correspond approximately to equivalent engine at MRP.

(4) Conditions for this run correspond approximately to equivalent engine at 14 percent of MRP.

(5) Conditions for this run correspond approximately to equivalent engine at minus 5 percent MRP.

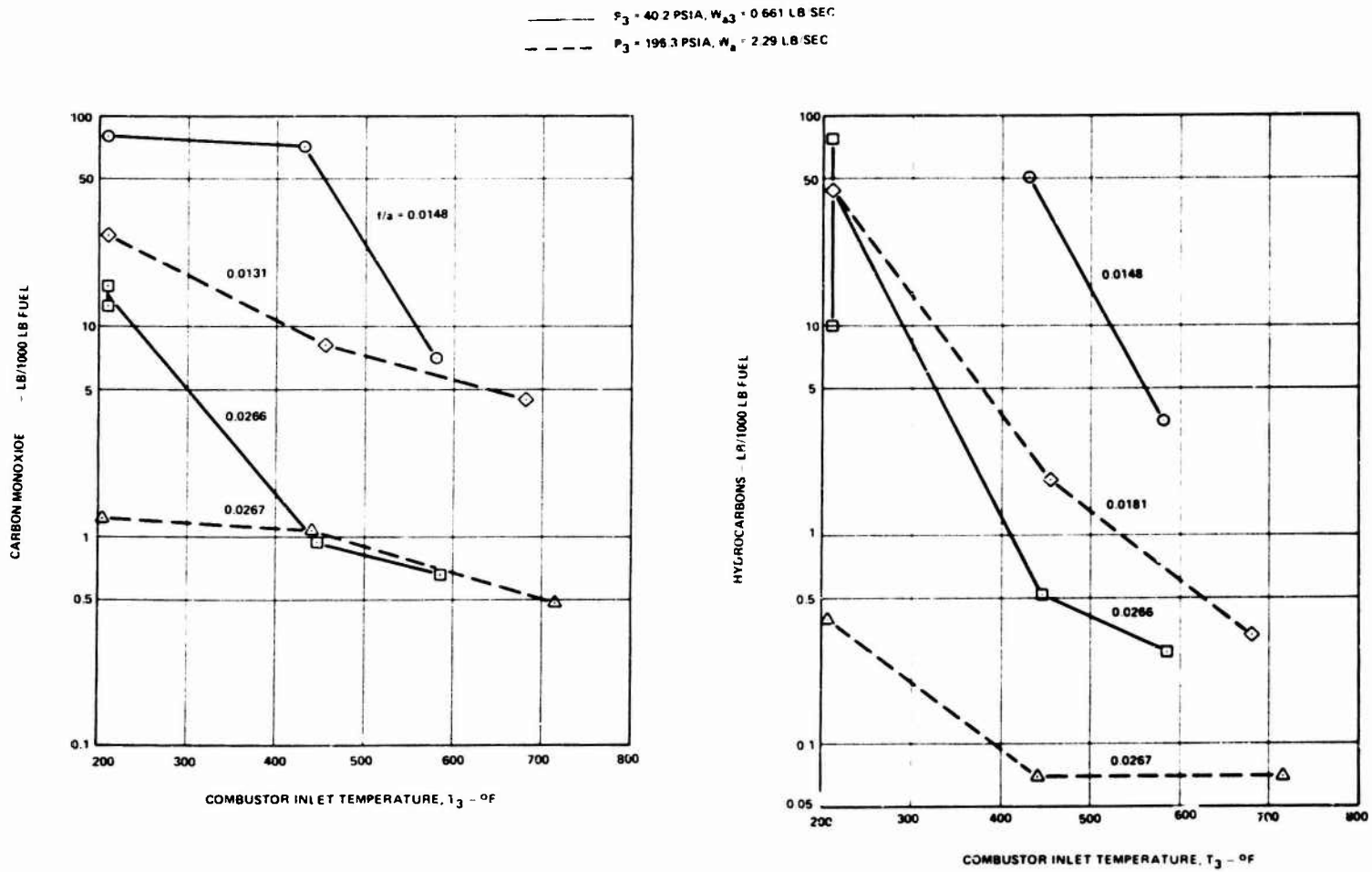

Figure 47. Effect of T_3 on Carbon Monoxide and Hydrocarbon Emissions of Combustor With P_3, W_{a3}, and f/a as Parameters.

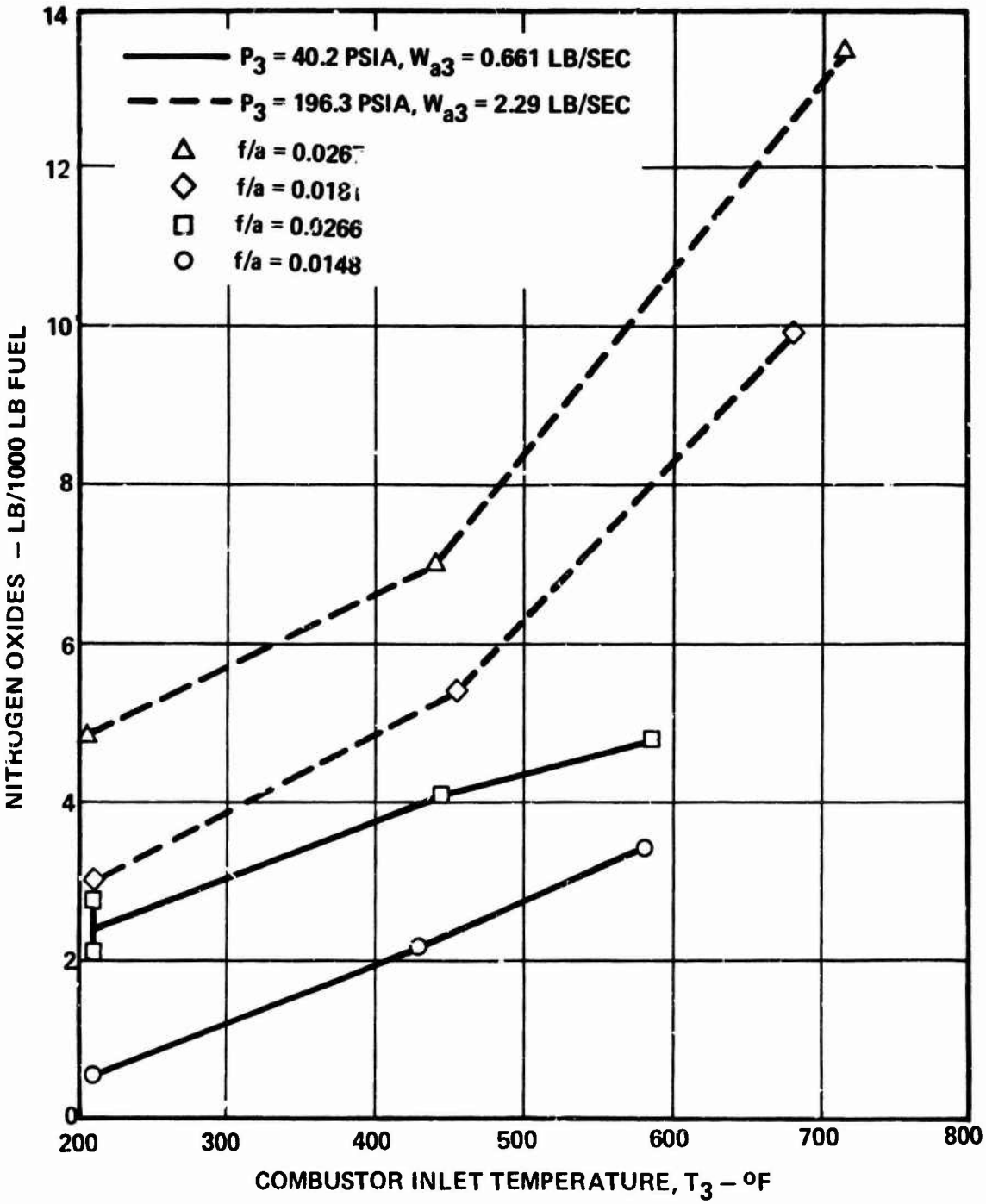

Figure 48. Variation of Nitrogen Oxide Emissions of Combustor With P_3, W_{a3}, and f/a as Parameters.

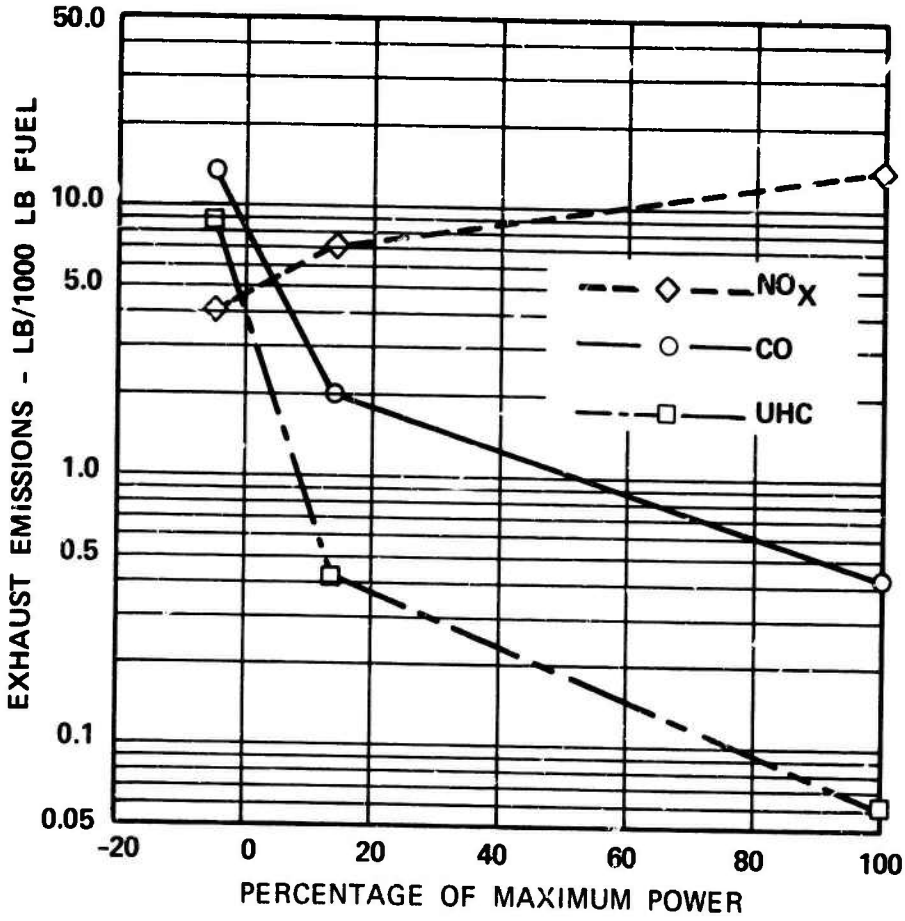

Figure 49. Exhaust Emissions of Combustor at Different Sea-Level Power Settings.

The general effect of each variable on exhaust emissions is summarized as follows:

- Concentration of CO decreases with increasing T_3, T_4, and/or P_3. Influence of P_3 diminishes with higher value of T_3.
- Concentration of UHC decreases with increasing T_3, T_4, and/or P_3.
- Concentration of NO_x increases with increasing T_3, T_4, and/or P_3.

Inlet conditions for Runs 16, 17 and 18 were set to correspond (approximately) to equivalent turboshaft engine gas generator speeds (N_{GG}) of 100, 80, and 70 percent. (These gas generator speeds correspond to MRP, 14-percent MRP, and minus 5-percent MRP, respectively). These results are arithmetic averages of gas samples obtained at the combustor exit plane by the same six-point averaging probe transversed through 16 circumferential positons.

Figure 49 also shows concentrations of pollutants at different power settings at sea-level static conditions. The trends are typical of gas turbine combustion systems in that CO and UHC decrease with increasing power, whereas NO_x increases. Figure 50 shows the comparison of the NO_x emission data with a curve that is somewhat representative of the state of the art and shows the effect of T_3 on NO_x emission index. As shown in Figure 49, NO_x emission level depends upon P_3 and T_4 (and other parameters such as type of injector, geometry, etc.) in addition to T_3. It can be tentatively concluded that the present combustor is slightly lower in NO_x emission than the state of the art. As shown in Table VI, Smoke Number (SAE ARP1179) was zero at all operating conditions as compared with a visible limit smoke number for this type and size of engine of more than 50.

In general, smoke number increases as the stability range is broadened. Therefore, since the smoke number of this combustor is so low, it is apparent that a significant increase in smoke number can be tolerated (and still stay below the visibility limit) in order to increase the stability range of the system.

The low levels of gaseous and particulate emissions produced by the combustion system are encouraging, particularly when considering the following:

- It is a high surface-to-volume combustion liner ($S/V = 1.6$ in.$^{-1}$).

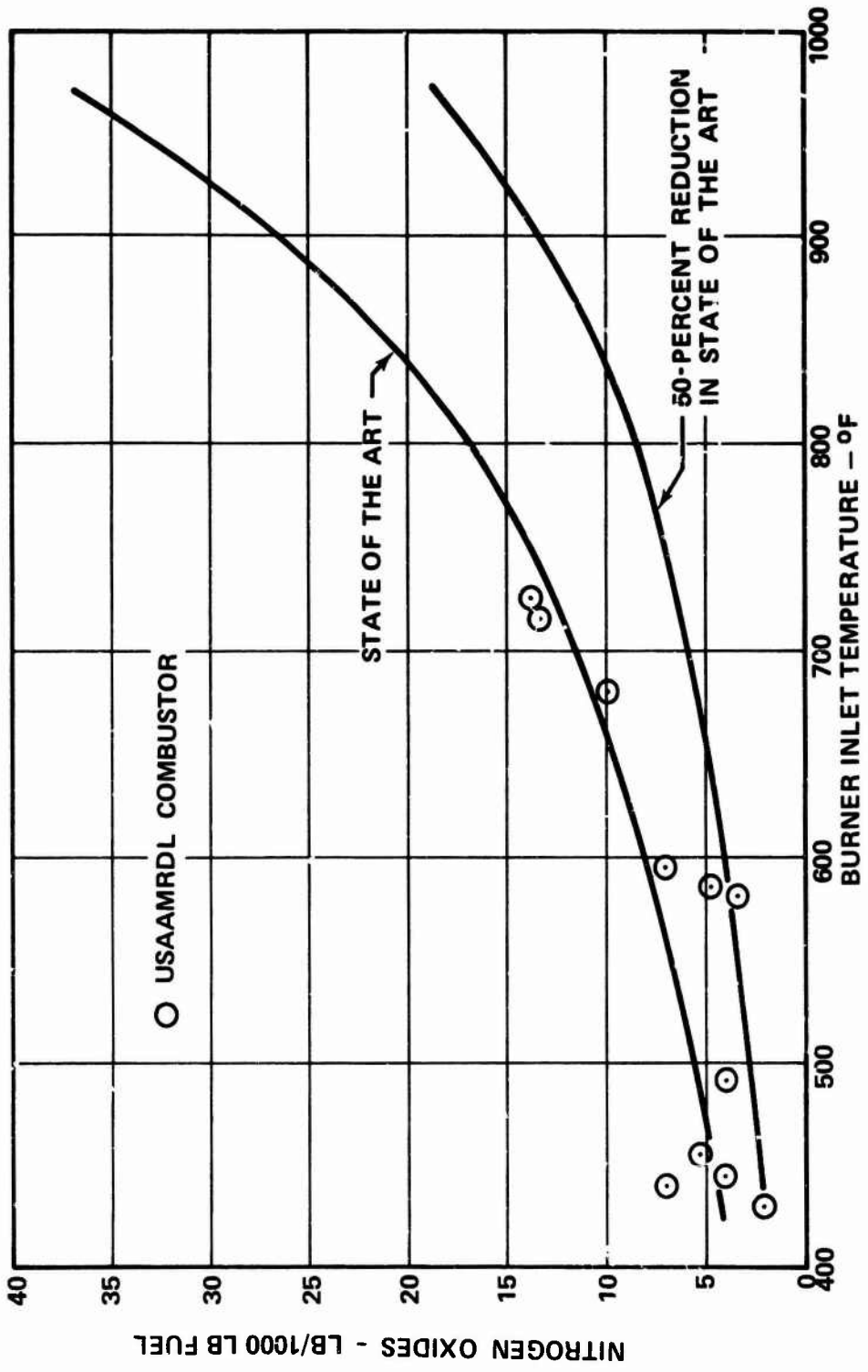

Figure 50. Comparison of Combustor NO_X Emissions With State of the Art.

- The fuel nozzle and primary zone configuration have not been developed.

Some improvement in the emission levels could perhaps be achieved with optimum matching of the fuel nozzle to the combustor.

3.4.5 Structural Durability Test

A combustor thermal cycle endurance test was conducted on the combustion rig. Fuel flow rates were varied from 200 to 98.8 pounds per hour (which was very close to the LBO point) while maintaining nearly constant airflow, pressure and temperature. The fuel flow rate step changes were made after each 2-minute interval of steady-state flow. Airflow conditions were P_{3} = 224.2 psia, T_3 = 731.3°F, and W_{a3} = 2.731 pounds per second. The test had to be discontinued after 128 cycles (compared to the 325 cycles required) because of a structural failure in the rig exhaust section. (It should be noted that the total test time on this combustor more than satisfied the cycle time requirement.) The rig was disassembled and the combustor was visually inspected. A combustor-mount bolt had vibrated loose, causing misalignment of the combustor and fuel manifold. A fuel nozzle tip was damaged, and tack-welds on three swirlers had broken. The above damages, were not considered to be significant problem areas, as they were due only to combustor fabrication techniques. Of more significance was the appearance of cracks on the inside of the dome. The dome was fabricated with a double wall to provide adequate support for the fuel nozzle swirler system. The cracks were confined to the inner wall closest to the flame.

A section was cut from the dome (Figure 51) and tested to determine the reason for this cracking.

Conclusions drawn from the materials analysis were:

- The inner sheet buckling and cracking mode of failure was thermal fatigue (regions A and B on Figure 51).

- Grain growth of the inner sheet was due to lack of cooling. The outer sheet plus the air gap space between the sheets prevented the inner sheet from receiving any form of cooling.

- No visible cracks existed on the outside sheet exposed to the cooling air.

- The dome wall must be fabricated from a single sheet thick enough to support the fuel nozzle swirler system.

As a further indication of the combustor and fuel system performance during the test program (including this thermal cycle endurance test), it was noted that there was no indication of carbon disposition or buildup on the liner at the conclusion of the tests. Occasionally, a very light soot film was present on the internal surface of the cover of some of the fuel nozzles.

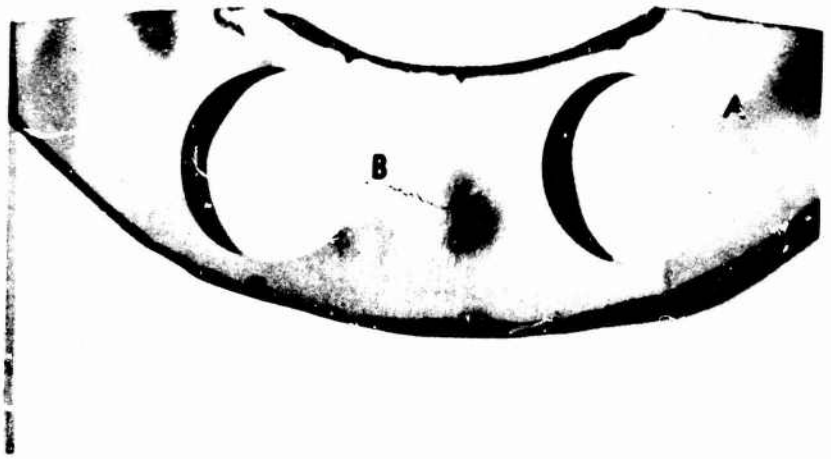

Figure 51. Combustor Dome Buckling and Crack Failure.

4.0 CONCLUSIONS AND RECOMMENDATIONS

The objective of Phase III of the program was to integrate the design and development information of Phases I and II into a working combustion system and to evaluate that system. Conclusions that were drawn from this phase of the program in light of Phases I and II of the program are listed in this section. Recommendations for further work in these areas are also listed.

4.1 CONCLUSIONS

The following conclusions were drawn from the test results and analysis of the combustor.

(a) The combustor system which produced the data presented in this report was essentially the initial configuration. The engine cycle and performance goals specified by the contract represent a difficult combustor design point and, to some extent, are unrealistic since technology for the compressor, turbine, seals, etc., does not exist. However, the combustor performance essentially met the stipulated design goals and therefore demonstrated a design methodology based on rational concepts; and aided by analysis rather than "cut and try" methods, it can significantly reduce combustor development time and cost.

(b) Although most of the combustor element models developed during Phases I and II helped in making rational design decisions, the fluid dynamic models (e.g., Primary Flow and Dilution Zone Models) need to be further developed to be useful as design tools, especially for predicting emission levels and methods for reducing them.

(c) The combustor, although a high surface-to-volume ratio, has the following efficiency and emission characteristics:

- Combustion efficiency not less than 99% over the entire rig-simulated engine operating range
- CO and UHC emissions well below the state of the art, even through the fuel system and primary zone are not properly matched

- o NO_x emission level somewhat lower than current state of the art
- o Zero smoke number
- o Pattern factor between 0.2 and 0.3 with pressure drop about 3 percent
- o High light-off and lean blowout fuel-air ratios which are due to using undeveloped air shear fuel injectors (because of time and money, not technical constraint)

4.2 RECOMMENDATIONS

Based on the successful application of the analytical models to the present combustor design, it is recommended that the available models be further developed and refined. This development should be conducted using an axisymmetric combustor of a size large enough to minimize the effects of probe diameter.

The present combustor system using air-shear fuel injection has demonstrated low emission characteristics. Development of this injection system would produce an efficient, inexpensive method of fuel injection.

The cooling requirement was shown to be a severely limiting factor in the design of small, high-pressure, high-temperature-rise combustors. Future work should include consideration of other forms of cooling and other materials.

LITERATURE CITED

1. Anderson, R.H., ADVANCED HIGH-TEMPERATURE COMBUSTOR RESEARCH FOR SMALL GAS TURBINE ENGINES, USAAVLABS Technical Report 68-63, U.S. Army Aviation Materiel Laboratories, Fort Eustis, Virginia, October 1968, AD681948.

2. Juhasz, A.J., and Market, C.J., COMBUSTION LINER FILM COOLING IN THE PRESENCE OF HIGH FREE-STREAM TURBULENCE, NASA TN D-6360, July 1971.

3. Dukler, A.E., and Moye, W., III, GAS LIQUID FLOW IN CONDUITS, Modern Chemical Engineering, Volume 1 (Ed. A. Avicos), Reinhold Publishing Co., New York, 1963.

4. Fraser, R.P., et al, THE ATOMIZATION OF A LIQUID SHEET BY AN IMPINGING AIR STREAM, Chemical Engineering Science, Volume 18, 1963, pp 339-353.

5. Levy, S., PREDICTION OF TWO-PHASE ANNULAR FLOW WITH LIQUID ENTRAINMENT, International Journal of Heat and Mass Transfer, Volume 9, 1966, pp 171-178.

6. Aiba, T., and Inove, M., INVESTIGATION OF THE AIR STREAM FROM AIR-ENTRY HOLES OF THE AERONAUTICAL GAS TURBINE COMBUSTOR, JSME 20, October 1971.

7. Greenhourh, V.W., and Lefebvre, A.H., SOME APPLICATIONS OF COMBUSTION THEORY TO GAS TURBINE DEVELOPMENT, Sixth Symposium (International) on Combustion, 1957, pp 858-869.

8. Montchiloff, I.N., and Gibson, M.M., THE DESIGN AND PERFORMANCE ANALYSIS OF GAS-TURBINE COMBUSTION CHAMBERS, Northern Research and Engineering Corporation, NREC Report No. 1082-1, 1964, pp 196-200.

APPENDIX
COMBUSTOR DESIGN AND PERFORMANCE DATA SUMMARY

PARAMETER	UNITS	COMBUSTOR	
		Goals	Achieved ①②
Configuration	-	N.D. ③	Annular straight through
Combustor Airflow	lb/sec	2.733	2.817
Combustion Efficiency (@ 5% Idle)	%	N.D.	99.7 ④
(@ 30% MRP)	%	N.D.	99.95
(@ 60% MRP)	%	N.D.	99.98
(@ MRP)	%	99.0	99.985
Estimated Airflow Split (Combustion)	%	N.D.	42.0
(Cooling)	%	N.D.	38.0
(Dilution)	%	N.D.	20.0
Inlet Total Pressure	psia	235.1	235.1
Total Pressure Loss	%	≤ 3.0	3.1
Inlet Total Temperature	°F	820	775 ⑤
Average Exit Total Temperature	°F	2500	2363
Temperature Rise	°F	1680	1588
Pattern Factor	-	0.20	0.239
Liner Surface Area (excluding transition duct)	in.②	N.D.	91.0
Liner Surface Area/Volume	in.①	N.D.	1.61
Liner Temperature (max)	°F	1600	1600
(avg)	°F	1400	1200-1300
Liner Wall Thickness	in.	N.D.	0.023
Material	-	N.D.	IN-586
Estimated Tolerance to Flow Discontinuity at Diffuser Exit	-	N.D.	Good
Overall f/a Ratio (Rich Blowout)	-	N.D.	> 0.12
Based on Total (MRP)	-	0.0285	0.026, T_4=2363°F
Combustor Airflow (Lean Blowout)	-	N.D.	0.0054
Primary Zone f/a Ratio	-	N.D.	0.057 (ϕ = 0.85)
Fuel Injector Type	-	N.D.	Air shear atomizer
Number of Fuel Injectors	-	N.D.	8
Minimum Fuel Passage Dimension	in.	N.D.	0.035
Fuel Flow Rate (Maximum)	lb/hr	280	280

Fuel System Pressure (MRP) (Light-Off)	psig	N.D. N.D.	370 370
Estimated Tolerance to Diffuser Exit Swirl Angle	-	N.D.	Good
Fuel Used	-	Multifuel	JP-4, JP-5, JP-8
Heat Release Rate	$\frac{Btu}{hr\text{-}ft^3\text{-}atm}$ ③	N.D.	9.96×10^6
Reference Flow Area	in^2 ②	N.D.	18.05
Primary Zone Reference Velocity	fps	N.D.	44.3
Estimated Smoke Index	SAE Smoke No.	Below Visible Limit	0
Number of Ignitors	-	N.D.	1 ⑥
Ignitor Energy Level (Stored) (Delivered)	Joules	N.D. N.D.	4.0 1.0
Gaseous Emissions	lb 1000 lb fuel	Low	
Unburned Hydrocarbons (Idle)			1.9
(MRP)			0.06
Carbon Monoxide (Idle)			5.1
(MRP)			0.41
Oxides of Nitrogen (Idle)			5.1
(MRP)			13.0

① The achieved performance was obtained with the initial configuration.
② All data for standard-day, sea-level static conditions unless otherwise specified.
③ N.D. = not defined.
④ Efficiency determined from gaseous emissions analysis.
⑤ Facility limitation at the specified airflow rate.
⑥ Although two ignitors were provided, only one was used during light-off tests.